

Numerical investigation of vacuum ultra-violet emission in Ar/O₂ inductively coupled plasmas

Michel Osca Engelbrecht¹, Jonathan Jenderny², Henrik Hylla^{2,3}, Dominik Filla^{2,3}, Peter Awakowicz², Ihor Korolov², Christopher P. Ridgers¹ and Andrew R. Gibson³

¹ York Plasma Institute, School of Physics, Engineering and Technology, University of York, York, UK

² Chair of Electrodynamics and Plasma Technology, Faculty of Electrical Engineering and Information Technology, Ruhr University Bochum, Bochum, Germany

³ Research Group for Biomedical Plasma Technology, Faculty of Electrical Engineering and Information Technology, Ruhr University Bochum, Bochum, Germany

E-mail: michel.osca@york.ac.uk

E-mail: andrew.gibson@rub.de

February 2023

Abstract. Controlling fluxes of vacuum ultraviolet (VUV) radiation is important in a number of industrial and biomedical applications of low pressure plasma sources because, depending on the process, VUV radiation may be desired, required to a certain degree, or unwanted. In this work, the emission of VUV radiation from O atoms is investigated in low-pressure Ar/O₂ inductively coupled plasmas via numerical simulations. For this purpose, a self-consistent Ar/O₂ plasma-chemical reaction scheme has been implemented in a zero dimensional plasma chemical kinetics model and is used to investigate VUV emission from excited O atoms ($3s\ ^5S_2^0$ and $3s\ ^3S_1^0$) at 130 and 135 nm. The model is extensively compared with experimental measurements of

absolute VUV emission intensities, electron densities and Ar excited state densities. In addition, VUV emission intensities are investigated as a function of pressure, Ar/O₂ mixture, and power deposition and the dominant reaction pathways leading to VUV emission are identified and described. In general terms, absolute VUV emission intensities increase with power and oxygen fraction over the ranges investigated and peak emission intensities are found for pressures between 5-50 Pa. The emission is dominated by the 130 nm resonance line from the decay of the O(3s ³S₁^o) state to the ground state. Besides, at low pressure (0.3-1 Pa), the flux of VUV photons to surfaces is much lower than that of positive ions, whereas VUV fluxes dominate at higher pressure, \gtrsim 5-50 Pa depending on O₂ fraction. Finally, oxygen atom fluxes to surfaces are, in general, larger than those of VUV photons for the parameter space investigated.

1. Introduction

Inductively coupled plasmas (ICPs) operated at low pressures are widely used for materials processing, microelectronics manufacturing¹⁻⁷ and are also investigated for applications in biomedicine.⁸⁻¹⁴ Control of vacuum ultraviolet (VUV) radiation in ICPs is important as, depending on the process, radiation may be desired^{14,15} required to some degree¹⁶⁻¹⁸ or unwanted.^{19,20} On the one hand, damage to the substrate by VUV radiation during plasma etching can be an important process in materials processing applications and is therefore an active topic of research.²¹ Otherwise, in some specific circumstances, VUV radiation can participate in synergistic processes,^{16,17,22} where they can be exploited for the benefit of materials processing. On the other hand, VUV fluxes may be used for the sterilisation of surfaces and are therefore of great interest in medical, pharmaceutical and food industry applications.⁹⁻¹³ In this context, VUV radiation for sterilisation purposes is of increasing interest as it can be an effective mechanism on 3-D, heat-sensitive objects and it enables sterilisation in dry environments, with short exposure times and without toxic residues.

VUV emission in ICPs has been investigated for different gas mixtures and under different operation conditions. Investigations of VUV radiation have been carried out in ICPs operated with different gases, such as Ar,²³⁻²⁸ N₂,^{27,29} O₂,^{27,28} He,²¹ H₂,^{27,29,30} Xe,^{21,27} Cl₂,³¹ Cl₂/BCl₃³² and fluorocarbon gases,^{23,24} with either experimental or numerical methods in power ranges between 150 and 1100 W and total pressure ranges between 1 and 100 mTorr (0.13-13 Pa). However, despite the number of investigations carried out, the understanding of the formation pathways of VUV photons in ICP applications remains relatively limited as the operating parameters investigated are comparatively few. Therefore, a comprehensive investigation of VUV emission in ICPs that describes the pathways leading to emission over a wide range of operating parameters would be useful to better understand and control ICPs for industrial and biomedical applications.

For this reason, an investigation of oxygen atom VUV emission in low pressure Ar/O₂ ICPs over the operating parameters of total pressure p_T , power P_{in} and oxygen mixture fraction χ_{O_2} is carried out in this work. Oxygen containing plasmas are widely used in industrial applications³³⁻³⁹ and are of interest for biomedical^{14,15,40} applications. Therefore, providing a detailed understanding of VUV radiation formed from O atoms in Ar/O₂ ICPs and the plasma-chemical pathways leading to it could be useful to improve plasma performance in these applications. In this work, the collisional radiative model developed in 28 has been extended and implemented in a zero-dimensional (0D) plasma chemical-kinetics global model (GM) that allows self-consistent simulations. The GM enables computationally inexpensive simulations and allows detailed study of plasma-chemical and radiative processes and is therefore well suited to the goals of this investigation.

The GM and reaction scheme for Ar/O₂ are presented in section 2. In parallel,

experimental work has been carried out in order to provide a validation of the simulated plasma properties and is described in section 3. The numerical GM results are first compared against experimental measurements carried out in this work, and available from previous studies, in 4.1 to provide confidence in the numerical model and the reaction scheme used. In this section simulations of electron densities and temperatures, dissociation fractions, argon metastable densities and absolute emission intensities are compared with experimental measurements. Following comparison with experimental data, a more extensive numerical investigation is carried out over a wide range of operating conditions in section 4.2. In this section variations of the operating parameters of total pressure ($p_T = 0.3\text{-}100\text{ Pa}$), input power ($P_{in} = 100\text{-}2000\text{ W}$) and oxygen fraction ($\chi_{O_2} = 0\text{-}0.2$) are conducted and oxygen VUV emission and its formation pathways investigated. The VUV emission is not only described in absolute values but also in comparison with ion and oxygen atom fluxes at the reactor walls to give a broad context on regimes of interest for optimising plasma processes that may be dependent on the fluxes of each different component to surfaces.

2. Numerical model description

The numerical method used for this investigation is a 0D plasma-chemical kinetics GM that solves fluid-based mass and energy balance equations for a system of volume V bounded by a surface area A . Under the assumption that mass and energy are relatively homogeneously distributed in space, time variations of species densities and energies are caused by plasma-chemical reactions, interactions with the system boundaries and input power. This type of model is widely used in the low temperature plasma research community^{41,42} as it enables fast simulations of plasmas with complex chemical reaction schemes and can provide robust insights into the scaling of important plasma parameters

under variations of external operating conditions.^{43–45}

For this work, a GM has been designed and developed in the Julia programming language.⁴⁶ The GM models a cylindrical plasma reactor, of length L and radius R , to which power P_{in} is coupled inductively. The experimental reactor is discussed in more detail in section 3.

The numerical execution structure consists of an initialization of the simulation environment and a five-step cycle, shown in figure 1, that updates the simulation system in time.

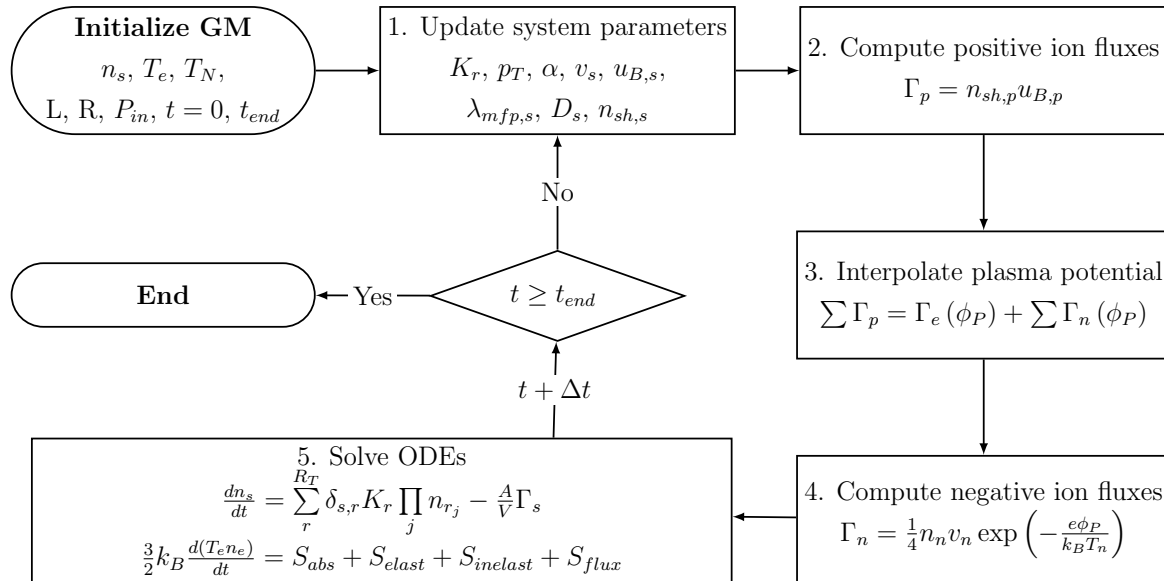


Figure 1: Flowchart of the 0D plasma-chemical kinetics GM. Steps 2-4 are described in section 2.4 and step 5 in sections 2.2 and 2.3.

The initial conditions for the density and temperature of each species, as well as the length L and radius R of the reactor, the applied power P_{in} and the simulation time length t_{end} must be defined in advance. After initialising the simulation parameters, the execution of the cycle computes a new electron temperature and species densities values and advances in time by Δt . The simulation ends when the final time condition is reached, $t \geq t_{end}$. The cycle consists of the following steps

- 1.- Computation of system parameters necessary for later steps: reaction rate coefficients K_r , species mean-free-path $\lambda_{mfp,s}$, diffusion coefficients D_s , electronegativity α , total pressure p_T , thermal speed v_s , Bohm velocity $u_{B,s}$ and number density at the plasma sheath edge $n_{sh,s}$.
- 2-4.- Computation of charged particle fluxes to the system walls, Γ , and plasma potential, ϕ_P . This is described in more detail in section 2.4.
- 5.- Solve the system of ordinary differential equations (ODEs) formed by mass and energy continuity equations. The ODE solver *Rosenbrock23* in the *DifferentialEquations* library⁴⁷ is used for this purpose. A detailed description of the mass and energy equations is found in sections 2.2 and 2.3, respectively.

The simulation results presented in section 4 use the following initial conditions, unless explicitly stated otherwise. A partially ionised plasma, where the neutral gas is formed only by ground state Ar and O₂ at total pressure p_T and with an arbitrary oxygen fraction $0 \leq \chi_{O_2} \leq 1$. The plasma is formed by electrons, O₂⁺ and Ar⁺ with an initial plasma density $n_P = 10^{14} \text{ m}^{-3}$. The initial density of the plasma species fulfils quasi-neutrality, and thus $n_P = n_e = n_{O_2^+} + n_{Ar^+}$, where $n_{Ar^+} = (1 - \chi_{O_2})n_P$ and $n_{O_2^+} = \chi_{O_2}n_P$ are in the same ratio as the Ar/O₂ gas mixture. The remaining neutral and charged species have an initial density of zero. The initial electron temperature is set to $T_e = 1.5 \text{ eV}$ and neutral and ion species have a fixed temperature T_N . Different values of T_N are used depending on the conditions, as discussed in more detail later. The reactor size is as the reactor described in the experimental section 3, with $L = R = 0.2 \text{ m}$. The simulation time is $t_{end} = 1 \text{ s}$, which has been tested to be long enough for the simulations to converge to a stable solution in all the results presented.

2.1. Species and plasma-chemical reaction scheme

The species list included in the model is based on previous works on the simulation of argon and oxygen containing plasmas,^{28,45,48} and is listed in table 1.

Table 1: Species included in the numerical model.

Species	Atomic level
e	
Ar	
Ar ⁺	
Ar(4p)	3s ² 3p ⁵ (2P _{3/2} ⁰)4p, 3s ² 3p ⁵ (2P _{1/2} ⁰)4p
Ar ^m	3s ² 3p ⁵ (2P _{3/2} ⁰)4s ₂ , 3s ² 3p ⁵ (2P _{1/2} ⁰)4s ₀
Ar ^r	3s ² 3p ⁵ (2P _{3/2} ⁰)4s ₁ , 3s ² 3p ⁵ (2P _{1/2} ⁰)4s ₁
O ₂	
O ₂ ⁺	
O ₂ ⁻	
O ₂ (a ¹ Δ _u)	
O ₂ (b ¹ Σ _u ⁺)	
O	2s ² 2p ⁴ ³ P _{2,1,0}
O ⁺	
O ⁻	
O(¹ D)	2s ² 2p ⁴ ¹ D ₀
O(¹ S)	2s ² 2p ⁴ ¹ S ₀
O(³ S)	2s ² 2p ³ (³ S ⁰) 3s ³ S ₁ ⁰
O(⁵ S)	2s ² 2p ³ (³ S ⁰) 3s ⁵ S ₂ ⁰
O(³ P)	2s ² 2p ³ (³ S ⁰) 3p ³ P _{1,2,0}
O(⁵ P)	2s ² 2p ³ (³ S ⁰) 3p ⁵ P _{1,2,3}
O ₃	
O ₃ (ν)	
O ₃ ⁺	
O ₃ ⁻	
O ₄	
O ₄ ⁺	
O ₄ ⁻	

The plasma-chemical reaction scheme included in the GM is a compendium of reactions used in 28,41,49 and the references therein. The reaction scheme consists of a

set of electron-oxygen reactions, in table A1, electron-argon, in table A2, oxygen-oxygen, in table A3, argon-argon, in table A4, oxygen-argon, in table A5, and recombination reactions, in table A6. Moreover, additional reactions are included for ion-wall interactions, in table 2, neutral-wall interactions, in table 3, atomic level transitions, in table 4, and oxygen reactions with radiative cascading processes, in table 5. Altogether there are a total of $R_T = 393$ reactions included. As is noted in the appendices, reaction rate coefficients for electron impact reactions are implemented as functions of electron temperature, assuming a Maxwellian electron energy distribution function.

Reactions #13, 31, 50 (in table A1) and 107 (table A2) are electron-neutral elastic collisions. Reactions #14, 32 and 51 (table A1) are rotational excitations, and #15-20, #33-38, and #52-57 (table A1) are vibrational excitations,⁴⁸ whose products are not explicitly simulated and therefore these reactions only act as an energy gain or loss mechanism. The reactions #62 (table A1) and #142 (table A2) have as product the vibrational state of O₂ but this is not included in the model and is replaced by the O₂ ground state.

The interactions between electrically charged particles and the reactor walls are described in more detail in section 2.4 and neutral-wall reactions are described in section 2.5. Besides, atomic level transitions and radiative processes, especially in oxygen, are described in section 2.6.

2.2. Mass balance equations

The basic formulation of the equations used in the model is adapted from Refs.^{41,45} The GM includes a mass balance equation for each species s , in table 1,

$$\frac{dn_s}{dt} = \sum_r \delta_{s,r} K_r \prod_j n_{r_j} - \frac{A}{V} \Gamma_s. \quad (1)$$

The left hand side represents the time variations of the density of the s -th species, n_s .

The first term on the right hand side accounts for the particle gain, or loss, due to the R_T reactions listed in tables A1, A2, A3, A4, A5, A6, 3, 4 and 5. The second term on the right hand side accounts for mass variations caused by particle fluxes of charges particles to the system walls, Γ_s , that are described in more detail in section 2.4. The surface area A and system volume V are determined by the cylindrical shape of the reactor, i.e. $A = 2\pi(R^2 + RL)$ and $V = \pi R^2 L$.

The mass variation caused by the r -th reaction is the product of the rate coefficient K_r with the densities of the j reacting species, n_{rj} . The factor $\delta_{s,r}$ is an integer that reflects the particle balance of species s in reaction r . For instance, in reaction #1 ($e + O \rightarrow 2e + O^+$ in table A1) electrons have a positive balance $\delta_{1,e} = 1$, atomic oxygen a negative balance $\delta_{1,O} = -1$, and oxygen ions a positive balance $\delta_{1,O^+} = 1$. Essentially, $\delta_{s,r} < 0$ represents a mass loss, $\delta_{s,r} > 0$ gain, and $\delta_{s,r} = 0$ equilibrium.

2.3. Energy conservation equation

The energy balance equation accounts for changes in species temperatures as a function of time. The energy balance equation is only solved for electrons, while the temperatures of heavy particles are assumed to be constant in time. Here, the shape of the EDF of electrons is assumed to be Maxwellian. The potential limitations of this assumption are discussed further later. The energy equation for electrons takes the following form

$$\frac{3}{2}k_B \frac{d(T_e n_e)}{dt} = S_{abs} + S_{elast} + S_{inelast} + S_{flux}, \quad (2)$$

where the electron temperature T_e is used as energy reference parameter, k_B is the Boltzmann constant, n_e is the electron density, S_{abs} is the input power absorbed per unit volume, S_{elast} represents energy changes caused by elastic collision processes, $S_{inelast}$ are energy changes caused by inelastic and superelastic collision processes, and S_{flux} is related to the kinetic energy lost by electron and ion fluxes through the plasma sheath.

The input power absorption rate in equation 2

$$S_{abs} = \frac{P_{in}}{V}, \quad (3)$$

represents the external inductive power P_{in} that is coupled to the electrons.

The term $S_{elastic}$ represents the electron energy gains and losses caused by elastic collisions, of the type $e + N \rightarrow e + N$ where N is a neutral species,

$$S_{elastic} = -3 \sum_l^{R_{elastic}} \frac{m_e}{m_N} k_B (T_e - T_N) K_l n_e n_N, \quad (4)$$

where $R_{elastic}$ is the set of elastic collisions present in the collision model, m_N is the mass of N , T_N is the temperature of N , and K_l is the rate coefficient of the l -th elastic scattering process.

Gains or losses of energy caused by inelastic and superelastic collision processes are accounted as

$$S_{inelast} = - \sum_r E_{thr,r} K_r \prod_{r_j} n_j. \quad (5)$$

where $E_{thr,r}$ is the energy released, or absorbed, by the r -th collision.

The last term in equation 2 accounts for the kinetic energy of electrons and positive ions that pass through the sheath and are lost at surfaces

$$S_{Flux} = -\frac{A}{V} \left[2k_B T_e \Gamma_e + \sum_p \Gamma_p \left(\frac{1}{2} k_B T_e + q_p \phi_P \right) \right], \quad (6)$$

where Γ is the particle flux at the system walls, the subscript p is for positive ions, ϕ_P is the plasma potential, and q_p is electric charge. The first term on the right hand side accounts for the kinetic energy taken to surfaces by electrons that have passed through the sheath and the second term accounts for the kinetic energy taken to surfaces by positive ions that have passed across the sheath.⁵⁰ How particle fluxes crossing the sheath are handled in the GM is described in more detail in the following section.

2.4. Ion fluxes to the reactor walls

Ion fluxes crossing the plasma sheaths and reaching the reactor walls play an important role in the mass and energy balance equations. Moreover, ion fluxes are also important to compute the plasma potential ϕ_P , which is required for the electron energy equation and for fluxes of negatively charged species. Positive ion (subscript p) fluxes are computed differently from negative ion (subscript n) and electron (subscript e) fluxes.

Positive ions, whose fluxes are given by

$$\Gamma_p = n_{sh,p} u_{B,p}, \quad (7)$$

where $n_{sp,p}$ is the density at the sheath, need to enter the sheath with the Bohm velocity $u_{B,p} = \sqrt{k_B T_e / m_p}$ in order to be able to reach the walls. The effective density at the sheath edge^{43,51}

$$n_{sh,p} = \frac{R^2 h_{L,p} + RL h_{R,p}}{R^2 + RL} n_p \quad (8)$$

is determined from bulk plasma densities, n_p using geometrical factors R and L as well as the parameters⁵²

$$h_{\{R,L\},p} = \left[\left(\frac{h_{\{R,L\}0}}{1 + 3\alpha/2} \right)^2 + h_c^2 \right]^{1/2} \quad (9)$$

where

$$h_{R0,p} = 0.8 \left[4 + \frac{\eta R}{\lambda_{mfp,p}} + \left(\frac{0.8 R u_{B,p}}{\chi_{01} J_1(\chi_{01}) D_{a,p}} \right)^2 \right]^{-1/2}, \quad (10)$$

$$h_{L0,p} = 0.86 \left[3 + \frac{\eta L}{2\lambda_{mfp,p}} + \left(\frac{0.86 L u_{B,p}}{\pi D_{a,p}} \right)^2 \right]^{-1/2}, \quad (11)$$

$$h_c = \frac{1}{\gamma_-^{1/2} + \gamma_+^{1/2} [n_{*,p}^{1/2} n_+ / n_-^{3/2}]}. \quad (12)$$

These parameters enable the computation of the sheath edge density from very low pressure regimes, where the ion mean free path is much larger than the system dimensions $\lambda_{mfp,p} \gg (L, R)$, to high pressures, where $\lambda_{mfp} \ll T_e / T_p(R, L)$.^{51,53} The

$h_{\{R,L\}0}$ parameters make use of $\chi_{01} \simeq 2.405$, the first zero of the zero order Bessel function J_0 , and the Bessel function 1 of the first kind J_1 . The plasma electronegativity is given by

$$\alpha = \frac{1}{n_e} \sum_n n_n. \quad (13)$$

The temperature ratio between positive and negative ions is given by

$$\eta = \frac{2T_+}{T_+ + T_-}, \quad (14)$$

where the subscript + and – refer to all positive and negative ion species, respectively.

The ambipolar diffusion coefficient is calculated as

$$D_{a,p} = D_p \frac{1 + \gamma_p + \gamma_p \alpha}{1 + \gamma_p \alpha} \quad (15)$$

where

$$\gamma_p = T_e/T_p, \quad (16)$$

is the temperature ratio between electrons and the ion species.

The diffusion coefficient for ions (and also for neutrals, as discussed in the next section) is defined as

$$D_p = \frac{1}{\sum_s \frac{1}{D_{ps}}} \quad (17)$$

which represents an approximation for the diffusion of a species in a multicomponent mixture. Here, $D_{ps} = k_B T_N / \mu_{ps} \nu_{ps}$ is the binary diffusion coefficient⁵⁴ between the given ion p and the s -th heavy mass species in the system, i.e. species with $m_s \gg m_e$. Besides, $\nu_{ps} = n_s \sum_r K_r$ is the total collision frequency between p and s , and μ_{ps} is the reduced mass.

The h_c parameter makes use of $\gamma_- = T_e/T_-$ and $\gamma_+ = T_e/T_+$, which in our case are the same as the temperature of ions and neutrals are equal $T_- = T_+ = T_N$, and

$$n_{*,p} = \frac{15}{56} \frac{\eta^2}{K_{rec} \lambda_{mfp,p}} v_p, \quad (18)$$

where K_{rec} is the total rate coefficient of the recombination reactions listed in table A6.

The total mean-free-path is estimated as

$$\lambda_{mfp,p} = \frac{1}{\sum_s n_s \sigma_{ps}^T} \quad (19)$$

where $\lambda_{mfp,ps} = 1/n_s \sigma_{ps}^T$ and σ_{ps}^T is the total collision cross-section between species p and s . Please note that s refers only to heavy mass species, and therefore the corresponding neutral-ion and ion-ion collisions listed in tables A3-A6, as well as elastic scattering, resonant charge-exchange and Coulomb collision processes are included in the calculation of the mean-free-path. The cross-section of the reactions in the above-mentioned tables are approximated with $\sigma_{ps} \simeq K_r/v_{ps}$ ⁵⁵ where $v_{ps} = \sqrt{8k_B T_N/\pi\mu_{ps}}$ is the mean speed of relative motion.⁵⁴ The cross-section of elastic scattering and resonant charge-exchange are extracted from 45, 54, 56, if available, otherwise they are calculated using the hard sphere model, $\sigma_{ps} = \pi(r_p + r_s)^2$, using the following atomic, and molecular, radii: $r_{Ar} = 188$ pm, $r_O = 152$ pm, $r_{O_2} = r_{O_3} = r_{O_4} = 197$ pm. For Coulomb collisions, a constant cross-section estimate of $5 \cdot 10^{-19}$ m² is used.⁵²

Negative ion fluxes to surfaces are described by the expression given in 44

$$\Gamma_n = \frac{1}{4} n_n v_n \exp\left(-\frac{e\phi_P}{k_B T_n}\right), \quad (20)$$

where the subscript n refers to negative ion species. The flux of these species are restricted to those particles with energies high enough to overcome the potential barrier of the plasma sheath, which is determined in ICPs by the plasma potential with respect to a floating wall. Note that $v_n = \sqrt{8k_B T_n/\pi m_n}$ is the thermal speed of the n -th negative ion. The same expression as in equation 20 is valid for the electron flux, Γ_e . To determine Γ_n and Γ_e the plasma potential ϕ_P must be known, which is obtained by solving the flux balance equation

$$\sum_p q_p \Gamma_p + q_e \Gamma_e + \sum_n q_n \Gamma_n = 0, \quad (21)$$

which states that the total particle flux, of positive, negative ions and electrons, must balance to ensure quasi-neutrality. The flux balance equation is solved for ϕ_P using an iterative method. ϕ_P is then used in the flux term of the energy balance equation, equation 6, and for computing the flux of negative ions and electrons, equation 20.

In order to maintain mass conservation in the system, both positive and negative ions are considered to be neutralised when they get in contact with the wall.⁴⁵ These reactions are listed in table 2, such that $A/V\Gamma_s = \delta_{s,r}n_sK_r$,⁴⁵ and are included in the mass balance (second term on rhs of equation 1) for the species on both left and right sides of the neutralization reactions. Note that the ion-wall neutralization reactions in Ref. 45 have been extended to the ion species included in this work.

Table 2: Ion-wall reactions.

#	Process	K_r [s ⁻¹]	Ref.
344	O ⁺ → O	$2u_{B,O^+}(R^2h_{L,O^+} + RLh_{R,O^+})/(R^2L)$	45
345	O ₂ ⁺ → O ₂	$2u_{B,O_2^+}(R^2h_{L,O_2^+} + RLh_{R,O_2^+})/(R^2L)$	45
346	O ₃ ⁺ → O ₃	$2u_{B,O_3^+}(R^2h_{L,O_3^+} + RLh_{R,O_3^+})/(R^2L)$	45 ^a
347	O ₄ ⁺ → 2O ₂	$2u_{B,O_4^+}(R^2h_{L,O_4^+} + RLh_{R,O_4^+})/(R^2L)$	45 ^a
348	Ar ⁺ → Ar	$2u_{B,Ar^+}(R^2h_{L,Ar^+} + RLh_{R,Ar^+})/(R^2L)$	45
349	O ⁻ → O	$(A/4V)v_{O^-} \exp(-e\phi_P/k_B T_{O^-})$	44
350	O ₂ ⁻ → O ₂	$(A/4V)v_{O_2^-} \exp(-e\phi_P/k_B T_{O_2^-})$	44 ^b
351	O ₃ ⁻ → O ₃	$(A/4V)v_{O_3^-} \exp(-e\phi_P/k_B T_{O_3^-})$	44 ^b
352	O ₄ ⁻ → 2O ₂	$(A/4V)v_{O_4^-} \exp(-e\phi_P/k_B T_{O_4^-})$	44 ^b

^a The expression is of the same form given in Ref. 45, but is extended here to all positively charged species

^b The expression is of the same form given in Ref. 44, but is extended here to all negatively charged species

2.5. Neutral particle diffusion to the reactor walls

Neutral particle diffusion within the plasma reactor plays an important role as it determines the flux of neutral species that interact with the reactor walls.^{42,43,51} This is important because metastable species reaching the walls are de-excited to ground

state, and atomic oxygen recombines into molecular oxygen. Therefore, neutral-wall interactions depend on the species diffusion properties. These types of reactions are included in the GM, and listed in table 3.

Table 3: Neutral-wall reactions. γ is the sticking coefficient.

#	Process	γ	K_r [s ⁻¹]	Ref.
353	$O \rightarrow \frac{1}{2}O_2$	equation 24	$\left[\frac{\Lambda^2}{D_O} + \frac{2V(2-\gamma_O)}{Av_O\gamma_O} \right]^{-1}$	45
354	$O(^1D) \rightarrow O$	1.0	$\left[\frac{\Lambda^2}{D_{O(^1D)}} + \frac{2V(2-\gamma_{O(^1D)})}{Av_{O(^1D)}\gamma_{O(^1D)}} \right]^{-1}$	28
355	$O(^1S) \rightarrow O$	1.0	$\left[\frac{\Lambda^2}{D_{O(^1S)}} + \frac{2V(2-\gamma_{O(^1S)})}{Av_{O(^1S)}\gamma_{O(^1S)}} \right]^{-1}$	28
356	$O(^3S) \rightarrow O$	1.0	$\left[\frac{\Lambda^2}{D_{O(^3S)}} + \frac{2V(2-\gamma_{O(^3S)})}{Av_{O(^3S)}\gamma_{O(^3S)}} \right]^{-1}$	28
357	$O(^5S) \rightarrow O$	1.0	$\left[\frac{\Lambda^2}{D_{O(^5S)}} + \frac{2V(2-\gamma_{O(^5S)})}{Av_{O(^5S)}\gamma_{O(^5S)}} \right]^{-1}$	28
358	$O(^3P) \rightarrow O$	1.0	$\left[\frac{\Lambda^2}{D_{O(^3P)}} + \frac{2V(2-\gamma_{O(^3P)})}{Av_{O(^3P)}\gamma_{O(^3P)}} \right]^{-1}$	28
359	$O(^5P) \rightarrow O$	1.0	$\left[\frac{\Lambda^2}{D_{O(^5P)}} + \frac{2V(2-\gamma_{O(^5P)})}{Av_{O(^5P)}\gamma_{O(^5P)}} \right]^{-1}$	28
360	$O_2(a^1\Delta_u) \rightarrow O_2$	0.007	$\left[\frac{\Lambda^2}{D_{O_2(a^1\Delta_u)}} + \frac{2V(2-\gamma_{O_2(a^1\Delta_u)})}{Av_{O_2(a^1\Delta_u)}\gamma_{O_2(a^1\Delta_u)}} \right]^{-1}$	45, 57
361	$O_2(b^1\Sigma_u^+) \rightarrow O_2$	0.007	$\left[\frac{\Lambda^2}{D_{O_2(b^1\Sigma_u^+)}} + \frac{2V(2-\gamma_{O_2(b^1\Sigma_u^+)})}{Av_{O_2(b^1\Sigma_u^+)}\gamma_{O_2(b^1\Sigma_u^+)}} \right]^{-1}$	45, 57
362	$Ar^m \rightarrow Ar$	1.0	$\left[\frac{\Lambda^2}{D_{Ar^m}} + \frac{2V(2-\gamma_{Ar^m})}{Av_{Ar^m}\gamma_{Ar^m}} \right]^{-1}$	45
363	$Ar^r \rightarrow Ar$	1.0	$\left[\frac{\Lambda^2}{D_{Ar^r}} + \frac{2V(2-\gamma_{Ar^r})}{Av_{Ar^r}\gamma_{Ar^r}} \right]^{-1}$	45
364	$Ar(4p) \rightarrow Ar$	1.0	$\left[\frac{\Lambda^2}{D_{Ar(4p)}} + \frac{2V(2-\gamma_{Ar(4p)})}{Av_{Ar(4p)}\gamma_{Ar(4p)}} \right]^{-1}$	45

The effective loss-rate coefficient for a neutral species N to the wall is given by^{58,59}

$$K_{D,N} = \left[\frac{\Lambda^2}{D_N} + \frac{2V(2-\gamma_N)}{Av_N\gamma_N} \right]^{-1} \quad (22)$$

where

$$\Lambda = \left[\left(\frac{\pi}{L} \right)^2 + \left(\frac{2.405}{R} \right)^2 \right]^{-1/2} \quad (23)$$

is the effective diffusion length for a cylindrical reactor,⁵⁸ D_N is the diffusion coefficient for neutrals, $v_N = \sqrt{8k_B T_N / \pi m_N}$ is the thermal speed and γ_N is the sticking coefficient. D_N and the mean free path $\lambda_{mfp,N}$ are defined as in equations 17 and 19 respectively, but

for neutrals instead of ions. The sticking coefficient depends, among other parameters, on the wall material and operating pressure.^{43,45} The GM uses γ_N values taken from 28,45 that conducted simulations under similar operating conditions. The γ_N values used, listed in table 3, are constant parameters except for atomic oxygen,⁴⁵ which is pressure dependent based on the following expression

$$\gamma_{\text{O}} = \begin{cases} (1 - p_{\text{O}_2}[\text{mTorr}])/4, & p_{\text{O}_2} < 2 \text{ mTorr} \\ 0.1438 \exp(2.5069/p_{\text{O}_2}[\text{mTorr}]), & \text{otherwise.} \end{cases} \quad (24)$$

2.6. Atomic energy transitions and radiative processes

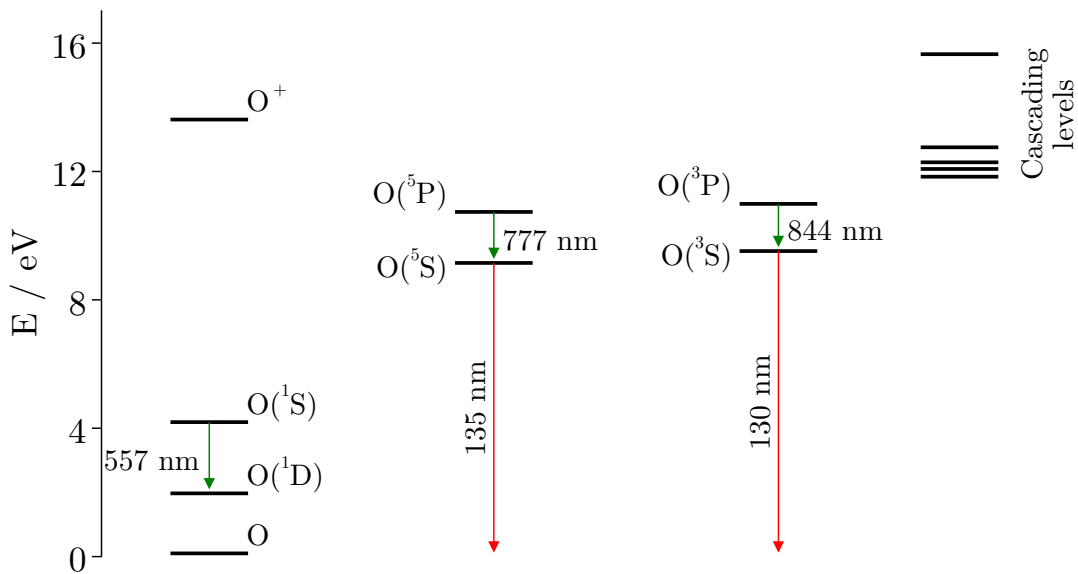


Figure 2: Energy diagram of atomic oxygen and radiative transitions taken into account in the numerical model. The cascading levels shown are only a representative subset of the existing high energy levels.⁶⁰ Figure adapted from Ref. 28.

Radiation processes from certain excited states when they decay to lower energy levels are included in the GM. The natural decay of excited species at energy level a to a lower energy level b emitting radiation at a wavelength λ_{ab} is a well-known physical phenomenon whose rates are described by Einstein coefficients for spontaneous emission. The radiative reactions included in the GM are sketched in figure 2 and listed in table 4.

The most important transitions for VUV emission are from the O(⁵S) and O(³S) states,

Table 4: Atomic transitions from state $a \rightarrow b$. λ_{ab} is the radiation wavelength, A_{ab} is the Einstein coefficient for spontaneous emission, g_a and g_b are the statistical weights of the a and b levels, respectively, and γ_{ab} is the escape factor.

#	Process	K_r [s ⁻¹]	λ_{ab} [nm]	A_{ab} [s ⁻¹]	g_p	g_k	Ref.
365	O(¹ S) \rightarrow O(¹ D)	$\gamma_{ab}A_{ab}$	557.7	1.26	1.0	5.0	28, 60
366	O(⁵ S) \rightarrow O	$0.5\gamma_{ab}A_{ab}$	135.6	$4.2 \cdot 10^3$	5.0	5.0	28, 60
367	O(⁵ S) \rightarrow O	$0.5\gamma_{ab}A_{ab}$	135.9	$1.4 \cdot 10^3$	5.0	3.0	28, 60
368	O(³ S) \rightarrow O	$0.33\gamma_{ab}A_{ab}$	130.2	$3.4 \cdot 10^8$	3.0	5.0	28, 60
369	O(³ S) \rightarrow O	$0.33\gamma_{ab}A_{ab}$	130.5	$2.0 \cdot 10^8$	3.0	3.0	28, 60
370	O(³ S) \rightarrow O	$0.33\gamma_{ab}A_{ab}$	130.6	$6.8 \cdot 10^7$	3.0	1.0	28, 60
371	O(⁵ P) \rightarrow O(⁵ S)	$0.47\gamma_{ab}A_{ab}$	777.2	$3.7 \cdot 10^7$	7.0	5.0	28, 60
372	O(⁵ P) \rightarrow O(⁵ S)	$0.33\gamma_{ab}A_{ab}$	777.4	$3.7 \cdot 10^7$	5.0	5.0	28, 60
373	O(⁵ P) \rightarrow O(⁵ S)	$0.2\gamma_{ab}A_{ab}$	777.5	$3.7 \cdot 10^7$	3.0	5.0	28, 60
374	O(³ P) \rightarrow O(³ S)	$0.11\gamma_{ab}A_{ab}$	844.6	$9.2 \cdot 10^7$	1.0	3.0	28, 60
375	O(³ P) \rightarrow O(³ S)	$0.56\gamma_{ab}A_{ab}$	844.6	$9.2 \cdot 10^7$	5.0	3.0	28, 60
376	O(³ P) \rightarrow O(³ S)	$0.33\gamma_{ab}A_{ab}$	844.7	$9.2 \cdot 10^7$	3.0	3.0	28, 60
377	Ar ^r \rightarrow Ar	A_{ab}		10^5			45, 61
378	Ar(4p) \rightarrow Ar	A_{ab}		$3.2 \cdot 10^7$			45, 62
379	Ar(4p) \rightarrow Ar ^m	A_{ab}		$3 \cdot 10^7$			45, 63
380	Ar(4p) \rightarrow Ar ^r	A_{ab}		$3 \cdot 10^7$			45, 63

as they emit photons at ~ 135 and ~ 130 nm when decaying to ground state. Other transitions between excited states of oxygen atoms defined in table 1, are included for completeness of the physical model. However, including all possible energy transitions would add significant complexity to the collisional radiative scheme, so instead, energy transitions at higher energy levels are simplified with so-called *cascade processes*.²⁸

Cascading processes gather several energy transition steps into one single reaction without needing to know the intermediate states. This usually includes electron impact excitation of O atoms, or dissociative excitation during electron collisions with O₂ molecules, that lead to the formation of high energy levels that subsequently decay to lower energy levels that are considered as species in the numerical model. The decay of

Table 5: Oxygen reactions with radiative cascading processes. The reaction rates are polynomials of the form $K_r(T_e) = a_0 + a_1T_e + a_2T_e^2 + a_3T_e^3 + a_4T_e^4$ where T_e is in eV.

#	Process	K_r [$10^{-17}\text{m}^3\text{s}^{-1}$]					Ref.
		a_0	a_1	a_2	a_3	a_4	
381	$e + \text{O} \rightarrow e + \text{O}(^5\text{S}) + \lambda_{777.5}$	-13.1	52.4	-65.4	29.3	-3.02	28, 49, 64 ^b
382	$e + \text{O}_2 \rightarrow e + 2\text{O} + \lambda_{130.4}$	-3.8	8.6	-6.5	1.9	-1.2	28, 49, 64
383	$e + \text{O}_2(\text{a}^1\Delta_u) \rightarrow e + 2\text{O} + \lambda_{130.4}$	-3.8	8.6	-6.5	1.9	-1.2	28, 49, 64 ^a
384	$e + \text{O}_2(\text{b}^1\Sigma_u^+) \rightarrow e + 2\text{O} + \lambda_{130.4}$	-3.8	8.6	-6.5	1.9	-1.2	28, 49, 64 ^a
385	$e + \text{O}_2 \rightarrow e + 2\text{O} + \lambda_{135.6}$	-9.20	21.2	-16.5	4.87	-0.331	28, 49, 64 ^b
386	$e + \text{O}_2(\text{a}^1\Delta_u) \rightarrow e + 2\text{O} + \lambda_{135.6}$	-9.20	21.2	-16.5	4.87	-0.331	28, 49, 64 ^{a,b}
387	$e + \text{O}_2(\text{b}^1\Sigma_u^+) \rightarrow e + 2\text{O} + \lambda_{135.6}$	-9.20	21.2	-16.5	4.87	-0.331	28, 49, 64 ^{a,b}
388	$e + \text{O}_2 \rightarrow e + \text{O} + \text{O}(^5\text{S}) + \lambda_{777.5}$	-2.91	6.40	-4.67	1.22	-0.0524	28, 49, 64 ^b
389	$e + \text{O}_2(\text{a}^1\Delta_u) \rightarrow e + \text{O} + \text{O}(^5\text{S}) + \lambda_{777.5}$	-2.91	6.40	-4.67	1.22	-0.0524	28, 49, 65 ^{a,b}
390	$e + \text{O}_2(\text{b}^1\Sigma_u^+) \rightarrow e + \text{O} + \text{O}(^5\text{S}) + \lambda_{777.5}$	-2.91	6.40	-4.67	1.22	-0.0524	28, 49, 65 ^{a,b}
391	$e + \text{O}_2 \rightarrow e + \text{O} + \text{O}(^3\text{S}) + \lambda_{844.6}$	-1.55	3.42	-2.51	0.658	-0.0284	28, 49, 65 ^b
392	$e + \text{O}_2(\text{a}^1\Delta_u) \rightarrow e + \text{O} + \text{O}(^3\text{S}) + \lambda_{844.6}$	-1.55	3.42	-2.51	0.658	-0.0284	28, 49, 65 ^{a,b}
393	$e + \text{O}_2(\text{b}^1\Sigma_u^+) \rightarrow e + \text{O} + \text{O}(^3\text{S}) + \lambda_{844.6}$	-1.55	3.42	-2.51	0.658	-0.0284	28, 49, 65 ^{a,b}

^a This reaction is given in Ref. 28 for electron collisions with ground state O₂ and is used here for electron collisions with excited states of O₂ with the same rate constant.

^b The constants were obtained from the polynomial fit to the data in the supplementary information in Ref. 49.

high energy levels may occur in a stepwise manner, called cascading, and modelling this using Einstein coefficients would add significant complexity to the species and chemistry schemes. The cascading processes incorporated to the GM are taken from Ref. 28 and are listed in table 5. These processes include atomic oxygen excitation to cascading levels that results in O(⁵S) and ~777 nm radiation, and dissociative excitation processes with O₂ that result in different excited oxygen atoms and radiation. Note that the dissociative excitation processes have been extended to all O₂ excited states included in the GM.

Self absorption of the emission line by the lower state of the given transition can be an important effect that has an impact on the population of the emitting species and the intensity of radiation leaving the plasma. Therefore it is important to account for this phenomena in the model. This is modelled by adding a so called escape factor γ_{ab} , as a correction to the Einstein coefficient for spontaneous emission. To do this, we follow the approach described in.²⁸ In general, the emission rate, K_{ab} , and intensity per

unit volume, I_{ab} for atomic transitions affected by self absorption are given by

$$K_{ab} = \gamma_{ab} A_{ab} \quad (25)$$

$$I_{ab} = K_{ab} n_a. \quad (26)$$

The definition of the escape factor used is the empirical formula given in 66

$$\gamma_{ab} = \frac{2 - \exp(-10^{-3} \kappa_{ab,0} R)}{1 + \kappa_{ab,0} R} \quad (27)$$

Under conditions where Doppler broadening is the dominant line broadening mechanism, as is the case for the low pressure conditions of interest in this work, the absorption coefficient at the centre of the emission line is given by⁶⁷

$$\kappa_{ab,0} = n_b A_{ab} \frac{g_p \lambda_{ab,0}^3}{g_b 8\pi} \sqrt{\frac{m_b}{2k_B T_b \pi}} \quad (28)$$

where $\lambda_{ab,0}$ is the central wavelength of the emission line.

As described in table 1, a number of the species considered in the model consist of grouped states. While the choice to group states whose energies are very similar is convenient for the plasma-chemical model, the fact that these states emit radiation at slightly different wavelengths needs to be accounted for to properly describe the line emission and self absorption. To do this, the density distribution of individual states within a grouped state needs to be estimated. For the wavelength ranges of interest in this work, two cases can be distinguished: (1) the upper state of the transition is represented in the model by a grouped state and the lower state is not and (2) the lower state is represented in the model by a grouped state and the upper state is not. The first case applies to emission around 777 nm (three emission lines, individual upper states: $2s^2 2p^3 ({}^3S^0) 3p {}^5P_{1,2,3}$, grouped state: O(5P)) and 844 nm (three emission lines individual upper states $2s^2 2p^3 ({}^3S^0) 3p {}^3P_{1,2,0}$, grouped state: O(3P)). The second case applies to emission around 130 (two emission lines individual lower states $2s^2 2p^4 {}^3P_{2,1}$, grouped state: O) and 135 nm (three emission lines, individual lower states $2s^2 2p^4$

³P_{2,1,0}, grouped state: O). We follow the approach used in 28 to estimate the densities of individual multiplet states within each grouped state. Here, the density of each multiplet level is estimated using the statistical weights of each level

$$n_m = \frac{g_m}{\sum_i g_{m_i}} n_g \quad (29)$$

where g_m are the statistical weights of each multiplet level within a grouped state with density n_g and $\sum_i g_{m_i}$ is the sum of the statistical weights of each multiplet level within the grouped state.

For emission around 777 and 844 nm, where the upper state is the grouped state, the densities of the individual upper states, n_a , used to calculate the emission intensity in equation 26 are determined using equation 29. On the other hand, for emission around 130 and 135 nm, where the lower state is the grouped state, the densities of the individual lower states, n_b required for the calculation of $\kappa_{ab,0}$ in equation 28 are determined by equation 29.

The small differences in emission wavelength of each multiplet are not relevant for the aims of the model and therefore, when presenting results, the emission intensities of the multiplet emission lines are added together. Specifically, the 135 nm emission line, I_{135} , is the sum of reactions #366 and 367 (in table 4), the 130 nm line, I_{130} , is the sum of reactions #367, 368 and 369, and the 777 nm line, I_{777} , is the sum of reactions #371-373.

3. Experimental setup

All experiments used for comparison to the simulation results were performed in a double inductively coupled plasma (DICP) reactor as depicted in figure 3. The reactor comprises a cylindrical stainless steel chamber, which is $L = 0.2$ m in height and $R = 0.2$ m in radius. Several flanges are attached at half-height to allow for characterisation

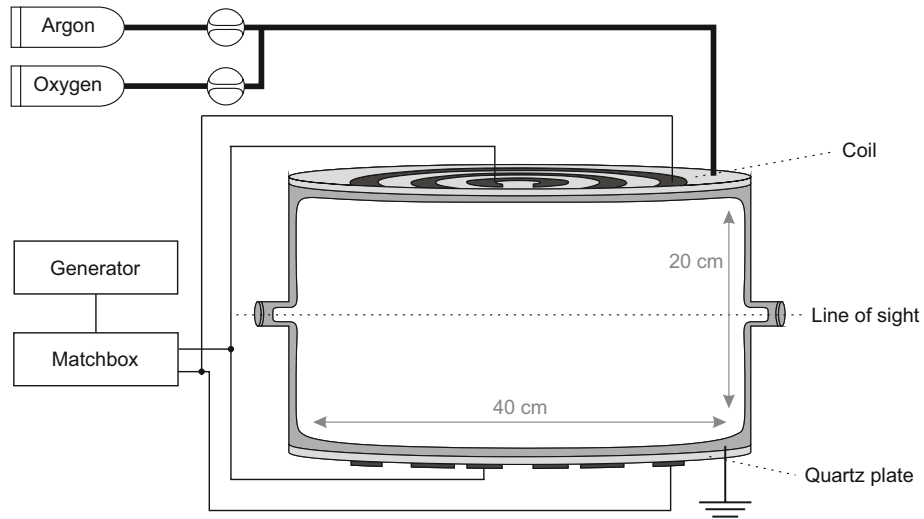


Figure 3: Schematic of the DICP used for experimental validation of the simulation results.

of plasma using optical and probe-based diagnostics. The top and bottom walls of the reactor consist of 20 mm thick quartz plates on which the inductive coils are mounted. The generator is equipped with a matching network and operates at a driving frequency of 13.56 MHz. Due to the reactor being powered from two sides, a relatively homogeneous plasma is obtained in the centre of the reactor. A more detailed description of the setup can be found elsewhere.^{28,68} For the experiments conducted in this work, a total gas flow of 100 sccm is kept constant for all measurements. The experiments include a variation in power from 200 W to 800 W, a variation in pressure from 2 Pa to 20 Pa and a variation of the oxygen content in the Ar/O₂ gas mixture from 0% to 20%.

Measurements of electron density are conducted using a multipole resonance probe (MRP). The MRP is based on active plasma resonance spectroscopy⁶⁹ and works by coupling an rf-signal into the plasma and measuring the response of the system. The rf-signal is varied in its bandwidth from the kHz to the GHz range, eventually inducing resonance of the electrons near the electron plasma frequency ω_{pe} . Using a mathematical model, the observed resonance can be correlated to electron density n_e and electron

temperature T_e .⁶⁹ Due to the MRP relying on electron resonance, it is well suited for applications involving deposition of insulators or reactive species such as oxygen, which can affect the performance of other probe-based diagnostics. The latter is of importance here due to Ar/O₂ gas mixture, which would lead to deterioration of e.g. the probe tip of a Langmuir probe and consequently have the potential to lead to measurement errors. A comparison between MRP and Langmuir probe measurements is given in Fiebrandt *et al* for the same setup.⁶⁸ More details on theory, operation and applications of the MRP can be found elsewhere.^{70–72} Measurements require a so-called “vacuum-trace”, which is a measurement performed without a plasma ignited for correction of conduction losses. This vacuum-trace is recorded separately for each measurement. For comparison with electron densities obtained from the GM, the probe is positioned in the centre of the setup at half-height for all measurements.

For observation of oxygen emission lines in the visible range, an echelle spectrometer ESA 4000 (LLA Instruments, Berlin) is used. The spectrometer records spectra in the range from $\lambda = 200$ nm to 800 nm and offers a resolution of between $\Delta\lambda = 0.015$ nm and 0.06 nm. For calculation of absolute emission intensities, the spectrometer is absolutely calibrated as described by Bibinov *et al*.⁷³ Measurements are performed line-of-sight integrated at half-height in front of a quartz window. The observed plasma volume is defined by an aperture mounted on the optical fibre (acceptance angle $\theta = 1.58^\circ$). Of particular interest with regards to comparing with the simulation results is the O(⁵P_{1,2,3}) → O(⁵S) transition, measured at 777 nm. By integrating the absolutely calibrated spectra over the emission lines from 777.07 nm to 777.65 nm, absolute intensities are obtained.

Tunable diode laser absorption spectroscopy (TDLAS) is performed to measure gas temperature and argon metastable densities. Specifically, the Ar(1s₅) metastable state

is measured using the Ar(1s₅ → 2p₆) transition at 772.376 nm. The system employed for the measurements consists of a laser head (DFB pro 100 mW, 772 nm + Fiberdock) and a laser controller (DLC pro). The laser beam traverses the plasma chamber in full diameter and is detected by a photodiode (Thorlabs DET10N2). In addition to a photodiode, a fraction of the laser power is coupled to a Fabry-Perot interferometer (Toptica FPI 100-750-3V0, 1 GHz free spectral range), allowing for monitoring of the change of the scanning laser wavelength. For each measurement point, four individual measurements are performed: (i) plasma on and laser on, (ii), plasma on and laser off, (iii), plasma off and laser on, (iv) plasma off and laser off. These four measurements are required for processing of the data. Gas temperatures and argon metastable densities are obtained by applying a Gaussian fit to the absorption profile. The gas temperature is calculated assuming that the line width, for the pressure range in this work, arises mainly from Doppler broadening, which can be directly related to the gas temperature. The calculation is performed by a semi-automatic LabVIEW software. The full setup of the TDLAS system and evaluation of the acquired data is described by Schulenberg *et al.*⁷⁴

4. Results

4.1. Characterization of Ar/O₂ DICP with numerical and experimental data

The influence of variations of total pressure p_T , power P_{in} and oxygen gas fraction χ_{O_2} on the plasma properties are presented. The total pressure is varied between $p_T = 2 - 20$ Pa the input power $P_{in} = 200 - 800$ W and the oxygen fraction $\chi_{O_2} = 0 - 0.20$. However, since the temperature of ions and neutrals, T_N , changes significantly under variations of p_T , P_{in} , and χ_{O_2} ,⁶⁸ and this is a fixed parameter in the GM, simulations are run with various values of T_N to ensure that variations of this parameter have been taken

into account in the final results. On the one hand, simulations have been performed varying T_N between 400 - 2000K in order to understand the impact of T_N on the plasma parameters. On the other hand, a second set of simulations has also been run using

Table 6: Neutral gas temperature experimental measurements, in K. The error shows the standard deviation obtained from three measurements for each operating condition.

χ_{O_2}	5 Pa			500 W		
	200 W	500 W	800 W	2 Pa	10 Pa	20 Pa
0.0	425±11	513± 8	569± 3	413±55	632± 5	787±12
0.04	567±11	657± 6	722±16	459± 5	680±10	780± 9
0.08	615±16	743±12	843±49	501± 8	675±31	446 ^a
0.12	626±36	801±10	862±10	538± 7	654±22	587±68 ^b
0.16	617±35	784±12	931±25	534± 7	661±12	
0.2	596± 7	793± 9	930± 1	526±22	726±22 ^b	

^a One valid measurement was taken.

^b Two valid measurements were taken.

values of T_N measured experimentally using TDLAS, listed in table 6, in order to better compare experiment and simulation. The results are compared with the experimental work described in section 3 and with results from Fiebrandt *et al* in 68, 75 and 28. The experimental work from Fiebrandt *et al* is conducted on the same plasma reactor and in similar operating conditions and thus its results are a useful reference. However, in the time since the earlier works of Fiebrandt *et al*, the reactor has undergone several changes including the replacement of the quartz plates separating the coils from the plasma. While these changes would not necessarily be expected to significantly affect the plasma properties, since the design of the reactor has not changed, the more recent measurements are generally not in exact agreement with the earlier data for otherwise identical operating conditions. This should also be kept in mind when interpreting the level of agreement between experiment and simulation. Therefore, the results presented in this section are not only used to provide a general characterization of Ar/O₂ plasmas

and its radiation behaviour of oxygen species, but also to validate the numerical results.

4.1.1. Electron density and temperature The electron density n_e , in figure 4, and temperature T_e , in figure 5, are the first parameters to evaluate the plasma results. The numerical results for n_e are compared with MRP measurements described in section 3 and also conducted in 75. Numerical results for T_e are compared with Langmuir probe data from 75.

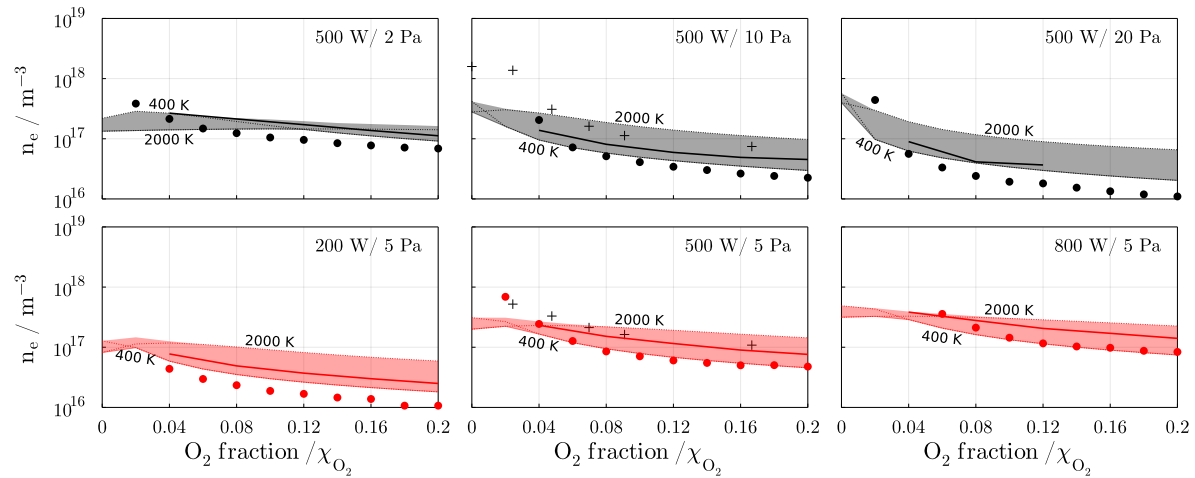


Figure 4: Electron density, n_e , for variations of p_T (top row), P_{in} (bottom row) and χ_{O_2} . Circle (●) markers are experimental data described in section 3, and + markers are experimental MRP results from 75. The shaded areas cover the model results when the neutral gas temperature, T_n , is varied between 400 and 2000 K (dotted lines). The solid lines are numerical results using the T_N experimental data listed in table 6.

First, n_e values are found between 10^{16} and 10^{18} m^{-3} and present decreasing trends with χ_{O_2} , as observed in 45, as well as with p_T . These trends are caused by a constant growth of dissociative attachment (reactions #25, 42 and 60 in table A1) acting as the main electron loss mechanism, while the main production mechanism transits from argon ionization (reaction #108 in table A2), dominant at low χ_{O_2} and p_T , to the recombination of O₂((a¹Δ_u) and O₂(b¹Σ_u⁺) with O₂⁻ (reactions #227 and 231 in table A3), and O with O⁻ (reaction #177 in table A3), at low χ_{O_2} and higher p_T ,

Besides, a positive trend in n_e with P_{in} is observed that is in line with the results

in 43. This is caused by a significant increase of argon ionization with increasing P_{in} .

The simulation results and experimental data are in good agreement with both showing similar trends for variations of p_T , P_{in} and χ_{O_2} . There is however a consistent difference between numerical and experimental results (circle markers), with the latter generally being slightly lower. A potential explanation for this may lie in the fact that the power defined for the simulation is that coupled into the plasma, that defined for the experiment is measured at the RF generator. It is generally well known that there can be significant differences between the power provided at the RF generator and the power coupled into the plasma in ICP systems.^{76–81} Since the electron density is strongly power dependent, any deviation between generator power and that coupled into the plasma would tend to decrease the experimentally measured electron density in comparison to the simulated electron density. However, since we are currently unable to characterise the power coupling efficiency in detail, the extent to which this effect can explain the differences between experiment and simulation is currently not known.

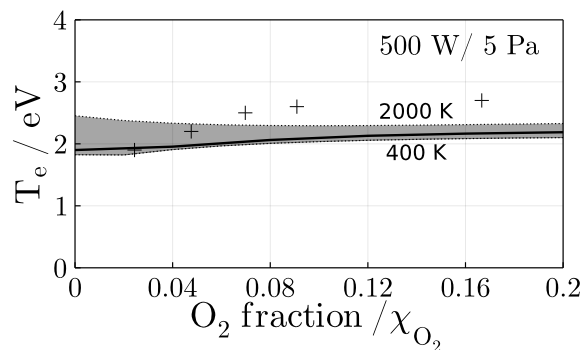


Figure 5: Electron temperature, T_e , for variations of O₂ fraction. The + markers are LP experimental results in 75. The shaded areas cover the model results when the neutral gas temperature, T_n , is varied between 400 and 2000 K (dotted lines). The solid lines are numerical results using the T_N experimental data listed in table 6.

The electron temperature data T_e , in figure 5, show values between approximately 2 and 3 eV for variations in χ_{O_2} . Both numerical and experimental values, show a slight positive trend that plateaus with increasing values of χ_{O_2} . The absolute T_e values

between experimental and numerical data differs less than 1 eV and therefore results are in reasonably good agreement. The assumption of a Maxwellian electron EDF, which does not hold for increasing χ_{O_2} ,^{19,43,75} is likely to be an important reason for the differences that do exist between experiment and simulation. While this is a weakness in the model formulation, the effect on the comparison between experimentally measured and simulated electron densities and temperatures is not severe for the cases compared here. A detailed study on the effects of the EDF shape on the properties of oxygen discharges for similar conditions has previously been carried out in 82. In general, EDFs of different shapes were found to change the absolute values of species densities and electron temperatures predicted by the global model used in that work, without strongly affecting the observed trends. Given this context and the n_e and T_e comparisons obtained here it can be concluded that the physics and chemistry modelled by the GM is as expected and is in good agreement with experimental work and previous literature.

4.1.2. Role of neutral gas temperature The variations of n_e and T_e caused by variations of T_N , shown in the figures by the shaded areas, are considerable but do not have a determining effect on the trends observed. The resulting plasma parameters remain within an order of magnitude for variations between 400 and 2000 K. Similar variations are observed for the other parameters described in this section, so it can be concluded that T_N has an important influence on the plasma properties, but does not have a strong influence on the qualitative trends presented in this work.

4.1.3. Neutral species densities With respect to neutral species densities, measured and simulated densities of Ar^m, n_{Ar^m} , and the O₂ dissociation fraction are compared.

In model, the species Ar^m represents an effective metastable state that includes the states Ar(1s₃) and Ar(1s₅).⁴⁵ However, the experimental measurements performed with

TDLAS, described in section 3, measure only the Ar(1s₅) state. Still, the comparison between the experimental and GM results is considered reasonable since the work performed in 68 with optical emission spectroscopy (OES), under similar operating conditions, infers the densities of both Ar(1s₃) and Ar(1s₅) states and shows that the former is typically an order of magnitude lower in density.

The results for n_{Ar^m} , in figure 6, show values between 10^{15} and 10^{17} m⁻³. The

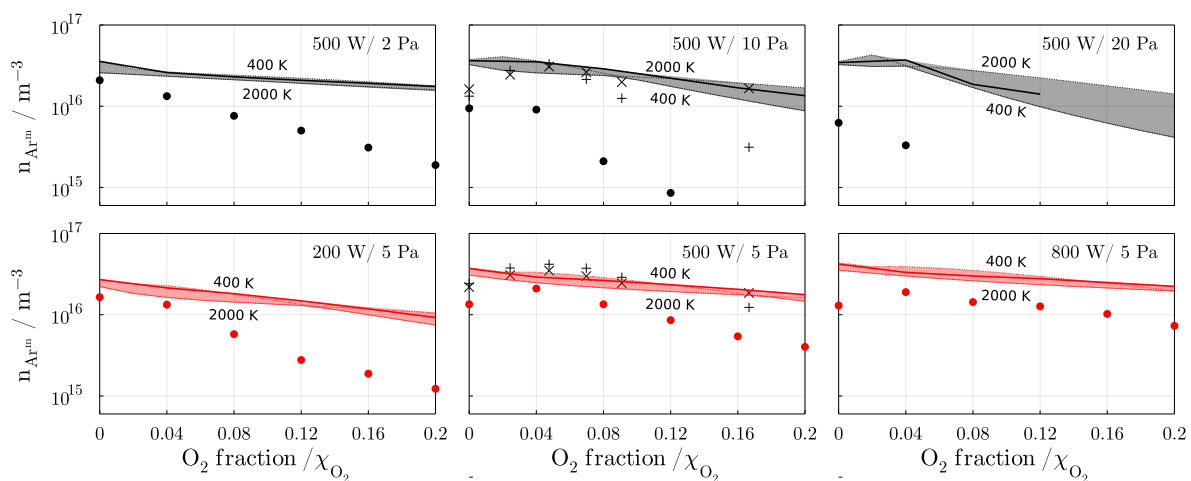


Figure 6: Ar^m density, n_{Ar^m} , for variations of p_T (top row), P_{in} (bottom row) and χ_{O_2} . Circle (●) markers are experimental TDLAS data described in section 3, + and × markers are TDLAS and OES results in 68, respectively. The shaded areas cover the model results when the neutral gas temperature, T_n , is varied between 400 and 2000 K (dotted lines). The solid lines are numerical results using the T_N experimental data listed in table 6. It should be noted that TDLAS measurements refer to the density of the Ar(1s₅) state, while the simulated densities and OES measurements represent an effective metastable state comprising the densities of both Ar(1s₃) and Ar(1s₅).

production of Ar^m is sustained by electron impact excitation from ground and radiative Ar^r states, reactions #109-110 and 123 in table A2 respectively, and the decay Ar(4p)→Ar^m, reaction #379 in table 4. These three reactions are of similar importance in the range of parameters studied. The loss mechanisms of Ar^m are dominated by electron impact collisions forming Ar^r and Ar(4p) (#116-117 in table A2), and the dissociation of O₂ by Ar^m impact (#276 and 282 in table A5), which is expected to be important when $\chi_{\text{O}_2} \rightarrow 1$,^{45,83-85} is only relevant for $P_{in} = 200$ W and $\chi_{\text{O}_2} \simeq 0.2$.

The GM results and the experimental measurements carried out in this work (circle markers) show reasonable agreement as they share similar trends and results are, mostly, within an order of magnitude in terms of absolute values. The differences between GM and experimental work become more pronounced for increasing p_T and χ_{O_2} . The reason for these divergences are not fully clear as there are many factors that could be involved, both from the experimental and the computational perspectives. On the experimental side, note that measurements carried out in 68 using TDLAS and OES, + and × markers respectively in figure 6, show better agreement with the GM results than the measurements done in this investigation. This may reflect changes in the experimental system between now and when the work of Fiebrandt was carried out, as discussed earlier. On the simulation side, the GM results are consistently above the experimental data, as also observed for n_e in figure 4, and therefore a discrepancy with the experimental data due to a non-unity inductive power coupling efficiency cannot be discarded.

Aside from comparing with experimental data, a series of simulations has also been carried out to compare with previous simulations of Ar excited state densities in Ar/O₂ plasmas with varying O₂ content.^{45,86} In general, very good agreement (not shown) is found in the excited state densities of Ar simulated in those previous works and using the GM developed here.

The oxygen dissociation percentage

$$\text{O}_2 \text{ diss. [\%]} = 100 \frac{\frac{1}{2}n_{\text{O}}^*}{\frac{1}{2}n_{\text{O}}^* + n_{\text{O}_2}^*}, \quad (30)$$

where n_{O}^* , and $n_{\text{O}_2}^*$, are the sum of all atomic, and molecular, oxygen species in table 1, reflecting the ratio between atomic and molecular oxygen present in the system. The dissociation percentage are shown in figure 7, where GM results are compared to the collisional-radiative model (CRM) results in 28. The CRM estimates volume averaged

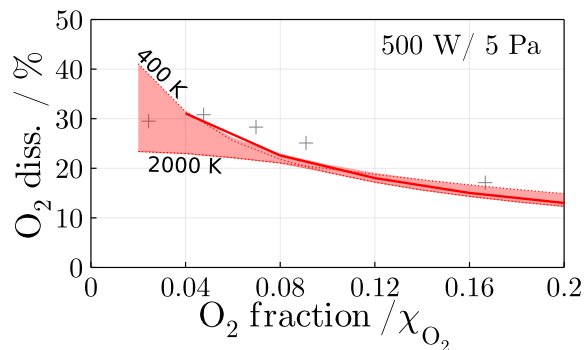


Figure 7: Oxygen dissociation percentage for variations of χ_{O_2} . The + markers are the collisional-radiative model results in 28. The shaded areas cover the model results when the neutral gas temperature, T_n , is varied between 400 and 2000 K (dotted lines). The solid lines are numerical results using the T_N experimental data listed in table 6.

atomic oxygen ground and excited state densities from experimental data. Both CRM and GM results are in good agreement, showing a decreasing trend for growing χ_{O_2} . This shows that GM results for the main oxygen species, i.e. the molecular and atomic species in the ground state, are computed as expected.

4.1.4. Oxygen radiation The simulation of radiation from oxygen species is tested with the 777 nm emission line, I_{777} , from the $\text{O}(^5\text{P}) \rightarrow \text{O}(^5\text{S})$ transition, and the VUV emission lines, $I_{\text{VUV}} = I_{130} + I_{135}$. The two most important VUV emission lines investigated are the 130 nm line, I_{130} , from the $\text{O}(^3\text{S}) \rightarrow \text{O}$ transition, and the 135 nm line, I_{135} , from the $\text{O}(^5\text{S}) \rightarrow \text{O}$ transition. These parameters are not only used to study the radiation of oxygen but also to verify the composition of excited states present in the gas.

The results for I_{777} , in figure 8, show emission intensities between 10^{19} and $10^{21} \text{ m}^{-3}\text{s}^{-1}$. The production of $\text{O}(^5\text{P})$ is mostly sustained by electron impact excitation from ground state (reaction #88 in table A1) and from $\text{O}(^5\text{S})$ (#99 in table A1), where the latter is more important when P_{in} is larger, p_T is lower, and/or $\chi_{\text{O}_2} \rightarrow 0$. The main loss mechanism of $\text{O}(^5\text{P})$ is the decay $\text{O}(^5\text{P}) \rightarrow \text{O}(^5\text{S})$ (#371-373 in table 4) that emits at

777 nm. Although O(⁵P) is directly responsible for the 777 nm line, the concentration of O(⁵S) is also important as it is closely related to the creation and destruction of O(⁵P). As expected, O(⁵S) is mainly created by electron impact excitation (reaction #86 in table A1) and the transition O(⁵P) → O(⁵S). However, the destruction of O(⁵S) is not only determined by electron impact excitation to O(³P), O(³S) and O(⁵P) but also by quenching with Ar, O and O₂. Quenching reactions become more important at increasing p_T and χ_{O_2} and are thus responsible for the decreasing trends with respect to these parameters.

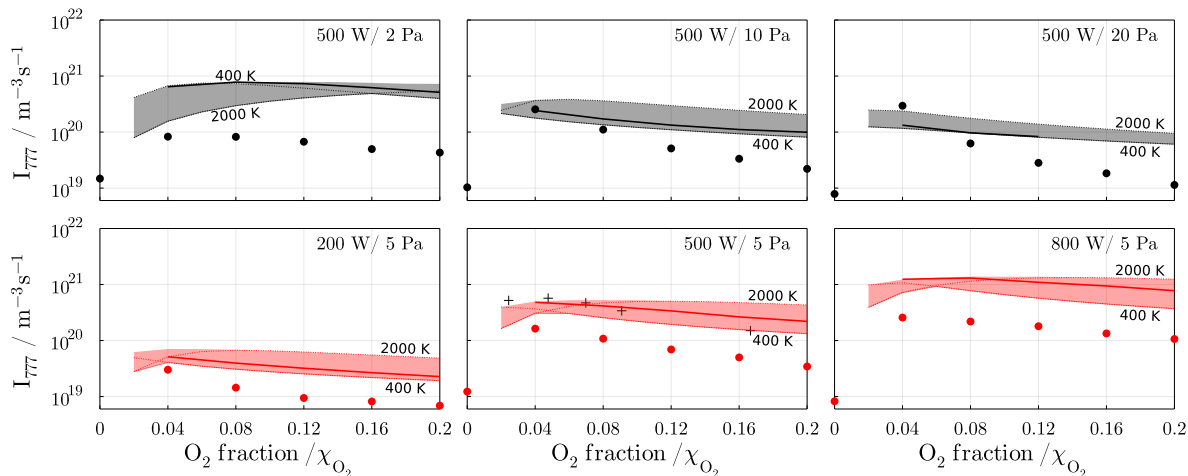


Figure 8: Emission intensity of the 777 nm line, from transition O(⁵P) → O(⁵S), for variations of p_T (top row), P_{in} (bottom row) and χ_{O_2} . Circle (●) markers are experimental spectrometer data described in section 3, and + spectrometer results in Refs. 14,28. The shaded areas cover the model results when the neutral gas temperature, T_n , is varied between 400 and 2000 K (dotted lines). The solid lines are numerical results using the T_N experimental data listed in table 6.

The results obtained with the GM are in reasonably good agreement with experimental measurements carried out in this work, as trends are similar and values differ less than an order of magnitude. The experimental data conducted in this investigation is systematically below the numerical data, and that of the previous work of Fiebrandt,^{14,28} as observed above for n_e and n_{Ar^m} . Although it is not yet clear what the cause of this difference is, the low power coupling efficiency could be an important factor

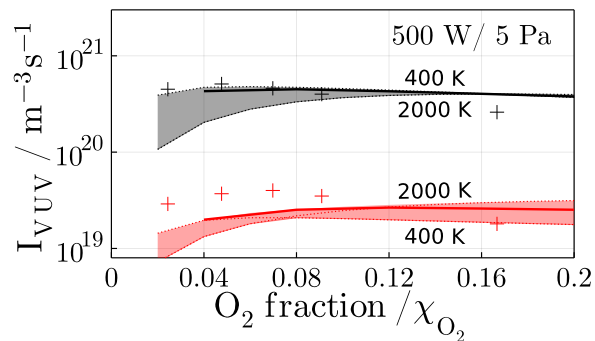


Figure 9: VUV emission intensities for variations of χ_{O_2} . In black, the 130 nm line transition $\text{O}(^3\text{S}) \rightarrow \text{O}$ and, in red, the 135 nm line transition $\text{O}(^5\text{S}) \rightarrow \text{O}$. The + markers are the results in 28. The shaded areas cover the model results when the neutral gas temperature, T_n , is varied between 400 and 2000 K (dotted lines). The solid lines are numerical results using the T_N experimental data listed in table 6.

to take into account, as the coupling efficiency decreases with low pressure and high power,⁷⁶ and this is in consistent with the observed differences between the experimental and numerical results. However, other factors must also be taken into account for the deviation between numerical and experimental data. Therefore, bearing in mind the simplifications made, the results of the GM are taken as acceptable.

The VUV emission results, shown in figure 9, show good agreement between the GM results and the experimental data in 28.. The 130 nm emission line, $I_{130} \sim 5 \cdot 10^{20} \text{m}^{-3} \text{s}^{-1}$, dominates the oxygen VUV radiation as it is an order of magnitude higher than the 135 nm line, $I_{135} \sim 5 \cdot 10^{19} \text{m}^{-3} \text{s}^{-1}$. For both emission lines, radiation comes from the natural decay of excited species, $\text{O}(^3\text{S}) \rightarrow \text{O}$ (reactions #368-370 in table 4) and $\text{O}(^5\text{S}) \rightarrow \text{O}$ (reactions #366-367 in table 4) respectively, and the contribution from cascading reactions (#382-387 in table 5) is negligible. This is in line with the description given in 27. Further analysis of oxygen VUV radiation is found in the following section.

4.2. Vacuum ultraviolet emission in oxygen species

After confirming that GM results are in good agreement with experimental reality, this second part of the results presents an extended numerical investigation of VUV radiation in Ar/O₂ plasmas. The results over a wider range of operating conditions, $P_T = 0.3$ -100 Pa and $p_T = 100$ -2000 W, are presented and analysed. The analysis of the results focuses on the VUV emission intensity of oxygen species, in absolute terms, I_{VUV} , but also with respect to the flux of ions, $\frac{V}{A}I_{VUV}/\Gamma_+$, and oxygen atoms, $I_{VUV}/R_{D,O}$, present in the DICP system, as these are quantities that are generally known to be important for the understanding and optimisation of various surface treatments.

4.2.1. Absolute VUV emission intensities The total VUV emission intensity from oxygen species, I_{VUV} , is shown in figure 10. These results show that, in general terms, the VUV radiation is higher at higher P_{in} and χ_{O_2} and finds a peak at a given range of p_T . This VUV peak with respect to p_T moves towards lower pressure values as the χ_{O_2} increases. The VUV emission, as noted in section 4.1.4 is dominated by the 130 nm line, specifically by the transition $O(^3S) \rightarrow O$.

The reaction pathways for the production of $O(^3S)$ species have been tracked to understand the most important source of oxygen VUV radiation. The main production mechanisms of $O(^3S)$ are electron impact excitation of atomic oxygen $e + O \rightarrow e + O(^3S)$ (reaction #87 in table A1), electron impact cross-excitation $e + O(^5S) \rightarrow e + O(^3S)$ (#98 in table A1), and the radiative decay $O(^3P) \rightarrow O(^3S)$ (#374-376 in table 4). The % of $O(^3S)$ produced by each of these reactions is shown in figure 11 for the case where $\chi_{O_2} = 0.1$. Interestingly, the most frequent production mechanism of $O(^3S)$ is via decay $O(^3P)$, about 60-70%, instead of the direct excitation through electron collision impact, 25-30%. This means that the most important oxygen VUV radiation mechanism is a three-step process that consist of i) electron impact excitation to $O(^3P)$ state, ii)

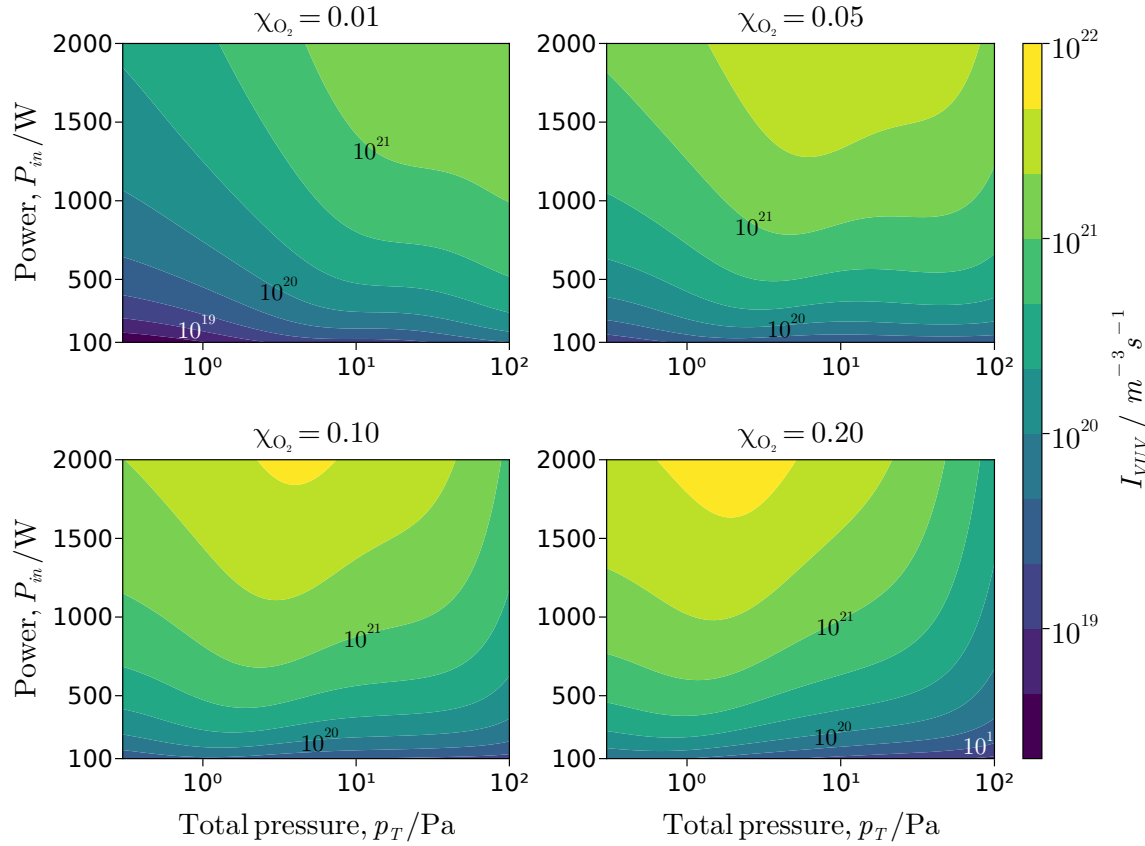


Figure 10: Absolute vacuum-ultraviolet (VUV) emission intensity, I_{VUV} , from oxygen species for variations of p_T , P_{in} , and χ_{O_2} .

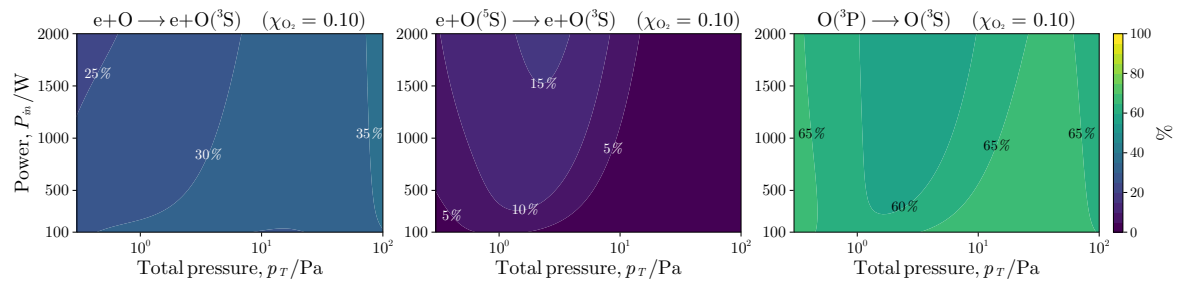


Figure 11: Most important O(³S) production processes as a % of the overall O(³S) production for $\chi_{O_2} = 0.1$.

radiative decay to O(³S), iii) radiative decay to ground state and photon emission at 130 nm.

In fact, the distribution of I_{VUV} in the (p_T, P_{in}) parameter space in figure 10, is determined by the density of O(³P). The reason for a peak in I_{VUV} is that electron

impact excitation from ground state (reactions #89-91 in table A1) dominates the production of O(³P), and n_e presents a peak in that pressure range which is consistent with the results presented in 82. With increasing p_T higher n_e are found. However, as the p_T increases further negative ion production, mainly O⁻, becomes more important at the expense of the electron population. Therefore at intermediate pressures, where electron impact ionization is large and negative ion production is relatively low, the electron density finds its maximum.

4.2.2. VUV emission to ion flux rate For some industrial processes it is of interest to know photon flux, $\frac{V}{A}I_{VUV}$, with respect to the ion fluxes reaching the reactor walls, Γ_+ , and therefore

$$r_{\Gamma_+} = \frac{\frac{V}{A}I_{VUV}}{\Gamma_+}, \quad (31)$$

is a useful parameter to evaluate VUV emission. Note that $\Gamma_+ = \sum_p \Gamma_p$ is the sum of the positive ion fluxes resulting from the reactions #344-348 (in table 2). This rate is shown in figure 12. The ion and VUV -photon fluxes are in the same order of magnitude and therefore it is possible to find operating conditions where either VUV emission dominates, $r_{\Gamma_+} \gg 1$, or ion fluxes dominates, $r_{\Gamma_+} \ll 1$.

The total positive ion flux, shown in figure 13, is strongly correlated with the plasma electronegativity $\alpha = n_-/n_e$ such that Γ_+ is largest when $\alpha \rightarrow 0$. In general terms at lower pressures, $p_T \leq 1$ Pa, Γ_+ is large and mostly dominated by Ar⁺, and for $p_T > 10$ Pa the electronegativity is large, $\alpha > 1$, and Γ_+ drops more than an order of magnitude. This pressure dependence of Γ_+ has a significant impact on r_{Γ_+} , such that, in general terms it grows with pressure. r_{Γ_+} becomes largest at high p_T and P_{in} as in these operating conditions I_{VUV} is maximum and Γ_+ drops significantly. With increasing χ_{O_2} the peak VUV intensity is displaced towards lower p_T , whereas Γ_+ does not change significantly, and therefore larger r_{Γ_+} values, close to unity, are already found

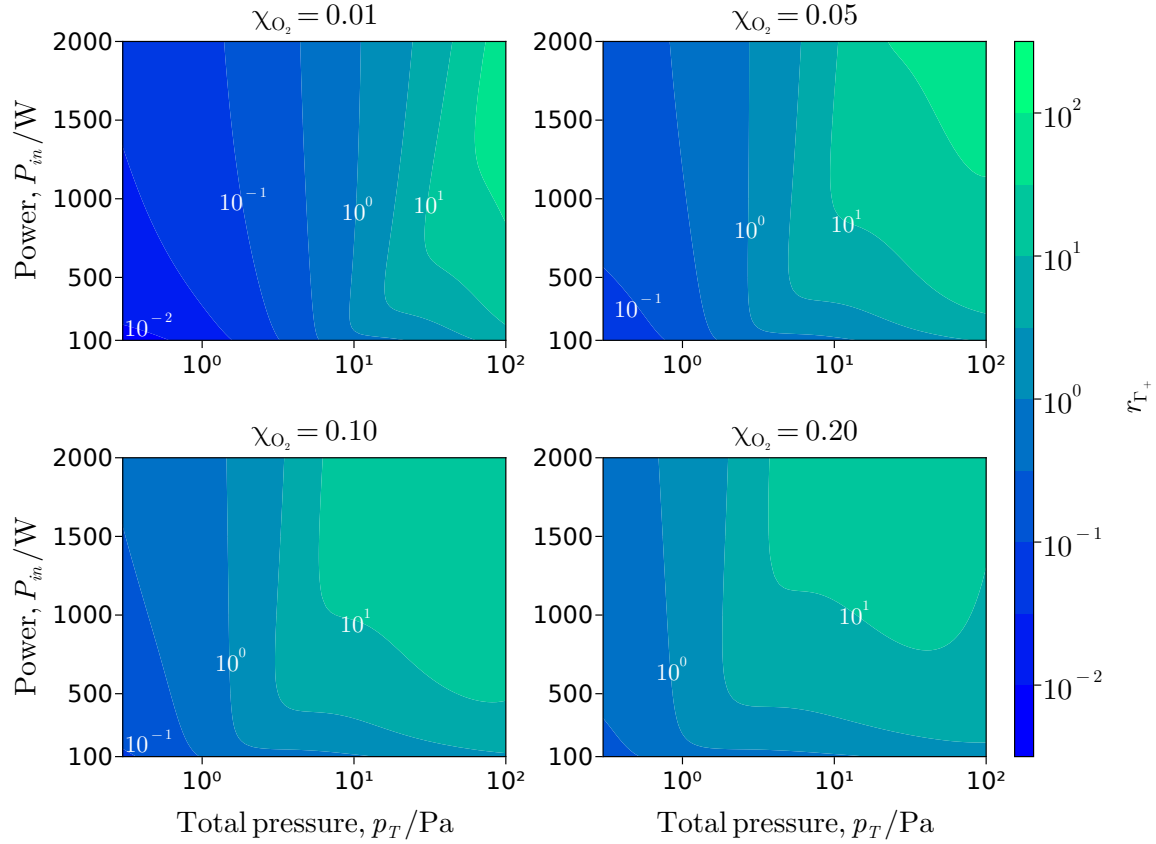


Figure 12: Vacuum-ultraviolet emission intensity to positive ion flux rate, r_{Γ^+} .

for $\chi_{\text{O}_2} \geq 0.1$ and $p_T \sim 1$ Pa.

4.2.3. *VUV emission to atomic oxygen diffusion to the wall* The ratio between I_{VUV} and atomic oxygen reaching the reactor walls may be of interest for industrial and biomedical applications as both oxygen radicals and VUV photons can readily interact with material leading to surface modifications. This ratio is defined as follow

$$r_{\text{O}} = \frac{I_{\text{VUV}}}{R_{D,\text{O}}}, \quad (32)$$

where $R_{D,\text{O}} = \sum_{\text{O}(X)} n_{\text{O}(X)} K_{D,\text{O}(X)}$ is the sum of neutral diffusion reaction rates of atomic oxygen species touching the walls, i.e. reactions #353-359 in table 3.

First, $R_{D,\text{O}}$ results are shown in figure 14. The flux of oxygen radicals to the wall due to diffusion is large, especially at $p_T > 10$ Pa and $P_{\text{in}} > 1000$ W and with increasing

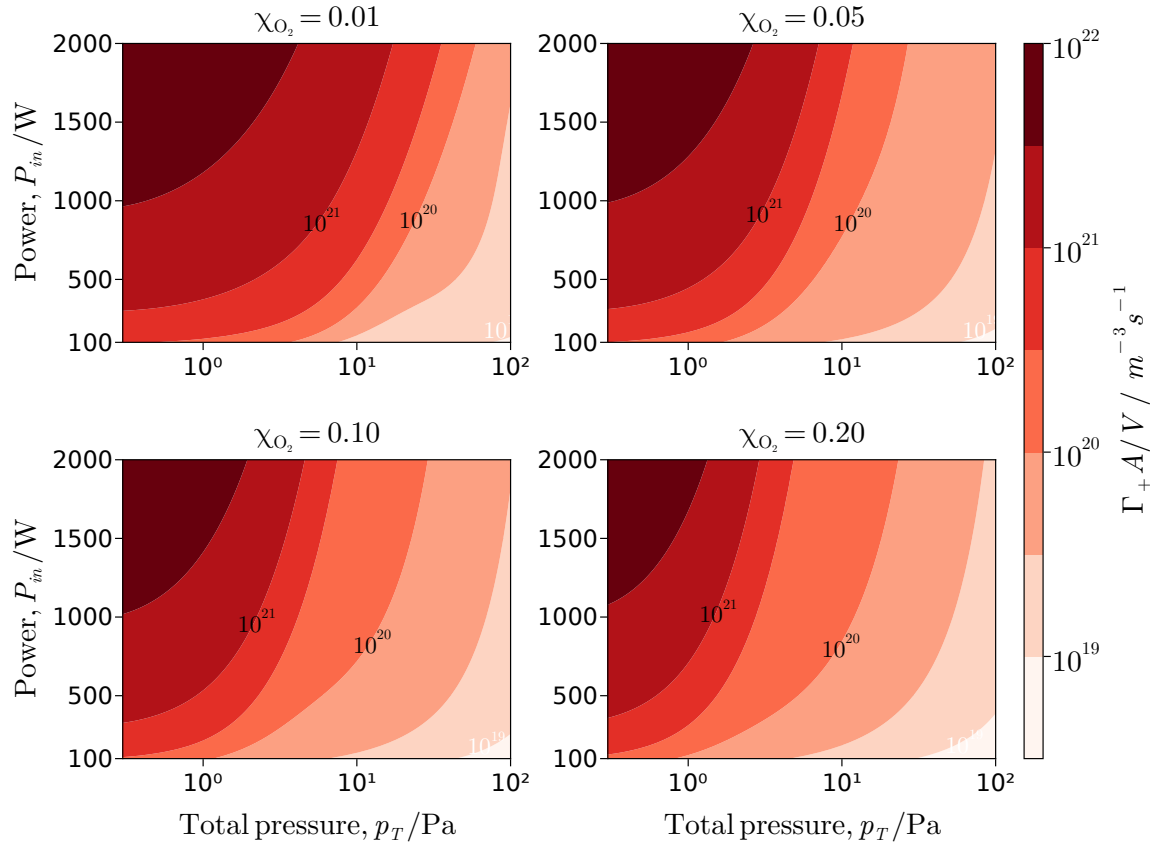


Figure 13: Total positive ion flux rate to the reactor walls.

χ_{O_2} . Only at very low pressure, < 0.6 Pa, these fluxes can be considered low. These trends correlate mainly with atomic oxygen density, which presents a similar distribution in the parameter space investigated.

The results for r_{O} are presented in figure 15. This data shows that I_{VUV} is always lower than $R_{D,\text{O}}$. The maximum values, $r_{\text{O}} \sim 0.4$, are found at minimum $p_T \sim 0.3$ Pa, and maximum power, $P_{in} \sim 2000$ W and decreases with increasing χ_{O_2} . The minimum values, $r_{\text{O}} \rightarrow 0$, are found in a larger region of high p_T and low p_T .

5. Summary

In this work we have conducted a numerical investigation of oxygen VUV emission in Ar/O₂ DICP. For this purpose we have developed a 0D plasma chemical-kinetics GM

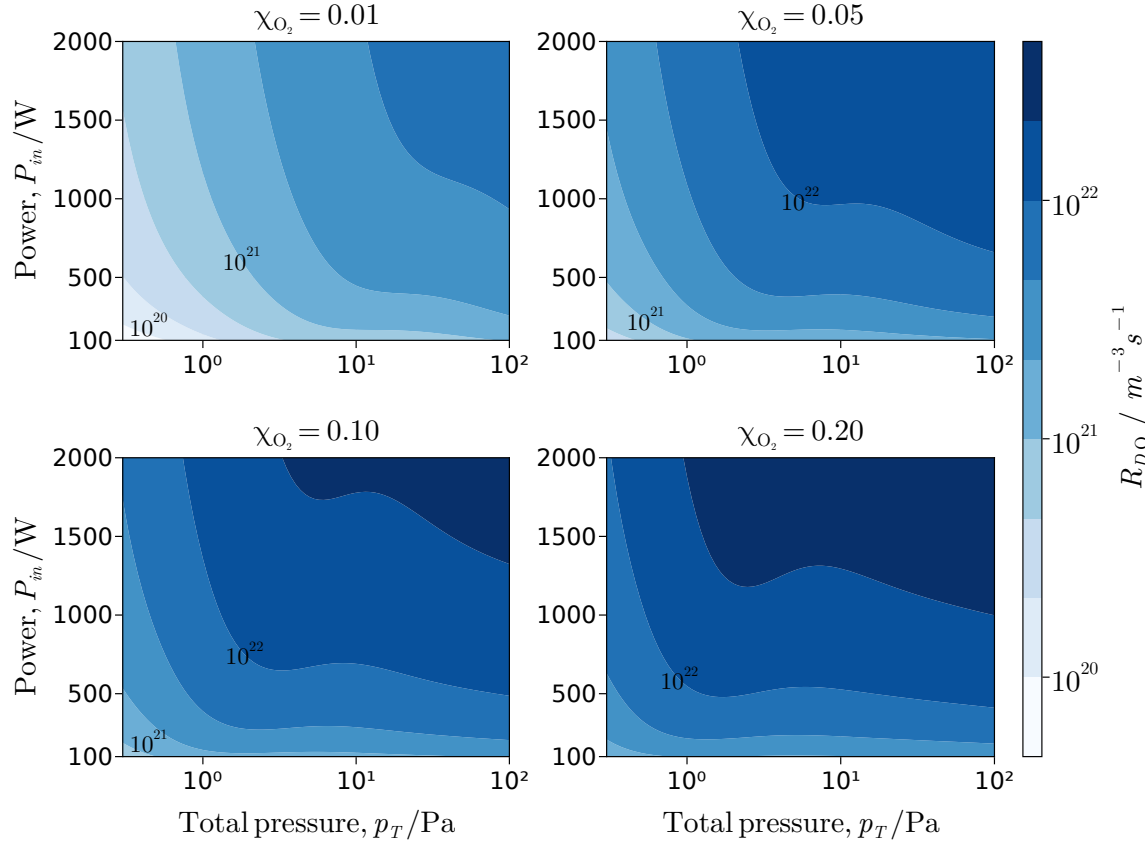


Figure 14: Atomic oxygen diffusion rate to the reactor walls.

that implements an extended chemical-radiative reaction scheme for Ar and O₂ species. The first part of the results investigates Ar/O₂ DICP for operating parameters between 200-800 W, 2-20 Pa and 0-0.20 O₂ fractions. Moreover, because the GM works with a fixed temperature T_N for neutrals and ions, T_N has also been varied between 400 and 2000 K to test the impact of T_N on the plasma results. The numerical results have been presented alongside experimental work conducted specifically for this investigation. The results show that the GM is performing correctly and that T_N does have an impact on the final results but within a relatively small range. The gas and plasma results, as well as the emission lines measured are as expected although some differences are observed for argon metastables. The source of these discrepancies is not yet clear, as they are not necessarily errors in the numerical method, and thus results are taken as valid. Oxygen

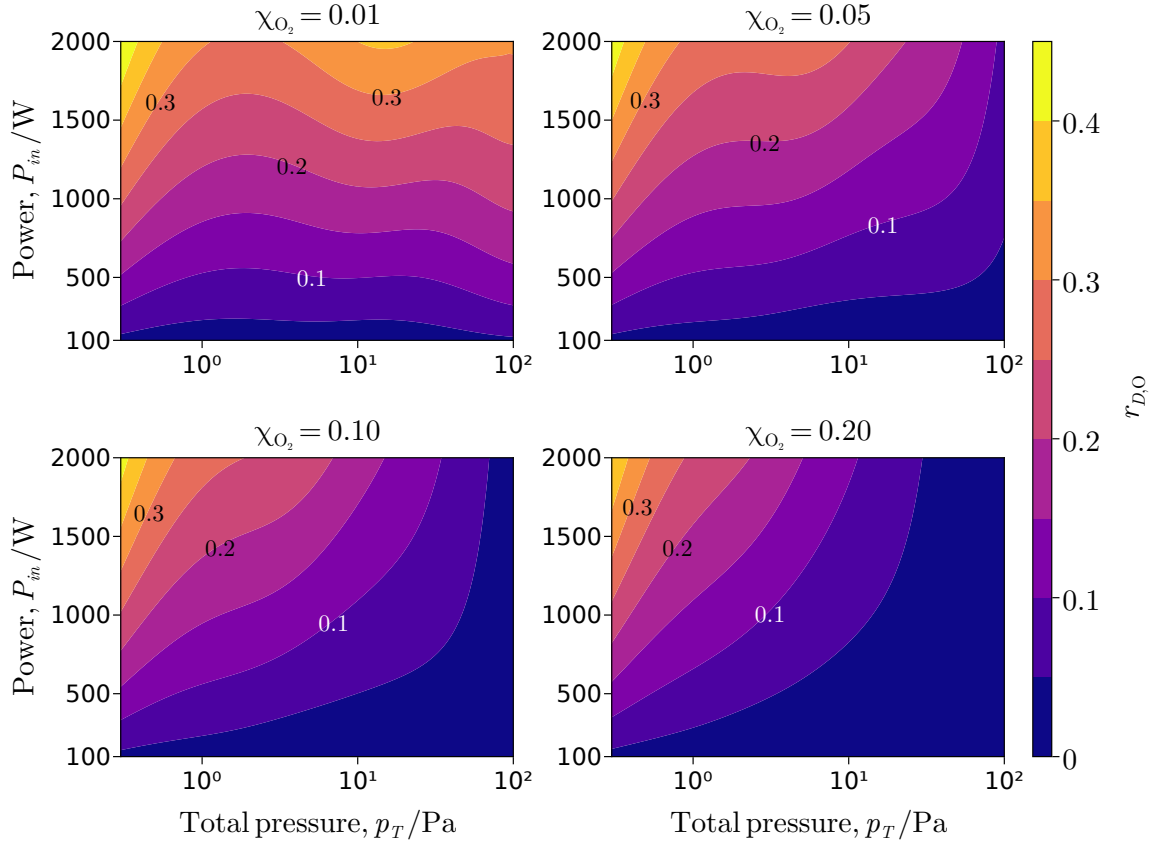


Figure 15: Vacuum-ultraviolet emission to atomic oxygen surface flux rate.

VUV emission results show good agreement, with the 130 nm line, from the $O(^3S) \rightarrow O$ transition, clearly dominating. The 135 nm line, from the $O(^5S) \rightarrow O$ transition, is an order of magnitude lower and emission from cascading reactions is negligible.

The second part of results investigates oxygen VUV emission over a broader range of total pressure and power. The GM results for plasmas with 0.3-100 Pa and 100-2000 W have shown that oxygen VUV emission, in general terms, increases within the investigated power and oxygen fraction and peak emission intensities are found for pressures between 5-50 Pa. The 130 nm line dominates for most of the parameter space investigated. Surprisingly the most frequent chemical pathway that generates $O(^3S)$ is not direct electron impact excitation from ground state, but excitation to $O(^3P)$ that then decays to $O(^3S)$.

Results of VUV emission intensities with respect to ion fluxes and oxygen diffusion to the reactor walls have also been presented. While VUV emission is largest with respect to ion fluxes at high pressures, oxygen diffusion is much larger than VUV emission for the parameter space investigated.

6. Acknowledgments

This project was undertaken on the Viking Cluster, which is a high performance computing facility provided by the University of York. We are grateful for computational support from the University of York High Performance Computing service, Viking and the Research Computing team. The authors wish to acknowledge financial support from the EPSRC Centre for Doctoral Training in Fusion Energy (EP/L01663X/1) and the UKRI Engineering and Physical Sciences. This has also been funded by the Deutsche Forschungsgemeinschaft (DFG, German Research Foundation) – project number 424927143. We also thank the team at House of Plasma GmbH for support in using the Multipole Resonance Probe.

References

- [1] Wang S B and Wendt A E 2001 *Journal of Vacuum Science & Technology A* **19** 2425–2432 ISSN 0734-2101 (Preprint https://pubs.aip.org/avs/jva/article-pdf/19/5/2425/7452738/2425_1_online.pdf) URL <https://doi.org/10.1116/1.1387056>
- [2] Athavale S D and Economou D J 1995 *Journal of Vacuum Science & Technology A* **13** 966–971 ISSN 0734-2101 (Preprint https://pubs.aip.org/avs/jva/article-pdf/13/3/966/11804066/966_1_online.pdf) URL <https://doi.org/10.1116/1.579659>
- [3] Schaepkens M, Oehrlein G S and Cook J M 2000 *Journal of Vacuum Science & Technology B: Microelectronics and Nanometer Structures Processing, Measurement, and Phenomena* **18** 848–855 ISSN 1071-1023 (Preprint https://pubs.aip.org/avs/jvb/article-pdf/18/2/848/8202100/848_1_online.pdf) URL <https://doi.org/10.1116/1.591285>
- [4] Barela M J, Anderson H M and Oehrlein G S 2005 *Journal of Vacuum Science & Technology A* **23** 408–416 ISSN 0734-2101 (Preprint https://pubs.aip.org/avs/jva/article-pdf/23/3/408/13968712/408_1_online.pdf) URL <https://doi.org/10.1116/1.1874173>
- [5] Banna S, Agarwal A, Tokashiki K, Cho H, Rauf S, Todorow V, Ramaswamy K, Collins K, Stout P, Lee J Y, Yoon J, Shin K, Choi S J, Cho H S, Kim H J, Lee C and Lymberopoulos D 2009 *IEEE Transactions on Plasma Science* **37** 1730–1746
- [6] Agarwal A, Stout P J, Banna S, Rauf S and Collins K 2011 *Journal of Vacuum Science & Technology A* **29** 011017 ISSN 0734-2101 (Preprint https://pubs.aip.org/avs/jva/article-pdf/doi/10.1116/1.3521315/15972238/011017_1_online.pdf) URL <https://doi.org/10.1116/1.3521315>
- [7] Diomede P, Economou D J and Donnelly V M 2011 *Journal of Applied Physics* **109** 083302 ISSN 0021-8979 (Preprint https://pubs.aip.org/aip/jap/article-pdf/doi/10.1063/1.3573488/14697695/083302_1_online.pdf) URL <https://doi.org/10.1063/1.3573488>
- [8] Fiebrandt M, Lackmann J W and Stapelmann K 2018 *Plasma Processes and Polymers* **15** 1800139 (Preprint <https://onlinelibrary.wiley.com/doi/pdf/10.1002/ppap.201800139>) URL <https://onlinelibrary.wiley.com/doi/abs/10.1002/ppap.201800139>
- [9] Abreu A C, Tavares R R, Borges A, Mergulhão F and Simões M 2013 *Journal of Antimicrobial Chemotherapy* **68** 2718–2732 ISSN 0305-7453 (Preprint <https://academic.oup.com/jac/article-pdf/68/12/2718/2055527/dkt281.pdf>) URL <https://doi.org/10.1093/jac/dkt281>

- [10] Gómez-López V M, Ragaert P, Debevere J and Devlieghere F 2008 *Critical Reviews in Food Science and Nutrition* **48** 487–495 PMID: 18568855 (Preprint <https://doi.org/10.1080/10408390701638878>) URL <https://doi.org/10.1080/10408390701638878>
- [11] Denis B, Steves S, Semmler E, Bibinov N, Novak W and Awakowicz P 2012 *Plasma Processes and Polymers* **9** 619–629 (Preprint <https://onlinelibrary.wiley.com/doi/pdf/10.1002/ppap.201100211>) URL <https://onlinelibrary.wiley.com/doi/abs/10.1002/ppap.201100211>
- [12] A F 2011 *Journal of Hospital Infection* **77**(3) 210–212
- [13] Siani H and Maillard J Y 2015 *European Journal of Clinical Microbiology & Infectious Diseases* **34** 1–11
- [14] Fiebrandt M, Hillebrand B, Lackmann J W, Raguse M, Moeller R, Awakowicz P and Stapelmann K 2018 *Journal of Physics D: Applied Physics* **51** 045401 URL <https://dx.doi.org/10.1088/1361-6463/aa9f0a>
- [15] Lerouge S, Fozza A C, Wertheimer M R, Marchand R and Yahia L 2000 *Plasmas and Polymers* **5** 31–46
- [16] Nest D, Graves D B, Engelmann S, Bruce R L, Weirnboeck F, Oehrlein G S, Andes C and Hudson E A 2008 *Applied Physics Letters* **92** 153113 ISSN 0003-6951 (Preprint https://pubs.aip.org/aip/apl/article-pdf/doi/10.1063/1.2912028/14393677/153113_1_online.pdf) URL <https://doi.org/10.1063/1.2912028>
- [17] Titus M J, Graves D B, Yamaguchi Y and Hudson E A 2011 *Journal of Physics D: Applied Physics* **44** 085204 URL <https://dx.doi.org/10.1088/0022-3727/44/8/085204>
- [18] Shin H, Zhu W, Donnelly V M and Economou D J 2012 *Journal of Vacuum Science & Technology A* **30** 021306 ISSN 0734-2101 (Preprint https://pubs.aip.org/avs/jva/article-pdf/doi/10.1116/1.3681285/15989562/021306_1_online.pdf) URL <https://doi.org/10.1116/1.3681285>
- [19] Lee H C, Hwang H J, Kim Y C, Kim J Y, Kim D H and Chung C W 2013 *Physics of Plasmas* **20** 033504 ISSN 1070-664X (Preprint https://pubs.aip.org/aip/pop/article-pdf/doi/10.1063/1.4794344/14797708/033504_1_online.pdf) URL <https://doi.org/10.1063/1.4794344>
- [20] Uchida S, Takashima S, Hori M, Fukasawa M, Ohshima K, Nagahata K and Tatsumi T 2008 *Journal of Applied Physics* **103** 073303 ISSN 0021-8979 (Preprint https://pubs.aip.org/aip/jap/article-pdf/doi/10.1063/1.2891787/15005554/073303_1_online.pdf) URL https://doi.org/10.1063/1.2891787/15005554/073303_1_online.pdf

[//doi.org/10.1063/1.2891787](https://doi.org/10.1063/1.2891787)

- [21] Tian P and Kushner M J 2015 *Plasma Sources Science and Technology* **24** 034017 URL <https://dx.doi.org/10.1088/0963-0252/24/3/034017>
- [22] Nakano T, Kumagai S and Samukawa S 2002 *Journal of Applied Physics* **92** 2990–2995 ISSN 0021-8979 (Preprint https://pubs.aip.org/aip/jap/article-pdf/92/6/2990/10622403/2990_1_online.pdf) URL <https://doi.org/10.1063/1.1501741>
- [23] Woodworth J R, Riley M E, Amatucci V A, Hamilton T W and Aragon B P 2001 *Journal of Vacuum Science & Technology A* **19** 45–55 (Preprint <https://doi.org/10.1116/1.1335685>) URL <https://doi.org/10.1116/1.1335685>
- [24] Jinnai B, Fukuda S, Ohtake H and Samukawa S 2010 *Journal of Applied Physics* **107** 043302 (Preprint <https://doi.org/10.1063/1.3313924>) URL <https://doi.org/10.1063/1.3313924>
- [25] Titus M J, Nest D G and Graves D B 2009 *Journal of Physics D: Applied Physics* **42**(15) 152001 ISSN 0022-3727 URL <https://iopscience.iop.org/article/10.1088/0022-3727/42/15/152001>
- [26] Boffard J B, Lin C C, Culver C, Wang S, Wendt A E, Radovanov S and Persing H 2014 *Journal of Vacuum Science & Technology A* **32** 021304 ISSN 0734-2101 (Preprint https://pubs.aip.org/avs/jva/article-pdf/doi/10.1116/1.4859376/13591302/021304_1_online.pdf) URL <https://doi.org/10.1116/1.4859376>
- [27] Boffard J B, Lin C C, Wang S, Wendt A E, Culver C, Radovanov S and Persing H 2014 *Journal of Vacuum Science & Technology A* **33** 021306 ISSN 0734-2101 (Preprint https://pubs.aip.org/avs/jva/article-pdf/doi/10.1116/1.4904036/15764486/021306_1_online.pdf) URL <https://doi.org/10.1116/1.4904036>
- [28] Fiebrandt M, Bibinov N and Awakowicz P 2020 *Plasma Sources Science and Technology* **29** 045018 URL <https://dx.doi.org/10.1088/1361-6595/ab7cbe>
- [29] Fantz U, Briefi S, Rauner D and Wunderlich D 2016 *Plasma Sources Science and Technology* **25** 045006 URL <https://dx.doi.org/10.1088/0963-0252/25/4/045006>
- [30] Wunderlich D, Briefi S, Friedl R and Fantz U 2021 *Review of Scientific Instruments* **92** 123510 ISSN 0034-6748 (Preprint https://pubs.aip.org/aip/rsi/article-pdf/doi/10.1063/5.0075491/16749716/123510_1_online.pdf) URL <https://doi.org/10.1063/5.0075491>
- [31] Tian P and Kushner M J 2017 *Plasma Sources Science and Technology* **26** 024005 URL

- <https://dx.doi.org/10.1088/1361-6595/26/2/024005>
- [32] Woodworth J R, Blain M G, Jarecki R L, Hamilton T W and Aragon B P 1999 *Journal of Vacuum Science & Technology A* **17** 3209–3217 (Preprint <https://doi.org/10.1116/1.582044>) URL <https://doi.org/10.1116/1.582044>
- [33] Cook J G, LeBrun L, Zhongming L and Ogryzlo E A 1995 *Journal of Applied Physics* **77** 1690–1695 ISSN 0021-8979 (Preprint https://pubs.aip.org/aip/jap/article-pdf/77/4/1690/8043375/1690_1_online.pdf) URL <https://doi.org/10.1063/1.358859>
- [34] Collart E J H, Baggerman J A G and Visser R J 1995 *Journal of Applied Physics* **78** 47–54 ISSN 0021-8979 (Preprint https://pubs.aip.org/aip/jap/article-pdf/78/1/47/10579037/47_1_online.pdf) URL <https://doi.org/10.1063/1.360630>
- [35] Korzec D, Schott M and Engemann J 1995 *Journal of Vacuum Science & Technology A* **13** 843–848 ISSN 0734-2101 (Preprint https://pubs.aip.org/avs/jva/article-pdf/13/3/843/11803594/843_1_online.pdf) URL <https://doi.org/10.1116/1.579839>
- [36] Kelly P and Arnell R 2000 *Vacuum* **56** 159–172 ISSN 0042-207X URL <https://www.sciencedirect.com/science/article/pii/S0042207X9900189X>
- [37] Depla D, Mahieu S and De Gryse R 2009 *Thin Solid Films* **517** 2825–2839 ISSN 0040-6090 URL <https://www.sciencedirect.com/science/article/pii/S0040609008015149>
- [38] Mitschker F, Dietrich J, Ozkaya B, de los Arcos T, Giner I, Awakowicz P and Grundmeier G 2015 *Plasma Processes and Polymers* **12** 1002–1009 (Preprint <https://onlinelibrary.wiley.com/doi/pdf/10.1002/ppap.201500085>) URL <https://onlinelibrary.wiley.com/doi/abs/10.1002/ppap.201500085>
- [39] Ries S, Bibinov N, Rudolph M, Schulze J, Mráz S, Schneider J M and Awakowicz P 2018 *Plasma Sources Science and Technology* **27** 094001 URL <https://dx.doi.org/10.1088/1361-6595/aad6d9>
- [40] Moisan, Michel, Boudam, Karim, Carignan, Denis, Kéroack, Danielle, Levif, Pierre, Barbeau, Jean, Séguin, Jacynthe, Kutasi, Kinga, Elmoualij, Benaïssa, Thellin, Olivier and Zorzi, Willy 2013 *Eur. Phys. J. Appl. Phys.* **63** 10001 URL <https://doi.org/10.1051/epjap/2013120510>
- [41] Hurlbatt A, Gibson A R, Schröter S, Bredin J, Foote A P S, Grondein P, O’Connell D and Gans T 2017 *Plasma Processes and Polymers* **14** 1600138 (Preprint <https://onlinelibrary.wiley.com/doi/pdf/10.1002/ppap.201600138>) URL <https://onlinelibrary.wiley.com/doi/abs/10.1002/ppap.201600138>

- [42] Lieberman M A and Lichtenberg A J 2005 *Particle and Energy Balance in Discharges* (John Wiley & Sons, Ltd) chap 10, pp 327–386 ISBN 9780471724254 (Preprint <https://onlinelibrary.wiley.com/doi/pdf/10.1002/0471724254.ch10>) URL <https://onlinelibrary.wiley.com/doi/abs/10.1002/0471724254.ch10>
- [43] Gudmundsson J T, Kimura T and Lieberman M A 1999 *Plasma Sources Science and Technology* **8**(1) 22–30 ISSN 0963-0252 URL <https://iopscience.iop.org/article/10.1088/0963-0252/8/1/003>
- [44] Gudmundsson J T, Marakhtanov A M, Patel K K, Gopinath V P and Lieberman M A 2000 *Journal of Physics D: Applied Physics* **33**(11) 1323–1331 ISSN 0022-3727 URL <https://iopscience.iop.org/article/10.1088/0022-3727/33/11/311>
- [45] Gudmundsson J T and Thorsteinsson E G 2007 *Plasma Sources Science and Technology* **16** 399 URL <https://dx.doi.org/10.1088/0963-0252/16/2/025>
- [46] Bezanson J, Edelman A, Karpinski S and Shah V B 2017 *SIAM Review* **59** 65–98 (Preprint <https://doi.org/10.1137/141000671>) URL <https://doi.org/10.1137/141000671>
- [47] Rackauckas C and Nie Q 2017 *Journal of Open Research Software* **5**
- [48] Turner M M 2015 *Plasma Sources Science and Technology* **24** 035027 URL <https://dx.doi.org/10.1088/0963-0252/24/3/035027>
- [49] Fiebrandt M, Awakowicz P, Brinkmann R P and Stapelmann K 2018 *Influence of photon energy and photon / particle fluxes on the inactivation efficiency of B. subtilis spores in low-pressure plasmas* Ph.D. thesis Fakultät für Elektrotechnik und Informationstechnik
- [50] Lieberman M A and Lichtenberg A J 2005 *Direct Current (DC) Sheaths* (John Wiley & Sons, Ltd) chap 6, pp 165–206 ISBN 9780471724254 (Preprint <https://onlinelibrary.wiley.com/doi/pdf/10.1002/0471724254.ch6>) URL <https://onlinelibrary.wiley.com/doi/abs/10.1002/0471724254.ch6>
- [51] Lieberman M A and Lichtenberg A J 2005 *Diffusion and Transport* (John Wiley & Sons, Ltd) chap 5, pp 133–163 ISBN 9780471724254 (Preprint <https://onlinelibrary.wiley.com/doi/pdf/10.1002/0471724254.ch5>) URL <https://onlinelibrary.wiley.com/doi/abs/10.1002/0471724254.ch5>
- [52] Thorsteinsson E G and Gudmundsson J T 2010 *Plasma Sources Science and Technology* **19** 055008 URL <https://dx.doi.org/10.1088/0963-0252/19/5/055008>
- [53] Lee C and Lieberman M A 1995 *Journal of Vacuum Science & Technology A* **13** 368–

- 380 ISSN 0734-2101 (*Preprint* https://pubs.aip.org/avs/jva/article-pdf/13/2/368/11935070/368_1_online.pdf) URL <https://doi.org/10.1116/1.579366>
- [54] Lieberman M A and Lichtenberg A J 2005 *Chemical Kinetics and Surface Processes* (John Wiley & Sons, Ltd) chap 9, pp 285–325 ISBN 9780471724254 (*Preprint* <https://onlinelibrary.wiley.com/doi/pdf/10.1002/0471724254.ch9>) URL <https://onlinelibrary.wiley.com/doi/abs/10.1002/0471724254.ch9>
- [55] Lieberman M A and Lichtenberg A J 2005 *Atomic Collisions* (John Wiley & Sons, Ltd) chap 3, pp 43–85 ISBN 9780471724254 (*Preprint* <https://onlinelibrary.wiley.com/doi/pdf/10.1002/0471724254.ch3>) URL <https://onlinelibrary.wiley.com/doi/abs/10.1002/0471724254.ch3>
- [56] Smirnov B M 1977 *Introduction to Plasma Physics* (Mir Publishers Moscow) chap Appendix I & II, pp 169–170 (*Preprint* <https://archive.org/embed/b.-m.-smirnov-introduction-to-plasma-physics-mir-1977>) URL <https://archive.org/embed/b.-m.-smirnov-introduction-to-plasma-physics-mir-1977>
- [57] Sharpless R L and Slanger T G 1989 *The Journal of Chemical Physics* **91** 7947–7950 ISSN 0021-9606 (*Preprint* https://pubs.aip.org/aip/jcp/article-pdf/91/12/7947/9730956/7947_1_online.pdf) URL <https://doi.org/10.1063/1.457211>
- [58] Chantry P J 1987 *Journal of Applied Physics* **62** 1141–1148
- [59] Booth J P and Sadeghi N 1991 *Journal of Applied Physics* **70** 611–620
- [60] Kramida A, Yu Ralchenko, Reader J and and NIST ASD Team 2022 NIST Atomic Spectra Database (ver. 5.10), [Online]. Available: <https://physics.nist.gov/asd> [2023, October 20]. National Institute of Standards and Technology, Gaithersburg, MD.
- [61] Hurst G S, Wagner E B and Payne M G 2003 *The Journal of Chemical Physics* **61** 3680–3685 ISSN 0021-9606 (*Preprint* https://pubs.aip.org/aip/jcp/article-pdf/61/9/3680/1144582/3680_1_online.pdf) URL <https://doi.org/10.1063/1.1682553>
- [62] Ashida S, Lee C and Lieberman M A 1995 *Journal of Vacuum Science & Technology A* **13** 2498–2507 ISSN 0734-2101 (*Preprint* https://pubs.aip.org/avs/jva/article-pdf/13/5/2498/11514434/2498_1_online.pdf) URL <https://doi.org/10.1116/1.579494>
- [63] Lee M H, Jang S H and Chung C W 2006 *Physics of Plasmas* **13** 053502 ISSN 1070-664X (*Preprint* https://pubs.aip.org/aip/pop/article-pdf/doi/10.1063/1.2193535/15799142/053502_1_online.pdf) URL <https://doi.org/10.1063/1.2193535>

- [64] Itikawa Y and Ichimura A 1990 *Journal of Physical and Chemical Reference Data* **19** 637–651 ISSN 0047-2689 (Preprint https://pubs.aip.org/aip/jpr/article-pdf/19/3/637/12060125/637_1_online.pdf) URL <https://doi.org/10.1063/1.555857>
- [65] McConkey J, Malone C, Johnson P, Winstead C, McKoy V and Kanik I 2008 *Physics Reports* **466** 1–103 ISSN 0370-1573 URL <https://www.sciencedirect.com/science/article/pii/S0370157308001488>
- [66] Mewe R 1967 *British Journal of Applied Physics* **18** 107
- [67] Holstein T 1947 *Phys. Rev.* **72**(12) 1212–1233 URL <https://link.aps.org/doi/10.1103/PhysRev.72.1212>
- [68] Fiebrandt M, Hillebrand B, Spiekermeier S, Bibinov N, Böke M and Awakowicz P 2017 *Journal of Physics D: Applied Physics* **50** 355202 URL <https://dx.doi.org/10.1088/1361-6463/aa7d67>
- [69] Lapke M, Oberrath J, Mussenbrock T and Brinkmann R P 2013 *Plasma Sources Science and Technology* **22** 025005 URL <https://dx.doi.org/10.1088/0963-0252/22/2/025005>
- [70] Lapke M, Oberrath J, Schulz C, Storch R, Styrnoll T, Zietz C, Awakowicz P, Brinkmann R P, Musch T, Mussenbrock T and Rolfes I 2011 *Plasma Sources Science and Technology* **20** 042001 URL <https://dx.doi.org/10.1088/0963-0252/20/4/042001>
- [71] Schulz C, Styrnoll T, Storch R, Awakowicz P, Musch T and Rolfes I 2014 *IEEE Sensors Journal* **14** 3408–3417
- [72] Pohle D, Schulz C, Oberberg M, Serwa A, Uhlig P, Awakowicz P and Rolfes I 2018 Progression of the multipole resonance probe: Advanced plasma sensors based on ltcc-technology 2018 48th *European Microwave Conference (EuMC)* pp 239–242
- [73] Bibinov N, Halfmann H, Awakowicz P and Wiesemann K 2007 *Measurement Science and Technology* **18** 1327 URL <https://dx.doi.org/10.1088/0957-0233/18/5/019>
- [74] Schulenberg D A, Korolov I, Donkó Z, Derzsi A and Schulze J 2021 *Plasma Sources Science and Technology* **30** 105003 URL <https://dx.doi.org/10.1088/1361-6595/ac2222>
- [75] Fiebrandt M, Oberberg M and Awakowicz P 2017 *Journal of Applied Physics* **122** 013302 ISSN 0021-8979 (Preprint https://pubs.aip.org/aip/jap/article-pdf/doi/10.1063/1.4991493/15194524/013302_1_online.pdf) URL <https://doi.org/10.1063/1.4991493>
- [76] Godyak V A 2011 *Plasma Sources Science and Technology* **20** 025004 URL <https://dx.doi.org/10.1088/0963-0252/20/2/025004>

- [77] Zielke D, Briefi S and Fantz U 2021 *Journal of Physics D: Applied Physics* **54** 155202 URL <https://dx.doi.org/10.1088/1361-6463/abd8ee>
- [78] Rauner D, Briefi S and Fantz U 2019 *Plasma Sources Science and Technology* **28** 095011 URL <https://dx.doi.org/10.1088/1361-6595/ab3d6a>
- [79] Elaissi S, Trabelsi A B G, Alkallas F H, Alrebdi T A and Charrada K 2022 *Materials* **15** ISSN 1996-1944 URL <https://www.mdpi.com/1996-1944/15/15/5213>
- [80] Rauner D, Mattei S, Briefi S, Fantz U, Hatayama A, Lettry J, Nishida K and Tran M Q 2017 *AIP Conference Proceedings* **1869** 030035 ISSN 0094-243X (Preprint https://pubs.aip.org/aip/acp/article-pdf/doi/10.1063/1.4995755/13750527/030035_1_online.pdf) URL <https://doi.org/10.1063/1.4995755>
- [81] Schwabedissen A, Benck E C and Roberts J R 1997 *Phys. Rev. E* **55**(3) 3450–3459 URL <https://link.aps.org/doi/10.1103/PhysRevE.55.3450>
- [82] Toneli D A, Pessoa R S, Roberto M and Gudmundsson J T 2015 *Journal of Physics D: Applied Physics* **48** 495203 URL <https://dx.doi.org/10.1088/0022-3727/48/49/495203>
- [83] Agarwal S, Quax G W W, van de Sanden M C M, Maroudas D and Aydil E S 2003 *Journal of Vacuum Science & Technology A* **22** 71–81 ISSN 0734-2101 (Preprint https://pubs.aip.org/avs/jva/article-pdf/22/1/71/7460668/71_1_online.pdf) URL <https://doi.org/10.1116/1.1627767>
- [84] Takechi K and Lieberman M A 2001 *Journal of Applied Physics* **90** 3205–3211 ISSN 0021-8979 (Preprint https://pubs.aip.org/aip/jap/article-pdf/90/7/3205/8059996/3205_1_online.pdf) URL <https://doi.org/10.1063/1.1398600>
- [85] Kitajima T, Nakano T and Makabe T 2006 *Applied Physics Letters* **88** 091501 ISSN 0003-6951 (Preprint https://pubs.aip.org/aip/apl/article-pdf/doi/10.1063/1.2180871/13350743/091501_1_online.pdf) URL <https://doi.org/10.1063/1.2180871>
- [86] Sato T and Makabe T 2008 *Journal of Physics D: Applied Physics* **41** 035211 URL <https://dx.doi.org/10.1088/0022-3727/41/3/035211>
- [87] Laher R R and Gilmore F R 1990 *Journal of Physical and Chemical Reference Data* **19** 277–305 ISSN 0047-2689 (Preprint https://pubs.aip.org/aip/jpr/article-pdf/19/1/277/11721454/277_1_online.pdf) URL <https://doi.org/10.1063/1.555872>
- [88] Deutsch H, Scheier P, Becker K and Märk T 2003 *Chemical Physics Letters* **382** 26–31 ISSN 0009-2614 URL <https://www.sciencedirect.com/science/article/pii/S0009261403017731>

- [89] Straub H C, Renault P, Lindsay B G, Smith K A and Stebbings R F 1996 *Phys. Rev. A* **54**(3) 2146–2153 URL <https://link.aps.org/doi/10.1103/PhysRevA.54.2146>
- [90] Lawton S A and Phelps A V 2008 *The Journal of Chemical Physics* **69** 1055–1068 ISSN 0021-9606 (*Preprint* https://pubs.aip.org/aip/jcp/article-pdf/69/3/1055/8133504/1055_1_online.pdf) URL <https://doi.org/10.1063/1.436700>
- [91] Tashiro M, Morokuma K and Tennyson J 2006 *Phys. Rev. A* **73**(5) 052707 URL <https://link.aps.org/doi/10.1103/PhysRevA.73.052707>
- [92] Jaffke T, Meinke M, Hashemi R, Christophorou L G and Illenberger E 1992 *Chemical Physics Letters* **193** 62–68 ISSN 0009-2614 URL <https://www.sciencedirect.com/science/article/pii/0009261492856832>
- [93] Hayashi D H D and Kadota K K K 1999 *Japanese Journal of Applied Physics* **38** 225 URL <https://dx.doi.org/10.1143/JJAP.38.225>
- [94] Deutsch H, Becker K, Probst M, Zhu W and Märk T 2008 *International Journal of Mass Spectrometry* **277** 151–154 ISSN 1387-3806 electron-induced atomic and molecular processes: A special issue honoring Eugen Illenberger on his 65th birthday URL <https://www.sciencedirect.com/science/article/pii/S1387380608001681>
- [95] Gupta M and Baluja K L 2005 *Journal of Physics B: Atomic, Molecular and Optical Physics* **38** 4057 URL <https://dx.doi.org/10.1088/0953-4075/38/22/010>
- [96] Rangwala S A, Kumar S V K, Krishnakumar E and Mason N J 1999 *Journal of Physics B: Atomic, Molecular and Optical Physics* **32** 3795 URL <https://dx.doi.org/10.1088/0953-4075/32/15/311>
- [97] Joshipura K N, Antony B K and Vinodkumar M 2002 *Journal of Physics B: Atomic, Molecular and Optical Physics* **35** 4211 URL <https://dx.doi.org/10.1088/0953-4075/35/20/308>
- [98] Zhaunerchyk V, Geppert W D, Österdahl F, Larsson M, Thomas R D, Bahati E, Bannister M E, Fogle M R and Vane C R 2008 *Phys. Rev. A* **77**(2) 022704 URL <https://link.aps.org/doi/10.1103/PhysRevA.77.022704>
- [99] Seiersen K, Bak J, Bluhme H, Jensen M J, Nielsen S B and Andersen L H 2003 *Phys. Chem. Chem. Phys.* **5**(21) 4814–4820 URL <http://dx.doi.org/10.1039/B309322K>
- [100] Flannery M 1996 *19960206 07C* 53
- [101] Bortner M and Baurer T 1978 *Space Div., General Electric Co.* **7**
- [102] Alge E, Adams N G and Smith D 1983 *Journal of Physics B: Atomic and Molecular Physics* **16**

- 1433 URL <https://dx.doi.org/10.1088/0022-3700/16/8/017>
- [103] Florescu-Mitchell A and Mitchell J 2006 *Physics Reports* **430** 277–374 ISSN 0370-1573 URL <https://www.sciencedirect.com/science/article/pii/S0370157306001463>
- [104] Queffelec J L, Rowe B R, Vallée F, Gomet J C and Morlais M 1989 *The Journal of Chemical Physics* **91** 5335–5342 ISSN 0021-9606 (Preprint https://pubs.aip.org/aip/jcp/article-pdf/91/9/5335/11163046/5335_1_online.pdf) URL <https://doi.org/10.1063/1.457582>
- [105] Dulaney J L, Biondi M A and Johnsen R 1988 *Phys. Rev. A* **37**(7) 2539–2542 URL <https://link.aps.org/doi/10.1103/PhysRevA.37.2539>
- [106] Gudmundsson J 2002 Notes on the electron excitation rate coefficients for argon and oxygen discharge-rh-21-2002 Tech. rep. Technical report, Science Institute-University of Iceland
- [107] Straub H C, Renault P, Lindsay B G, Smith K A and Stebbings R F 1995 *Phys. Rev. A* **52**(2) 1115–1124 URL <https://link.aps.org/doi/10.1103/PhysRevA.52.1115>
- [108] Tachibana K 1986 *Phys. Rev. A* **34**(2) 1007–1015 URL <https://link.aps.org/doi/10.1103/PhysRevA.34.1007>
- [109] Eggarter E 2008 *The Journal of Chemical Physics* **62** 833–847 ISSN 0021-9606 (Preprint https://pubs.aip.org/aip/jcp/article-pdf/62/3/833/11156575/833_1_online.pdf) URL <https://doi.org/10.1063/1.430534>
- [110] Kannari F, Obara M and Fujioka T 1985 *Journal of Applied Physics* **57** 4309–4322 ISSN 0021-8979 (Preprint https://pubs.aip.org/aip/jap/article-pdf/57/9/4309/7987701/4309_1_online.pdf) URL <https://doi.org/10.1063/1.334590>
- [111] Ferreira C M, Loureiro J and Ricard A 1985 *Journal of Applied Physics* **57** 82–90 ISSN 0021-8979 (Preprint https://pubs.aip.org/aip/jap/article-pdf/57/1/82/7985758/82_1_online.pdf) URL <https://doi.org/10.1063/1.335400>
- [112] Demore W B, Sander S P, Golden D M, Hampson R F, Kurylo M J, Howard C J, Ravishankara A R, Kolb C E and Molina M J 1992 *NASA Technical Report* **12** URL <https://www.osti.gov/biblio/6317172>
- [113] Slinger T G and Black G 1978 *The Journal of Chemical Physics* **68** 998–1000 ISSN 0021-9606 (Preprint https://pubs.aip.org/aip/jcp/article-pdf/68/3/998/11138866/998_1_online.pdf) URL <https://doi.org/10.1063/1.435839>
- [114] Niemi K, von der Gathen V S and Döbele H F 2005 *Plasma Sources Science and Technology* **14**

- 375 URL <https://dx.doi.org/10.1088/0963-0252/14/2/021>
- [115] Dagdigian P J, Forch B E and Miziolek A W 1988 *Chemical Physics Letters* **148** 299–308 ISSN 0009-2614 URL <https://www.sciencedirect.com/science/article/pii/0009261488872762>
- [116] Roth E P, Perner D and Dreyer J W 1973 *Zeitschrift für Naturforschung A* **28** 725–729 URL <https://doi.org/10.1515/zna-1973-0533>
- [117] Johnston H S 1968 *US Government Printing Office Washington, DC*
- [118] Rawlins W T, Caledonia G E and Armstrong R A 1987 *The Journal of Chemical Physics* **87** 5209–5221 ISSN 0021-9606 (Preprint https://pubs.aip.org/aip/jcp/article-pdf/87/9/5209/11285583/5209_1_online.pdf) URL <https://doi.org/10.1063/1.453689>
- [119] Slanger T G and Copeland R A 2003 *Chemical Reviews* **103** 4731–4766 pMID: 14664631 (Preprint <https://doi.org/10.1021/cr0205311>) URL <https://doi.org/10.1021/cr0205311>
- [120] Sobral J H A, Takahashi H, Abdu M A, Muralikrishna P, Sahai Y, Zamlutti C J, de Paula E R and Batista P P 1993 *Journal of Geophysical Research: Space Physics* **98** 7791–7798 (Preprint <https://agupubs.onlinelibrary.wiley.com/doi/pdf/10.1029/92JA01839>) URL <https://agupubs.onlinelibrary.wiley.com/doi/abs/10.1029/92JA01839>
- [121] Schofield K 1978 *Journal of Photochemistry* **9** 55–68 ISSN 0047-2670 URL <https://www.sciencedirect.com/science/article/pii/0047267078870063>
- [122] Sander S, Burkholder J, Abbatt J, Barker J, Cappa C, Crouse J, Dibble T, Huie R, Kolb C, Kurylo M, Orkin V, Percival C, Wilmouth D and Wine P 2011 *Technical Report Jet Propulsion Laboratory*
- [123] Atkinson R, Baulch D L, Cox R A, Crowley J N, Hampson R F, Hynes R G, Jenkin M E, Rossi M J and Troe J 2004 *Atmospheric Chemistry and Physics* **4** 1461–1738 URL <https://acp.copernicus.org/articles/4/1461/2004/>
- [124] Baulch D L, Cox R A, Hampson R F J, Kerr (Chairman) J A, Troe J and Watson R T 1984 *Journal of Physical and Chemical Reference Data* **13** 1259–1380 ISSN 0047-2689 (Preprint https://pubs.aip.org/aip/jpr/article-pdf/13/4/1259/9766232/1259_1_online.pdf) URL <https://doi.org/10.1063/1.555721>
- [125] Wine P H, Nicovich J M, Thompson R J and Ravishankara A R 1983 *The Journal of Physical Chemistry* **87** 3948–3954 (Preprint <https://doi.org/10.1021/j100243a030>) URL <https://doi.org/10.1021/j100243a030>

- [126] Steinfeld J I, Adler-Golden S M and Gallagher J W 1987 *Journal of Physical and Chemical Reference Data* **16** 911–951 ISSN 0047-2689 (Preprint https://pubs.aip.org/aip/jpr/article-pdf/16/4/911/11742557/911_1_online.pdf) URL <https://doi.org/10.1063/1.555796>
- [127] Kenner R and Ogryzlo E 1982 *Journal of Photochemistry* **18** 379–382 ISSN 0047-2670 URL <https://www.sciencedirect.com/science/article/pii/0047267082870275>
- [128] Slanger T G and Black G 1981 *The Journal of Chemical Physics* **75** 2247–2251 ISSN 0021-9606 (Preprint https://pubs.aip.org/aip/jcp/article-pdf/75/5/2247/11122784/2247_1_online.pdf) URL <https://doi.org/10.1063/1.442284>
- [129] Slanger T G and Black G 1981 *Geophysical Research Letters* **8** 535–538 (Preprint <https://agupubs.onlinelibrary.wiley.com/doi/pdf/10.1029/GL008i005p00535>) URL <https://agupubs.onlinelibrary.wiley.com/doi/abs/10.1029/GL008i005p00535>
- [130] Knickelbein M B, Marsh K L, Ulrich O E and Busch G E 1987 *The Journal of Chemical Physics* **87** 2392–2393 ISSN 0021-9606 (Preprint https://pubs.aip.org/aip/jcp/article-pdf/87/4/2392/11027225/2392_1_online.pdf) URL <https://doi.org/10.1063/1.453120>
- [131] Lilienfeld H V, Carr P A G and Hovis F E 1984 *The Journal of Chemical Physics* **81** 5730–5736 ISSN 0021-9606 (Preprint https://pubs.aip.org/aip/jcp/article-pdf/81/12/5730/14115120/5730_1_online.pdf) URL <https://doi.org/10.1063/1.447624>
- [132] Ard S G, Melko J J, Jiang B, Li Y, Shuman N S, Guo H and Viggiano A A 2013 *The Journal of Chemical Physics* **139** 144302 ISSN 0021-9606 (Preprint https://pubs.aip.org/aip/jcp/article-pdf/doi/10.1063/1.4824018/14784861/144302_1_online.pdf) URL <https://doi.org/10.1063/1.4824018>
- [133] Belostotsky S G, Economou D J, Lopaev D V and Rakhimova T V 2005 *Plasma Sources Science and Technology* **14** 532 URL <https://dx.doi.org/10.1088/0963-0252/14/3/016>
- [134] Ikezoe Y 1987 *Ion Reaction Research Group of the Mass Spectroscopy Society of Japan*
- [135] Eichelberger B R, Snow T P and Bierbaum V M 2003 *Journal of the American Society for Mass Spectrometry* **14** 501–505 PMID: 12745219 (Preprint [https://doi.org/10.1016/S1044-0305\(03\)00134-X](https://doi.org/10.1016/S1044-0305(03)00134-X)) URL [https://doi.org/10.1016/S1044-0305\(03\)00134-X](https://doi.org/10.1016/S1044-0305(03)00134-X)
- [136] Langevin M 1905 Une formule fondamentale de théorie cinétique *Annales de chimie et de physique, Series* vol 5 pp 245–288
- [137] Nesbet R K 1977 *Phys. Rev. A* **16**(1) 1–5 URL <https://link.aps.org/doi/10.1103/PhysRevA.>

16.1

- [138] Miller T M 2000 *CRC Handbook of Chemistry and Physics (Boca Raton, FL: CRC Press)* **77** 193–202
- [139] Anicich V G 1993 *Journal of Physical and Chemical Reference Data* **22** 1469–1569 ISSN 0047-2689 (Preprint https://pubs.aip.org/aip/jpr/article-pdf/22/6/1469/11008088/1469_1_online.pdf) URL <https://doi.org/10.1063/1.555940>
- [140] Midey A, Dotan I and Viggiano A A 2008 *The Journal of Physical Chemistry A* **112** 3040–3045 pMID: 18331008 (Preprint <https://doi.org/10.1021/jp710539s>) URL <https://doi.org/10.1021/jp710539s>
- [141] Lifshitz C, Wu R L C, Haartz J C and Tiernan T O 2008 *The Journal of Chemical Physics* **67** 2381–2382 ISSN 0021-9606 (Preprint https://pubs.aip.org/aip/jcp/article-pdf/67/5/2381/11003599/2381_1_online.pdf) URL <https://doi.org/10.1063/1.435078>
- [142] Böhringer H and Arnold F 1982 *The Journal of Chemical Physics* **77** 5534–5541 ISSN 0021-9606 (Preprint https://pubs.aip.org/aip/jcp/article-pdf/77/11/5534/11300773/5534_1_online.pdf) URL <https://doi.org/10.1063/1.443758>
- [143] de Petris G 2003 *Mass Spectrometry Reviews* **22** 251–271 (Preprint <https://analyticalsciencejournals.onlinelibrary.wiley.com/doi/pdf/10.1002/mas.10053>) URL <https://analyticalsciencejournals.onlinelibrary.wiley.com/doi/abs/10.1002/mas.10053>
- [144] Bassett N L and Economou D J 1994 *Journal of Applied Physics* **75** 1931–1939 ISSN 0021-8979 (Preprint https://pubs.aip.org/aip/jap/article-pdf/75/4/1931/10578546/1931_1_online.pdf) URL <https://doi.org/10.1063/1.356340>
- [145] King D L, Piper L G and Setser D W 1977 *J. Chem. Soc., Faraday Trans. 2* **73**(2) 177–200 URL <http://dx.doi.org/10.1039/F29777300177>
- [146] Midey A J and Viggiano A A 1998 *The Journal of Chemical Physics* **109** 5257–5263 ISSN 0021-9606 (Preprint https://pubs.aip.org/aip/jcp/article-pdf/109/13/5257/10792897/5257_1_online.pdf) URL <https://doi.org/10.1063/1.477142>
- [147] Gaucherel P and Rowe B 1977 *International Journal of Mass Spectrometry and Ion Physics* **25** 211–227 ISSN 0020-7381 URL <https://www.sciencedirect.com/science/article/pii/0020738177800508>
- [148] Velazco J E, Kolts J H and Setser D W 2008 *The Journal of Chemical Physics* **69** 4357–4373 ISSN

- 0021-9606 (Preprint https://pubs.aip.org/aip/jcp/article-pdf/69/10/4357/11140652/4357_1_online.pdf) URL <https://doi.org/10.1063/1.436447>
- [149] Balamuta J and Golde M F 1982 *The Journal of Physical Chemistry* **86** 2765–2769 (Preprint <https://doi.org/10.1021/j100211a041>) URL <https://doi.org/10.1021/j100211a041>
- [150] Piper L G, Clyne M A A and Monkhouse P B 1982 *J. Chem. Soc., Faraday Trans. 2* **78**(8) 1373–1382 URL <http://dx.doi.org/10.1039/F29827801373>
- [151] Piper L G 1974 *Chemical Physics Letters* **28** 276–279 ISSN 0009-2614 URL <https://www.sciencedirect.com/science/article/pii/0009261474800722>
- [152] Miller T M, Shuman N S and Viggiano A A 2012 *The Journal of Chemical Physics* **136** 204306 ISSN 0021-9606 (Preprint https://pubs.aip.org/aip/jcp/article-pdf/doi/10.1063/1.4720499/13887025/204306_1_online.pdf) URL <https://doi.org/10.1063/1.4720499>
- [153] Biondi M A 1969 *Canadian Journal of Chemistry* **47** 1711–1719 (Preprint <https://doi.org/10.1139/v69-282>) URL <https://doi.org/10.1139/v69-282>

Appendix A. Plasma-chemical reaction scheme

Please note that the rate coefficients for the reactions from 28, 49 were generated assuming a Maxwellian energy distribution function (EDF) for electrons with temperatures between 1.5 and 4 eV.

Table A1: Electron-oxygen reactions. Electron temperature, T_e , in eV and neutral temperature, T_N , in K. N_r is the number of reactants.

#	Reaction	E_{thr} [eV]	K_r [$\text{m}^{3+3(N_r-2)}\text{s}^{-1}$]	Ref.
1	$e + \text{O} \rightarrow 2e + \text{O}^+$	13.6	$4.93 \cdot 10^{-15} T_e^{0.723} \exp(-13.20/T_e)$	[48, reaction 12], 87
2	$e + \text{O} \rightarrow e + \text{O}(^1\text{D})$	1.96	$8.45 \cdot 10^{-15} T_e^{-0.306} \exp(-3.13/T_e)$	[48, reaction 13], 87
3	$e + \text{O} \rightarrow e + \text{O}(^1\text{S})$	4.18	$1.04 \cdot 10^{-15} T_e^{-0.134} \exp(-4.19/T_e)$	[48, reaction 14], 87
4	$e + \text{O}(^1\text{D}) \rightarrow 2e + \text{O}^+$	11.65	$4.93 \cdot 10^{-15} T_e^{0.723} \exp(-11.64/T_e)$	[48, reaction 15]
5	$e + \text{O}(^1\text{D}) \rightarrow e + \text{O}$	-1.96	$8.45 \cdot 10^{-15} T_e^{0.306} \exp(-1.17/T_e)$	[48, reaction 16], 87
6	$e + \text{O}(^1\text{S}) \rightarrow 2e + \text{O}^+$	9.43	$4.93 \cdot 10^{-15} T_e^{0.723} \exp(-9.42/T_e)$	[48, reaction 17]
7	$e + \text{O}(^1\text{S}) \rightarrow e + \text{O}$	-4.18	$1.04 \cdot 10^{-15} T_e^{-0.134} \exp(-0.73/T_e)$	[48, reaction 18], 87
8	$e + \text{O}^- \rightarrow 2e + \text{O}$	3.44	$9.33 \cdot 10^{-14} T_e^{0.178} \exp(-3.13/T_e)$	[48, reaction 19], 88
9	$e + \text{O}_2 \rightarrow 2e + \text{O} + \text{O}^+$	18.73	$8.60 \cdot 10^{-16} T_e^{1.110} \exp(-19.84/T_e)$	[48, reaction 20], 65, 89
10	$e + \text{O}_2 \rightarrow 2e + \text{O}_2^+$	12.06	$2.32 \cdot 10^{-15} T_e^{0.990} \exp(-12.51/T_e)$	[48, reaction 21], 65, 89
11	$e + \text{O}_2 \rightarrow e + \text{O} + \text{O}(^1\text{D})$	8.5	$3.12 \cdot 10^{-14} T_e^{0.017} \exp(-8.05/T_e)$	[48, reaction 22], 90
12	$e + \text{O}_2 \rightarrow e + \text{O} + \text{O}(^1\text{D})$	9.97	$1.56 \cdot 10^{-17} T_e^{1.500} \exp(-4.68/T_e)$	[48, reaction 23], 90
13	$e + \text{O}_2 \rightarrow e + \text{O}_2$	0.0	$4.15 \cdot 10^{-14} T_e^{0.599} \exp(-0.016/T_e)$	[48, reaction 24], 90
14	$e + \text{O}_2 \rightarrow e + \text{O}_2$	0.02	$3.88 \cdot 10^{-17} T_e^{-1.220} \exp(-0.55/T_e)$	[48, reaction 25], 90
15	$e + \text{O}_2 \rightarrow e + \text{O}_2$	0.19	$4.32 \cdot 10^{-16} T_e^{-1.570} \exp(-0.586/T_e)$	[48, reaction 26], 90
16	$e + \text{O}_2 \rightarrow e + \text{O}_2$	0.19	$2.76 \cdot 10^{-14} T_e^{-1.030} \exp(-6.96/T_e)$	[48, reaction 27], 90
17	$e + \text{O}_2 \rightarrow e + \text{O}_2$	0.57	$5.40 \cdot 10^{-15} T_e^{-0.916} \exp(-6.6/T_e)$	[48, reaction 28], 90
18	$e + \text{O}_2 \rightarrow e + \text{O}_2$	0.38	$1.64 \cdot 10^{-16} T_e^{-1.410} \exp(-0.723/T_e)$	[48, reaction 29], 90
19	$e + \text{O}_2 \rightarrow e + \text{O}_2$	0.38	$1.20 \cdot 10^{-14} T_e^{-1.015} \exp(-6.9/T_e)$	[48, reaction 30], 90
20	$e + \text{O}_2 \rightarrow e + \text{O}_2$	0.75	$5.27 \cdot 10^{-15} T_e^{-1.130} \exp(-7.57/T_e)$	[48, reaction 31], 90
21	$e + \text{O}_2 \rightarrow e + \text{O}_2(\text{a}^1\Delta_u)$	0.977	$2.10 \cdot 10^{-15} T_e^{-0.232} \exp(-2.87/T_e)$	[48, reaction 32], 90
22	$e + \text{O}_2 \rightarrow e + \text{O}_2(\text{b}^1\Sigma_u^+)$	1.627	$3.97 \cdot 10^{-16} T_e^{-0.089} \exp(-2.67/T_e)$	[48, reaction 33], 90
23	$e + \text{O}_2 \rightarrow e + \text{O}_2(\text{b}^1\Sigma_u^+)$	4.5	$1.28 \cdot 10^{-14} T_e^{-1.160} \exp(-7.00/T_e)$	[48, reaction 34], 90
24	$e + \text{O}_2 \rightarrow e + \text{O}_2(\text{b}^1\Sigma_u^+)$	6.0	$1.98 \cdot 10^{-14} T_e^{-0.779} \exp(-7.36/T_e)$	[48, reaction 35], 90
25	$e + \text{O}_2 \rightarrow \text{O} + \text{O}^-$	0.0	$1.32 \cdot 10^{-15} T_e^{-1.400} \exp(-1.40/T_e)$	[48, reaction 36], 90
26	$e + \text{O}_2(\text{a}^1\Delta_u) \rightarrow 2e + \text{O} + \text{O}^+$	17.75	$8.60 \cdot 10^{-16} T_e^{1.110} \exp(-18.86/T_e)$	[48, reaction 37]
27	$e + \text{O}_2(\text{a}^1\Delta_u) \rightarrow 2e + \text{O}_2^+$	11.08	$2.32 \cdot 10^{-15} T_e^{0.990} \exp(-11.53/T_e)$	[48, reaction 38]
28	$e + \text{O}_2(\text{a}^1\Delta_u) \rightarrow e + \text{O} + \text{O}(^1\text{D})$	7.52	$3.12 \cdot 10^{-14} T_e^{0.017} \exp(-7.07/T_e)$	[48, reaction 39]
29	$e + \text{O}_2(\text{a}^1\Delta_u) \rightarrow e + \text{O} + \text{O}(^1\text{D})$	9.0	$1.56 \cdot 10^{-17} T_e^{1.500} \exp(-3.70/T_e)$	[48, reaction 40]
30	$e + \text{O}_2(\text{a}^1\Delta_u) \rightarrow e + \text{O}_2$	-0.977	$2.10 \cdot 10^{-15} T_e^{-0.232} \exp(-1.89/T_e)$	[48, reaction 41], 90
31	$e + \text{O}_2(\text{a}^1\Delta_u) \rightarrow e + \text{O}_2(\text{a}^1\Delta_u)$	0.0	$4.15 \cdot 10^{-15} T_e^{0.599} \exp(-0.016/T_e)$	[48, reaction 42], 90, 91
32	$e + \text{O}_2(\text{a}^1\Delta_u) \rightarrow e + \text{O}_2(\text{a}^1\Delta_u)$	0.02	$3.88 \cdot 10^{-17} T_e^{-1.220} \exp(-0.55/T_e)$	[48, reaction 43]

Continuation of table A1: Electron-oxygen reactions.

#	Reaction	E_{thr} [eV]	K_r [$\text{m}^{3+3(N_r-2)}\text{s}^{-1}$]	Ref.
33	$e + \text{O}_2(\text{a}^1\Delta_u) \rightarrow e + \text{O}_2(\text{a}^1\Delta_u)$	0.19	$4.32 \cdot 10^{-16} T_e^{-1.570} \exp(-0.586/T_e)$	[48, reaction 44]
34	$e + \text{O}_2(\text{a}^1\Delta_u) \rightarrow e + \text{O}_2(\text{a}^1\Delta_u)$	0.19	$2.76 \cdot 10^{-14} T_e^{-1.030} \exp(-6.96/T_e)$	[48, reaction 45]
35	$e + \text{O}_2(\text{a}^1\Delta_u) \rightarrow e + \text{O}_2(\text{a}^1\Delta_u)$	0.38	$1.64 \cdot 10^{-16} T_e^{-1.410} \exp(-0.723/T_e)$	[48, reaction 46]
36	$e + \text{O}_2(\text{a}^1\Delta_u) \rightarrow e + \text{O}_2(\text{a}^1\Delta_u)$	0.38	$1.20 \cdot 10^{-15} T_e^{-1.015} \exp(-6.9/T_e)$	[48, reaction 47]
37	$e + \text{O}_2(\text{a}^1\Delta_u) \rightarrow e + \text{O}_2(\text{a}^1\Delta_u)$	0.57	$5.40 \cdot 10^{-15} T_e^{-0.916} \exp(-6.6/T_e)$	[48, reaction 48]
38	$e + \text{O}_2(\text{a}^1\Delta_u) \rightarrow e + \text{O}_2(\text{a}^1\Delta_u)$	0.75	$5.27 \cdot 10^{-15} T_e^{-1.130} \exp(-7.57/T_e)$	[48, reaction 49]
39	$e + \text{O}_2(\text{a}^1\Delta_u) \rightarrow e + \text{O}_2(\text{b}^1\Sigma_u^+)$	0.657	$5.25 \cdot 10^{-15} T_e^{-0.440} \exp(-1.49/T_e)$	[48, reaction 50], 91
40	$e + \text{O}_2(\text{a}^1\Delta_u) \rightarrow e + \text{O}_2(\text{b}^1\Sigma_u^+)$	3.52	$1.28 \cdot 10^{-14} T_e^{-1.160} \exp(-6.02/T_e)$	[48, reaction 51]
41	$e + \text{O}_2(\text{a}^1\Delta_u) \rightarrow e + \text{O}_2(\text{b}^1\Sigma_u^+)$	5.02	$1.98 \cdot 10^{-14} T_e^{-0.779} \exp(-6.38/T_e)$	[48, reaction 52]
42	$e + \text{O}_2(\text{a}^1\Delta_u) \rightarrow \text{O} + \text{O}^-$	3.0	$4.14 \cdot 10^{-15} T_e^{-1.340} \exp(-5.15/T_e)$	[48, reaction 53], 92
43	$e + \text{O}_2(\text{a}^1\Delta_u) \rightarrow \text{O}({}^1\text{D}) + \text{O}^-$	3.0	$9.20 \cdot 10^{-16} T_e^{-1.260} \exp(-6.55/T_e)$	[48, reaction 54], 92
44	$e + \text{O}_2(\text{b}^1\Sigma_u^+) \rightarrow 2e + \text{O} + \text{O}^+$	17.1	$8.60 \cdot 10^{-16} T_e^{1.110} \exp(-18.21/T_e)$	[48, reaction 55]
45	$e + \text{O}_2(\text{b}^1\Sigma_u^+) \rightarrow 2e + \text{O}_2^+$	10.43	$2.32 \cdot 10^{-15} T_e^{0.990} \exp(-10.88/T_e)$	[48, reaction 56]
46	$e + \text{O}_2(\text{b}^1\Sigma_u^+) \rightarrow e + \text{O} + \text{O}({}^1\text{D})$	6.87	$3.12 \cdot 10^{-14} T_e^{0.017} \exp(-6.42/T_e)$	[48, reaction 57]
47	$e + \text{O}_2(\text{b}^1\Sigma_u^+) \rightarrow e + \text{O} + \text{O}({}^1\text{D})$	8.34	$1.56 \cdot 10^{-17} T_e^{1.500} \exp(-3.05/T_e)$	[48, reaction 58]
48	$e + \text{O}_2(\text{b}^1\Sigma_u^+) \rightarrow e + \text{O}_2$	-1.627	$3.97 \cdot 10^{-16} T_e^{-0.089} \exp(-1.04/T_e)$	[48, reaction 59], 90
49	$e + \text{O}_2(\text{b}^1\Sigma_u^+) \rightarrow e + \text{O}_2(\text{a}^1\Delta_u)$	-0.657	$5.25 \cdot 10^{-15} T_e^{-0.440} \exp(-0.833/T_e)$	[48, reaction 60], 91
50	$e + \text{O}_2(\text{b}^1\Sigma_u^+) \rightarrow e + \text{O}_2(\text{b}^1\Sigma_u^+)$	0.0	$4.15 \cdot 10^{-14} T_e^{0.599} \exp(-0.016/T_e)$	[48, reaction 61], 90, 91
51	$e + \text{O}_2(\text{b}^1\Sigma_u^+) \rightarrow e + \text{O}_2(\text{b}^1\Sigma_u^+)$	0.02	$3.88 \cdot 10^{-17} T_e^{-1.220} \exp(-0.55/T_e)$	[48, reaction 62]
52	$e + \text{O}_2(\text{b}^1\Sigma_u^+) \rightarrow e + \text{O}_2(\text{b}^1\Sigma_u^+)$	0.19	$4.32 \cdot 10^{-16} T_e^{-1.570} \exp(-0.586/T_e)$	[48, reaction 63]
53	$e + \text{O}_2(\text{b}^1\Sigma_u^+) \rightarrow e + \text{O}_2(\text{b}^1\Sigma_u^+)$	0.19	$2.76 \cdot 10^{-14} T_e^{-1.030} \exp(-6.96/T_e)$	[48, reaction 64]
54	$e + \text{O}_2(\text{b}^1\Sigma_u^+) \rightarrow e + \text{O}_2(\text{b}^1\Sigma_u^+)$	0.38	$1.64 \cdot 10^{-16} T_e^{-1.410} \exp(-0.723/T_e)$	[48, reaction 65]
55	$e + \text{O}_2(\text{b}^1\Sigma_u^+) \rightarrow e + \text{O}_2(\text{b}^1\Sigma_u^+)$	0.38	$1.20 \cdot 10^{-15} T_e^{-1.015} \exp(-6.9/T_e)$	[48, reaction 66]
56	$e + \text{O}_2(\text{b}^1\Sigma_u^+) \rightarrow e + \text{O}_2(\text{b}^1\Sigma_u^+)$	0.57	$5.40 \cdot 10^{-15} T_e^{-0.916} \exp(-6.6/T_e)$	[48, reaction 67]
57	$e + \text{O}_2(\text{b}^1\Sigma_u^+) \rightarrow e + \text{O}_2(\text{b}^1\Sigma_u^+)$	0.75	$5.27 \cdot 10^{-15} T_e^{-1.130} \exp(-7.57/T_e)$	[48, reaction 68]
58	$e + \text{O}_2(\text{b}^1\Sigma_u^+) \rightarrow e + \text{O}_2(\text{b}^1\Sigma_u^+)$	2.87	$1.28 \cdot 10^{-14} T_e^{-1.160} \exp(-5.37/T_e)$	[48, reaction 69]
59	$e + \text{O}_2(\text{b}^1\Sigma_u^+) \rightarrow e + \text{O}_2(\text{b}^1\Sigma_u^+)$	4.37	$1.98 \cdot 10^{-14} T_e^{-0.779} \exp(-5.73/T_e)$	[48, reaction 70]
60	$e + \text{O}_2(\text{b}^1\Sigma_u^+) \rightarrow \text{O} + \text{O}^-$	0.0	$7.11 \cdot 10^{-16} T_e^{-1.040} \exp(-0.23/T_e)$	[48, reaction 71], 93
61	$e + \text{O}_2^- \rightarrow 2e + \text{O}_2$	4.68	$1.57 \cdot 10^{-14} T_e^{1.010} \exp(-1.77/T_e)$	[48, reaction 72], 94
62	$e + \text{O}_3 \rightarrow e + \text{O} + \text{O}_2$	2.6	$1.70 \cdot 10^{-14} T_e^{-0.570} \exp(-2.48/T_e)$	[48, reaction 73], 95
63	$e + \text{O}_3 \rightarrow e + \text{O}({}^1\text{D}) + \text{O}_2(\text{a}^1\Delta_u)$	5.72	$3.22 \cdot 10^{-13} T_e^{-1.180} \exp(-9.17/T_e)$	[48, reaction 74], 95
64	$e + \text{O}_3 \rightarrow \text{O} + \text{O}_2^-$	0.0	$1.02 \cdot 10^{-15} T_e^{-1.300} \exp(-1.03/T_e)$	[48, reaction 75], 96
65	$e + \text{O}_3 \rightarrow \text{O}^- + \text{O}_2$	0.0	$3.45 \cdot 10^{-15} T_e^{-0.960} \exp(-1.00/T_e)$	[48, reaction 76], 96
66	$e + \text{O}_3 \rightarrow 2e + \text{O}_3^+$	12.43	$5.96 \cdot 10^{-15} T_e^{0.978} \exp(-12.55/T_e)$	[48, reaction 77], 65, 97
67	$e + \text{O}_3^+ \rightarrow 3\text{O}$	-6.27	$2.07 \cdot 10^{-13} T_e^{-0.550}$	[48, reaction 78], 98
68	$e + \text{O}_3^+ \rightarrow 2\text{O} + \text{O}({}^1\text{D})$	-4.3	$6.69 \cdot 10^{-13} T_e^{-0.550}$	[48, reaction 79], 98
69	$e + \text{O}_3^+ \rightarrow \text{O} + 2\text{O}({}^1\text{D})$	-2.33	$1.55 \cdot 10^{-13} T_e^{-0.550}$	[48, reaction 80], 98
70	$e + \text{O}_3^- \rightarrow 2e + \text{O}_3$	2.1	$2.12 \cdot 10^{-14} T_e^{0.510} \exp(-5.87/T_e)$	[48, reaction 81], 99
71	$e + \text{O}_3^- \rightarrow 2e + \text{O} + \text{O}_2$	3.2	$7.12 \cdot 10^{-14} T_e^{-0.132} \exp(-5.94/T_e)$	[48, reaction 82], 99

Continuation of table A1: Electron-oxygen reactions.

#	Reaction	E_{thr} [eV]	K_r [$\text{m}^{3+3(N_r-2)}\text{s}^{-1}$]	Ref.
72	$e + \text{O}_3^- \rightarrow 2e + 3\text{O}$	8.4	$1.42 \cdot 10^{-14} T_e^{-0.520} \exp(-9.3/T_e)$	[48, reaction 83], 99
73	$2e + \text{O}^+ \rightarrow e + \text{O}$	0.0	$2.00 \cdot 10^{-39} T_e^{-4.5}$	[48, reaction 142], 100
74	$2e + \text{O}_2^+ \rightarrow e + \text{O}_2$	0.0	$2.00 \cdot 10^{-39} T_e^{-4.5}$	[48, reaction 143], 100
75	$2e + \text{O}_4^+ \rightarrow e + 2\text{O}_2$	0.0	$2.00 \cdot 10^{-39} T_e^{-4.5}$	[48, reaction 144], 100
76	$e + \text{O} + \text{O}_2 \rightarrow \text{O} + \text{O}_2^-$	0.0	$1.00 \cdot 10^{-43}$	[48, reaction 145], 101
77	$e + \text{O}^+ \rightarrow \text{O}(^1\text{D})$	0.0	$2.70 \cdot 10^{-19} T_e^{-0.7}$	[48, reaction 146], 101
78	$e + \text{O}^+ + \text{O}_2 \rightarrow \text{O} + \text{O}_2$	0.0	$3.30 \cdot 10^{-44} T_e^{-2.5}$	[48, reaction 147], 100
79	$e + 2\text{O}_2 \rightarrow \text{O}_2 + \text{O}_2^-$	0.0	$3.62 \cdot 10^{-43} T_e^{-1.0} \exp(-0.052/T_e)$	[48, reaction 148], 101
80	$e + \text{O}_2 + \text{O}_2^+ \rightarrow 2\text{O}_2$	0.0	$3.30 \cdot 10^{-44} T_e^{-2.5}$	[48, reaction 149], 100
81	$e + \text{O}_2 + \text{O}_3 \rightarrow \text{O}_2 + \text{O}_3^-$	0.0	$3.62 \cdot 10^{-43} T_e^{-1.0} \exp(-0.052/T_e)$	[48, reaction 150]
82	$e + \text{O}_2^+ \rightarrow \text{O} + \text{O}(^1\text{D})$	0.0	$9.10 \cdot 10^{-15} T_e^{-0.7}$	[48, reaction 151], 102–104
83	$e + \text{O}_2^+ \rightarrow \text{O}(^1\text{D}) + \text{O}(^1\text{S})$	0.0	$6.00 \cdot 10^{-15} T_e^{-0.7}$	[48, reaction 152], 102–104
84	$e + \text{O}_4^+ \rightarrow \text{O} + \text{O}(^1\text{D}) + \text{O}_2$	0.0	$2.02 \cdot 10^{-14} T_e^{-0.4}$	[48, reaction 153], 103, 105
85	$e + \text{O}_4^+ \rightarrow \text{O}(^1\text{D}) + \text{O}(^1\text{S}) + \text{O}_2$	0.0	$1.35 \cdot 10^{-14} T_e^{-0.4}$	[48, reaction 154], 103, 105
86	$e + \text{O} \rightarrow e + \text{O}(^5\text{S})$	9.15	$-9.0 \cdot 10^{-17} + 5.4 \cdot 10^{-17} \exp(T_e/2.4)$	[49, reaction 3]
87	$e + \text{O} \rightarrow e + \text{O}(^3\text{S})$	9.52	$-9.4 \cdot 10^{-17} + 3.9 \cdot 10^{-17} \exp(T_e/1.5)$	[49, reaction 4]
88	$e + \text{O} \rightarrow e + \text{O}(^5\text{P})$	10.74	$-2.8 \cdot 10^{-17} + 1.2 \cdot 10^{-17} \exp(T_e/1.5)$	[49, reaction 5]
89	$e + \text{O} \rightarrow e + \text{O}(^3\text{P})$	10.99	$-4.6 \cdot 10^{-17} + 1.6 \cdot 10^{-17} \exp(T_e/1.3)$	[49, reaction 6]
90	$e + \text{O} \rightarrow e + \text{O}(^3\text{P})$	10.74	$-6.53 \cdot 10^{-18} + 2.41 \cdot 10^{-18} \exp(T_e)$	[49, reaction 7]
91	$e + \text{O} \rightarrow e + \text{O}(^3\text{P})$	13.0	$-5.68 \cdot 10^{-17} + 1.30 \cdot 10^{-17} \exp(T_e/1.0)$	[49, reaction 8]
92	$e + \text{O}(^1\text{D}) \rightarrow e + \text{O}(^1\text{S})$	2.22	$1.4 \cdot 10^{-15} - 1.7 \cdot 10^{-15} \exp(-T_e/2.7)$	[49, reaction 10]
93	$e + \text{O}(^1\text{D}) \rightarrow e + \text{O}(^3\text{S})$	9.52	$-1.1 \cdot 10^{-18} + 5.8 \cdot 10^{-19} \exp(T_e/2.0)$	[49, reaction 11]
94	$e + \text{O}(^1\text{D}) \rightarrow e + \text{O}(^3\text{P})$	9.02	$-4.0 \cdot 10^{-18} + 1.9 \cdot 10^{-18} \exp(T_e/1.8)$	[49, reaction 12]
95	$e + \text{O}(^1\text{D}) \rightarrow e + \text{O}(^3\text{P})$	10.01	$-4.0 \cdot 10^{-17} + 1.5 \cdot 10^{-17} \exp(T_e/1.4)$	[49, reaction 13]
96	$e + \text{O}(^1\text{S}) \rightarrow e + \text{O}(^3\text{P})$	6.8	$-1.5 \cdot 10^{-17} + 1.2 \cdot 10^{-17} \exp(T_e/4.7)$	[49, reaction 15]
97	$e + \text{O}(^1\text{S}) \rightarrow e + \text{O}(^3\text{P})$	6.8		[49, reaction 16]
			$-1.64 \cdot 10^{-17} + 4.53 \cdot 10^{-17} T_e - 4.74 \cdot 10^{-17} T_e^2 + 2.34 \cdot 10^{-17} T_e^3 - 5.30 \cdot 10^{-18} T_e^4 + 4.57 \cdot 10^{-19} T_e^5$	
98	$e + \text{O}(^5\text{S}) \rightarrow e + \text{O}(^3\text{S})$	0.37		[49, reaction 17]
			$3.17 \cdot 10^{-14} + 1.91 \cdot 10^{-14} T_e - 1.68 \cdot 10^{-14} T_e^2 + 4.36 \cdot 10^{-15} T_e^3 - 3.85 \cdot 10^{-16} T_e^4$	
99	$e + \text{O}(^5\text{S}) \rightarrow e + \text{O}(^5\text{P})$	1.59		[49, reaction 18]
			$-1.64 \cdot 10^{-13} + 3.56 \cdot 10^{-13} T_e - 8.72 \cdot 10^{-14} T_e^2 + 9.88 \cdot 10^{-15} T_e^3 - 3.88 \cdot 10^{-16} T_e^4$	
100	$e + \text{O}(^5\text{S}) \rightarrow e + \text{O}(^3\text{P})$	1.84		[49, reaction 19]
			$-1.84 \cdot 10^{-14} + 4.19 \cdot 10^{-14} T_e - 1.88 \cdot 10^{-14} T_e^2 + 3.72 \cdot 10^{-15} T_e^3 - 2.81 \cdot 10^{-16} T_e^4$	
101	$e + \text{O}(^3\text{S}) \rightarrow e + \text{O}(^5\text{P})$	1.22		[49, reaction 20]
			$-2.94 \cdot 10^{-14} + 1.35 \cdot 10^{-13} T_e - 7.07 \cdot 10^{-14} T_e^2 + 1.55 \cdot 10^{-14} T_e^3 - 1.25 \cdot 10^{-15} T_e^4$	
102	$e + \text{O}(^3\text{S}) \rightarrow e + \text{O}(^3\text{P})$	1.47		[49, reaction 21]
			$-1.1 \cdot 10^{-13} + 3.6 \cdot 10^{-13} T_e - 1.5 \cdot 10^{-13} T_e^2 + 3.0 \cdot 10^{-14} T_e^3 - 2.2 \cdot 10^{-15} T_e^4$	
103	$e + \text{O}(^5\text{P}) \rightarrow e + \text{O}(^3\text{P})$	0.25		[49, reaction 22]
			$4.5 \cdot 10^{-14} + 4.9 \cdot 10^{-14} T_e - 3.5 \cdot 10^{-14} T_e^2 + 8.5 \cdot 10^{-15} T_e^3 - 7.3 \cdot 10^{-16} T_e^4$	

Continuation of table A1: Electron-oxygen reactions.

#	Reaction	E_{thr} [eV]	K_r [$\text{m}^{3+3(N_r-2)}\text{s}^{-1}$]	Ref.
104	$e + \text{O}_2 \rightarrow e + \text{O} + \text{O}(^1\text{S})$	0.0	$7.868 \cdot 10^{-20} \exp(T_e/0.8) - 5.1 \cdot 10^{-19}$	[49, reaction 26]
105	$e + \text{O}_2(\text{a}^1\Delta_u) \rightarrow e + \text{O} + \text{O}(^1\text{S})$	0.0	$7.868 \cdot 10^{-20} \exp(T_e/0.8) - 5.1 \cdot 10^{-19}$	[49, reaction 26]
106	$e + \text{O}_2(\text{b}^1\Sigma_u^+) \rightarrow e + \text{O} + \text{O}(^1\text{S})$	0.0	$7.868 \cdot 10^{-20} \exp(T_e/0.8) - 5.1 \cdot 10^{-19}$	[49, reaction 26]

Table A2: Electron-argon reactions. Electron temperature, T_e , in eV, and N_r is the number of reactants.

#	Process	E_{thr} [eV]	K_r [$\mathbf{m}^{3+3(N_r-2)}\mathbf{s}^{-1}$]	Ref.
107	$e + \text{Ar} \rightarrow e + \text{Ar}$	0.0	$2.336 \cdot 10^{-14} T_e^{1.609} \cdot \exp[0.0618(\log T_e)^2 - 0.1171(\log T_e)^3]$	41,106
108	$e + \text{Ar} \rightarrow \text{Ar}^+ + 2e$	15.76	$2.3 \cdot 10^{-14} T_e^{0.59} \exp(-17.44/T_e)$	45,107
109	$e + \text{Ar} \rightarrow \text{Ar}^m + e$	11.55	$5.0 \cdot 10^{-15} \exp(-12.64/T_e)$	45,108
110	$e + \text{Ar} \rightarrow \text{Ar}^m + e$	11.72	$1.4 \cdot 10^{-15} \exp(-12.42/T_e)$	45,108
111	$e + \text{Ar} \rightarrow \text{Ar}^r + e$	11.62	$1.9 \cdot 10^{-15} \exp(-12.60/T_e)$	45,108
112	$e + \text{Ar} \rightarrow \text{Ar}^r + e$	11.83	$2.7 \cdot 10^{-16} \exp(-12.14/T_e)$	45,108
113	$e + \text{Ar} \rightarrow \text{Ar}(4p) + e$	13.22	$2.1 \cdot 10^{-14} \exp(-13.13/T_e)$	45,109
114	$e + \text{Ar}^m \rightarrow \text{Ar} + e$	0.0	$4.3 \cdot 10^{-16} T_e^{0.74}$	45,62
115	$e + \text{Ar}^m \rightarrow \text{Ar}^+ + 2e$	4.12	$6.8 \cdot 10^{-15} T_e^{0.67} \exp(-4.2/T_e)$	45,110
116	$e + \text{Ar}^m \rightarrow \text{Ar}^r + e$	0.09	$3.7 \cdot 10^{-13}$	45,111
117	$e + \text{Ar}^m \rightarrow \text{Ar}(4p) + e$	1.57	$8.9 \cdot 10^{-13} T_e^{0.51} \exp(-1.59/T_e)$	45,110
118	$e + \text{Ar}(4p) \rightarrow \text{Ar}^+ + 2e$	2.55	$1.8 \cdot 10^{-13} T_e^{0.61} \exp(-2.61/T_e)$	45,110
119	$e + \text{Ar}(4p) \rightarrow \text{Ar}^r + e$	0.0	$3.0 \cdot 10^{-13} T_e^{0.51}$	45,62
120	$e + \text{Ar}(4p) \rightarrow \text{Ar}^m + e$	0.0	$3.0 \cdot 10^{-13} T_e^{0.51}$	45,62
121	$e + \text{Ar}(4p) \rightarrow \text{Ar} + e$	0.0	$3.9 \cdot 10^{-16} T_e^{0.71}$	45,62
122	$e + \text{Ar}^r \rightarrow \text{Ar} + e$	0.0	$4.3 \cdot 10^{-16} T_e^{0.74}$	45,62
123	$e + \text{Ar}^r \rightarrow \text{Ar}^m + e$	0.0	$9.1 \cdot 10^{-13}$	45,111
124	$e + \text{Ar}^r \rightarrow \text{Ar}(4p) + e$	1.48	$8.9 \cdot 10^{-13} T_e^{0.51} \exp(-1.59/T_e)$	45,110

Table A3: Oxygen-oxygen reactions. Electron temperature, T_e , in eV and neutral and ion temperature, T_N , in K. N_r is the number of reactants.

#	Reaction	K_r [$\text{m}^{3+3(N_r-2)}\text{s}^{-1}$]	Ref.
125	$3\text{O} \rightarrow \text{O} + \text{O}_2$	$3.80 \cdot 10^{-44}(300/T_N) \exp(-170/T_N)$	[48, reaction 92], 117
126	$3\text{O} \rightarrow \text{O} + \text{O}_2(\text{b}^1\Sigma_u^+)$	$1.40 \cdot 10^{-42} \exp(-650/T_N)$	[48, reaction 93], 101
127	$2\text{O} + \text{O}_2 \rightarrow \text{O} + \text{O}_3$	$4.20 \cdot 10^{-47} \exp(1056/T_N)$	[48, reaction 94], 117, 118
128	$2\text{O} + \text{O}_2 \rightarrow \text{O} + \text{O}_3(\nu)$	$9.80 \cdot 10^{-47} \exp(1056/T_N)$	[48, reaction 95], 117, 118
129	$2\text{O} + \text{O}_2 \rightarrow \text{O}_2(\text{a}^1\Delta_u) + \text{O}_2$	$6.50 \cdot 10^{-45}(300/T_N) \exp(-170/T_N)$	[48, reaction 96], 117, 119
130	$2\text{O} + \text{O}_2 \rightarrow \text{O}_2(\text{b}^1\Sigma_u^+) + \text{O}_2$	$6.50 \cdot 10^{-45}(300/T_N) \exp(-170/T_N)$	[48, reaction 97], 117, 119
131	$\text{O} + \text{O}({}^1\text{D}) \rightarrow 2\text{O}$	$2.00 \cdot 10^{-18}$	[48, reaction 98], 120
132	$\text{O} + \text{O}({}^1\text{S}) \rightarrow 2\text{O}$	$2.50 \cdot 10^{-17} \exp(-300/T_N)$	[48, reaction 99], 121
133	$\text{O} + \text{O}({}^1\text{S}) \rightarrow \text{O} + \text{O}({}^1\text{D})$	$2.50 \cdot 10^{-17} \exp(-300/T_N)$	[48, reaction 100], 121
134	$\text{O} + 2\text{O}_2 \rightarrow \text{O}_2 + \text{O}_3$	$1.80 \cdot 10^{-46}(300/T_N)^{2.6}$	[48, reaction 101], 118, 122, 123
135	$\text{O} + 2\text{O}_2 \rightarrow \text{O}_2 + \text{O}_3(\nu)$	$4.20 \cdot 10^{-46}(300/T_N)^{2.6}$	[48, reaction 102], 118, 122, 123
136	$\text{O} + \text{O}_2 + \text{O}_2(\text{a}^1\Delta_u) \rightarrow \text{O} + 2\text{O}_2$	$1.10 \cdot 10^{-44}$	[48, reaction 103], 118
137	$\text{O} + \text{O}_2 + \text{O}_3 \rightarrow 2\text{O}_3$	$1.40 \cdot 10^{-47} \exp(-1050/T_N)$	[48, reaction 104], 118
138	$\text{O} + \text{O}_2 + \text{O}_3 \rightarrow \text{O}_3 + \text{O}_3(\nu)$	$3.27 \cdot 10^{-47} \exp(-1050/T_N)$	[48, reaction 105], 118
139	$\text{O} + \text{O}_2(\text{a}^1\Delta_u) \rightarrow \text{O} + \text{O}_2$	$1.00 \cdot 10^{-22}$ ($E_{th} = -2.14$ eV)	[48, reaction 106], 122
140	$\text{O} + \text{O}_2(\text{b}^1\Sigma_u^+) \rightarrow \text{O} + \text{O}_2(\text{a}^1\Delta_u)$	$8.00 \cdot 10^{-20}$ ($E_{th} = -0.65$ eV)	[48, reaction 107], 122, 123
141	$\text{O} + \text{O}_3 \rightarrow 2\text{O} + \text{O}_2$	$1.20 \cdot 10^{-15} \exp(-11400/T_N)$	[48, reaction 108], 117
142	$\text{O} + \text{O}_3 \rightarrow 2\text{O}_2$	$8.00 \cdot 10^{-18} \exp(-2060/T_N)$	[48, reaction 109], 122–125
143	$\text{O} + \text{O}_3(\nu) \rightarrow 2\text{O}_2$	$4.50 \cdot 10^{-18}$	[48, reaction 110], 126
144	$\text{O} + \text{O}_3(\nu) \rightarrow \text{O}_3 + \text{O}$	$1.05 \cdot 10^{-17}$	[48, reaction 111], 126
145	$\text{O}({}^1\text{D}) + \text{O}_2 \rightarrow \text{O} + \text{O}_2$	$4 \cdot 10^{-17}$	28, 112
146	$\text{O}({}^1\text{D}) + \text{O}_2(\text{a}^1\Delta_u) \rightarrow \text{O} + \text{O}_2$	$4 \cdot 10^{-17}$	28, 112 ^a
147	$\text{O}({}^1\text{D}) + \text{O}_2(\text{b}^1\Sigma_u^+) \rightarrow \text{O} + \text{O}_2$	$4 \cdot 10^{-17}$	28, 112 ^a
148	$\text{O}({}^1\text{D}) + \text{O}_2 \rightarrow \text{O} + \text{O}_2(\text{b}^1\Sigma_u^+)$	$2.64 \cdot 10^{-17} \exp(55/T_N)$	[48, reaction 112], 122
149	$\text{O}({}^1\text{D}) + \text{O}_2 \rightarrow \text{O} + \text{O}_2(\text{a}^1\Delta_u)$	$6.60 \cdot 10^{-18} \exp(55/T_N)$	[48, reaction 113], 122
150	$\text{O}({}^1\text{D}) + \text{O}_3 \rightarrow 2\text{O} + \text{O}_2$	$1.20 \cdot 10^{-16}$	[48, reaction 114], 122, 123, 126
151	$\text{O}({}^1\text{D}) + \text{O}_3 \rightarrow 2\text{O}_2$	$1.20 \cdot 10^{-16}$	[48, reaction 115], 122, 123, 126
152	$\text{O}({}^1\text{S}) + \text{O}_2 \rightarrow \text{O} + \text{O}_2$	$3.00 \cdot 10^{-18} \exp(-850/T_N)$	[48, reaction 116], 101, 113
153	$\text{O}({}^1\text{S}) + \text{O}_2(\text{a}^1\Delta_u) \rightarrow \text{O} + \text{O}_2$	$3.00 \cdot 10^{-18} \exp(-850/T_N)$	[48, reactopn 116]101, 113 ^b
154	$\text{O}({}^1\text{S}) + \text{O}_2(\text{b}^1\Sigma_u^+) \rightarrow \text{O} + \text{O}_2$	$3.00 \cdot 10^{-18} \exp(-850/T_N)$	[48, reactopn 116]101, 113 ^b
155	$\text{O}({}^1\text{S}) + \text{O}_2 \rightarrow \text{O}({}^1\text{D}) + \text{O}_2$	$1.30 \cdot 10^{-18} \exp(-850/T_N)$	[48, reaction 117], 101, 113
156	$\text{O}({}^1\text{S}) + \text{O}_2(\text{a}^1\Delta_u) \rightarrow 3\text{O}$	$3.20 \cdot 10^{-17}$	[48, reaction 118], 127–129
157	$\text{O}({}^1\text{S}) + \text{O}_2(\text{a}^1\Delta_u) \rightarrow \text{O} + \text{O}_2(\text{b}^1\Sigma_u^+)$	$1.30 \cdot 10^{-16}$	[48, reaction 119], 127–129
158	$\text{O}({}^1\text{S}) + \text{O}_2(\text{a}^1\Delta_u) \rightarrow \text{O}({}^1\text{D}) + \text{O}_2$	$3.60 \cdot 10^{-17}$	[48, reaction 120], 128, 129
159	$\text{O}({}^1\text{S}) + \text{O}_3 \rightarrow \text{O} + \text{O}({}^1\text{D}) + \text{O}_2$	$1.93 \cdot 10^{-16}$	[48, reaction 121], 126
160	$\text{O}({}^1\text{S}) + \text{O}_3 \rightarrow 2\text{O}_2$	$1.93 \cdot 10^{-16}$	[48, reaction 122], 126
161	$\text{O}({}^1\text{S}) + \text{O}_3 \rightarrow 2\text{O} + \text{O}_2$	$1.93 \cdot 10^{-16}$	[48, reaction 123], 126

Continuation of table A3: Oxygen-oxygen reactions

#	Reaction	K_r [$\text{m}^{3+3(N_r-2)}\text{s}^{-1}$]	Ref.
162	$2\text{O}_2 \rightarrow 2\text{O} + \text{O}_2$	$6.60 \cdot 10^{-15} (300/T_N)^{1.5} \exp(-59000/T_N)$	[48, reaction 124], 101
163	$\text{O}_2 + \text{O}_2(\text{a}^1\Delta_u) \rightarrow 2\text{O}_2$	$3.60 \cdot 10^{-24} \exp(-220/T_N)$	[48, reaction 126], 122
164	$\text{O}_2 + \text{O}_2(\text{b}^1\Sigma_u^+) \rightarrow \text{O}_2 + \text{O}_2(\text{a}^1\Delta_u)$	$3.90 \cdot 10^{-23}$	[48, reaction 128], 122, 130
165	$\text{O}_2 + \text{O}_3 \rightarrow \text{O} + 2\text{O}_2$	$7.26 \cdot 10^{-16} \exp(-11435/T_N)$	[48, reaction 130], 126
166	$\text{O}_2 + \text{O}_3(\nu) \rightarrow \text{O}_2 + \text{O}_3$	$4.00 \cdot 10^{-20}$	[48, reaction 131], 126
167	$2\text{O}_2(\text{a}^1\Delta_u) \rightarrow \text{O}_2 + \text{O}_2(\text{b}^1\Sigma_u^+)$	$2.70 \cdot 10^{-23}$	[48, reaction 132], 131
168	$\text{O}_2(\text{a}^1\Delta_u) + \text{O}_2(\text{b}^1\Sigma_u^+) \rightarrow \text{O}_2 + \text{O}_2(\text{b}^1\Sigma_u^+)$	$2.70 \cdot 10^{-23}$	[48, reaction 133]
169	$2\text{O}_2(\text{b}^1\Sigma_u^+) \rightarrow \text{O}_2 + \text{O}_2(\text{b}^1\Sigma_u^+)$	$2.70 \cdot 10^{-23}$	[48, reaction 134]
170	$\text{O}_2(\text{a}^1\Delta_u) + \text{O}_3 \rightarrow \text{O} + 2\text{O}_2$	$5.20 \cdot 10^{-17} \exp(-2840/T_N)$	[48, reaction 135], 122
171	$\text{O}_2(\text{a}^1\Delta_u) + \text{O}_3(\nu) \rightarrow \text{O}_2 + \text{O}_3$	$5.00 \cdot 10^{-17}$	[48, reaction 136], 126
172	$\text{O}_2(\text{b}^1\Sigma_u^+) + \text{O}_3 \rightarrow \text{O} + 2\text{O}_2$	$2.40 \cdot 10^{-17} \exp(-135/T_N)$	[48, reaction 137], 122
173	$\text{O}_2(\text{b}^1\Sigma_u^+) + \text{O}_3 \rightarrow \text{O}_2 + \text{O}_3$	$5.50 \cdot 10^{-18} \exp(-135/T_N)$	[48, reaction 138], 122
174	$\text{O}_2(\text{b}^1\Sigma_u^+) + \text{O}_3 \rightarrow \text{O}_2(\text{a}^1\Delta_u) + \text{O}_3$	$5.50 \cdot 10^{-18} \exp(-135/T_N)$	[48, reaction 139], 122
175	$2\text{O}_3 \rightarrow \text{O} + \text{O}_2 + \text{O}_3$	$1.65 \cdot 10^{-15} \exp(-11435/T_N)$	[48, reaction 140], 126
176	$\text{O}_3 + \text{O}_3(\nu) \rightarrow 2\text{O}_3$	$1.00 \cdot 10^{-19}$	[48, reaction 141], 126
177	$\text{O} + \text{O}^- \rightarrow e + \text{O}_2$	$2.30 \cdot 10^{-16} (300/T_N)^{1.3}$	[48, reaction 155], 132, 133
178	$\text{O} + \text{O}_2^- \rightarrow \text{O}^- + \text{O}_2$	$8.50 \cdot 10^{-17} (300/T_N)^{1.8}$	[48, reaction 156], 132
179	$\text{O} + \text{O}_2^- \rightarrow e + \text{O}_3$	$8.50 \cdot 10^{-17} (300/T_N)^{1.8}$	[48, reaction 157], 132
180	$\text{O} + \text{O}_3^- \rightarrow e + 2\text{O}_2$	$1.00 \cdot 10^{-17}$	[48, reaction 158], 101
181	$\text{O} + \text{O}_3^- \rightarrow \text{O}_2 + \text{O}_2^-$	$2.50 \cdot 10^{-16}$	[48, reaction 159], 134
182	$\text{O} + \text{O}_4^+ \rightarrow \text{O}_3 + \text{O}_2^+$	$3.00 \cdot 10^{-16}$	[48, reaction 160], 134
183	$\text{O} + \text{O}_4^- \rightarrow \text{O}_2 + \text{O}_3^-$	$4.00 \cdot 10^{-16}$	[48, reaction 161], 101, 134
184	$\text{O}(^1\text{D}) + \text{O}^- \rightarrow e + 2\text{O}$	$7.40 \cdot 10^{-16}$	[48, reaction 162], 135–137
185	$\text{O}(^1\text{D}) + \text{O}_2^- \rightarrow e + \text{O}_3$	$8.50 \cdot 10^{-17} (300/T_N)^{1.8}$	[48, reaction 163]
186	$\text{O}(^1\text{D}) + \text{O}_2^- \rightarrow \text{O}^- + \text{O}_2$	$8.50 \cdot 10^{-17} (300/T_N)^{1.8}$	[48, reaction 164]
187	$\text{O}(^1\text{D}) + \text{O}_3^+ \rightarrow 2\text{O} + \text{O}_2^+$	$3.00 \cdot 10^{-16}$	[48, reaction 165], 135, 136, 138
188	$\text{O}(^1\text{D}) + \text{O}_3^- \rightarrow \text{O} + \text{O}_2 + \text{O}^-$	$3.00 \cdot 10^{-16}$	[48, reaction 166], 135, 136, 138
189	$\text{O}(^1\text{D}) + \text{O}_3^- \rightarrow \text{O} + \text{O}_3 + e$	$3.00 \cdot 10^{-16}$	[48, reaction 167], 135–137
190	$\text{O}(^1\text{D}) + \text{O}_4^+ \rightarrow \text{O} + \text{O}_2 + \text{O}_2^+$	$3.00 \cdot 10^{-16}$	[48, reaction 168], 135–137
191	$\text{O}(^1\text{D}) + \text{O}_4^+ \rightarrow \text{O}_3 + \text{O}_2^+$	$3.00 \cdot 10^{-16}$	[48, reaction 169], 135–137
192	$\text{O}(^1\text{D}) + \text{O}_4^- \rightarrow e + \text{O} + 2\text{O}_2$	$2.00 \cdot 10^{-16}$	[48, reaction 170], 135, 136, 138
193	$\text{O}(^1\text{D}) + \text{O}_4^- \rightarrow \text{O} + \text{O}_2 + \text{O}_2^-$	$2.00 \cdot 10^{-16}$	[48, reaction 171], 135, 136, 138
194	$\text{O}(^1\text{D}) + \text{O}_4^- \rightarrow 2\text{O}_2 + \text{O}^-$	$2.00 \cdot 10^{-16}$	[48, reaction 172], 135, 136, 138
195	$\text{O}(^1\text{D}) + \text{O}_4^- \rightarrow \text{O} + \text{O}_2 + \text{O}_2^-$	$7.40 \cdot 10^{-16}$	[48, reaction 173], 135–137
196	$\text{O}(^1\text{S}) + \text{O}_2^- \rightarrow \text{O}^- + \text{O}_2$	$8.50 \cdot 10^{-17} (300/T_N)^{1.8}$	[48, reaction 174]
197	$\text{O}(^1\text{S}) + \text{O}_2^- \rightarrow e + \text{O}_3$	$8.50 \cdot 10^{-17} (300/T_N)^{1.8}$	[48, reaction 175]
198	$\text{O}(^1\text{S}) + \text{O}_3^+ \rightarrow 2\text{O} + \text{O}_2^+$	$2.00 \cdot 10^{-16}$	[48, reaction 176], 135, 136, 138
199	$\text{O}(^1\text{S}) + \text{O}_3^- \rightarrow e + \text{O} + \text{O}_3$	$2.00 \cdot 10^{-16}$	[48, reaction 177], 135, 136, 138
200	$\text{O}(^1\text{S}) + \text{O}_3^- \rightarrow 2\text{O} + \text{O}_2^-$	$2.00 \cdot 10^{-16}$	[48, reaction 178], 135, 136, 138

Continuation of table A3: Oxygen-oxygen reactions

#	Reaction	K_r [$\text{m}^{3+3(N_r-2)}\text{s}^{-1}$]	Ref.
201	$\text{O}(^1\text{S}) + \text{O}_3^- \rightarrow \text{O} + \text{O}^- + \text{O}_2$	$2.00 \cdot 10^{-16}$	[48, reaction 179], 135,136,138
202	$\text{O}(^1\text{S}) + \text{O}_4^+ \rightarrow \text{O} + \text{O}_2 + \text{O}_2^+$	$3.00 \cdot 10^{-16}$	[48, reaction 180], 135–137
203	$\text{O}(^1\text{S}) + \text{O}_4^+ \rightarrow \text{O}_2^+ + \text{O}_3$	$3.00 \cdot 10^{-16}$	[48, reaction 181], 135–137
204	$\text{O}(^1\text{S}) + \text{O}_4^- \rightarrow e + \text{O} + 2\text{O}_2$	$2.00 \cdot 10^{-16}$	[48, reaction 182], 135,136,138
205	$\text{O}(^1\text{S}) + \text{O}_4^- \rightarrow \text{O} + \text{O}_2 + \text{O}_2^-$	$2.00 \cdot 10^{-16}$	[48, reaction 183], 135,136,138
206	$\text{O}(^1\text{S}) + \text{O}_4^- \rightarrow \text{O}^- + 2\text{O}_2$	$2.00 \cdot 10^{-16}$	[48, reaction 184], 135,136,138
207	$\text{O}^+ + \text{O} + \text{O}_2 \rightarrow \text{O}_2 + \text{O}_2^+$	$4.00 \cdot 10^{-42}(300/T_N)^{2.93}$	[48, reaction 185]
208	$\text{O}^+ + \text{O}_2 \rightarrow \text{O} + \text{O}_2^+$	$2.10 \cdot 10^{-17}(300/T_N)^{0.4}$	[48, reaction 189], 101,139
209	$\text{O}^+ + \text{O}_3 \rightarrow \text{O}_2 + \text{O}_2^+$	$1.20 \cdot 10^{-15}$	[48, reaction 193], 135,136,138
210	$\text{O}^- + \text{O}_2 \rightarrow \text{O}_3 + e$	$1.00 \cdot 10^{-18}$	[48, reaction 198], 134
211	$\text{O}^- + \text{O}_2 \rightarrow \text{O}_2^- + \text{O}$	$1.00 \cdot 10^{-18}$	[48, reaction 199], 134
212	$\text{O}^- + 2\text{O}_2 \rightarrow \text{O}_2 + \text{O}_3^-$	$1.10 \cdot 10^{-42}$	[48, reaction 200], 101
213	$\text{O}^- + \text{O}_2(\text{a}^1\Delta_u) \rightarrow \text{O} + \text{O}_2^-$	$7.90 \cdot 10^{-16} \exp(-890/T_N)$	[48, reaction 203], 140
214	$\text{O}^- + \text{O}_2(\text{a}^1\Delta_u) \rightarrow \text{O}_3 + e$	$6.10 \cdot 10^{-17}$	[48, reaction 204], 140
215	$\text{O}^- + \text{O}_2(\text{b}^1\Sigma_u^+) \rightarrow \text{O} + \text{O}_2^-$	$7.90 \cdot 10^{-16} \exp(-890/T_N)$	[48, reaction 205]
216	$\text{O}^- + \text{O}_2(\text{b}^1\Sigma_u^+) \rightarrow \text{O}_3 + e$	$6.10 \cdot 10^{-17}$	[48, reaction 206]
217	$\text{O}^- + \text{O}_3 \rightarrow e + 2\text{O}_2$	$3.00 \cdot 10^{-16}$	[48, reaction 209], 134,141
218	$\text{O}^- + \text{O}_3 \rightarrow \text{O} + \text{O}_3^-$	$2.00 \cdot 10^{-16}$	[48, reaction 210], 134,141
219	$\text{O}^- + \text{O}_3 \rightarrow \text{O}_2 + \text{O}_2^-$	$1.00 \cdot 10^{-17}$	[48, reaction 211], 134,141
220	$2\text{O}_2 + \text{O}_2^+ \rightarrow \text{O}_2 + \text{O}_4^+$	$4.00 \cdot 10^{-42}(300/T_N)^{2.93}$	[48, reaction 215], 142
221	$2\text{O}_2 + \text{O}_2^- \rightarrow \text{O}_2 + \text{O}_4^-$	$3.50 \cdot 10^{-43}(300/T_N)$	[48, reaction 216], 101
222	$\text{O}_2 + \text{O}_2^- \rightarrow e + 2\text{O}_2$	$2.70 \cdot 10^{-16}(T_N/300)^{0.5} \exp(-5590/T_N)$	[48, reaction 217], 101
223	$\text{O}_2 + \text{O}_2^- \rightarrow \text{O} + \text{O}_3^-$	$3.50 \cdot 10^{-21}$	[48, reaction 218], 134
224	$\text{O}_2 + \text{O}_3^+ \rightarrow \text{O}_2^+ + \text{O}_3$	$6.70 \cdot 10^{-16}$	[48, reaction 221], 135,136,138,143
225	$\text{O}_2 + \text{O}_4^+ \rightarrow 2\text{O}_2 + \text{O}_2^+$	$1.00 \cdot 10^{-11}(300/T_N)^{4.2} \exp(-5400/T_N)$	[48, reaction 222], 101,134
226	$\text{O}_2 + \text{O}_4^- \rightarrow 2\text{O}_2 + \text{O}_2^-$	$2.20 \cdot 10^{-11}(300/T_N) \exp(-6300/T_N)$	[48, reaction 227], 101
227	$\text{O}_2(\text{a}^1\Delta_u) + \text{O}_2^- \rightarrow e + 2\text{O}_2$	$7.00 \cdot 10^{-16}$	[48, reaction 228], 140
228	$\text{O}_2(\text{a}^1\Delta_u) + \text{O}_4^+ \rightarrow 2\text{O}_2 + \text{O}_2^+$	$6.00 \cdot 10^{-16}$	[48, reaction 229], 135,136,138
229	$\text{O}_2(\text{a}^1\Delta_u) + \text{O}_4^- \rightarrow 3\text{O}_2 + e$	$3.00 \cdot 10^{-16}$	[48, reaction 230], 135,136,138
230	$\text{O}_2(\text{a}^1\Delta_u) + \text{O}_4^- \rightarrow 2\text{O}_2 + \text{O}_2^-$	$3.00 \cdot 10^{-16}$	[48, reaction 231], 135,136,138
231	$\text{O}_2(\text{b}^1\Sigma_u^+) + \text{O}_2^- \rightarrow e + 2\text{O}_2$	$7.00 \cdot 10^{-16}$	[48, reaction 232]
232	$\text{O}_2(\text{b}^1\Sigma_u^+) + \text{O}_3^- \rightarrow \text{O}^- + 2\text{O}_2$	$6.70 \cdot 10^{-16} \exp(-1300/T_N)$	[48, reaction 233], 135,136,138
233	$\text{O}_2(\text{b}^1\Sigma_u^+) + \text{O}_4^+ \rightarrow 2\text{O}_2 + \text{O}_2^+$	$6.00 \cdot 10^{-16}$	[48, reaction 234]
234	$\text{O}_2(\text{b}^1\Sigma_u^+) + \text{O}_4^- \rightarrow e + 3\text{O}_2$	$3.00 \cdot 10^{-16}$	[48, reaction 235], 135,136,138
235	$\text{O}_2(\text{b}^1\Sigma_u^+) + \text{O}_4^- \rightarrow 2\text{O}_2 + \text{O}_2^-$	$3.00 \cdot 10^{-16}$	[48, reaction 236], 135,136,138
236	$\text{O}_2^- + \text{O}_3 \rightarrow \text{O}_2 + \text{O}_3^-$	$6.00 \cdot 10^{-16}$	[48, reaction 247], 134
237	$\text{O}_3 + \text{O}_4^- \rightarrow 2\text{O}_2 + \text{O}_3^-$	$8.00 \cdot 10^{-16}$	[48, reaction 251], 135,136,138
238	$\text{O}_3^- + \text{O}_3 \rightarrow e + 3\text{O}_2$	$8.50 \cdot 10^{-16}$	[48, reaction 254], 135,136,138
239	$\text{O}(^3\text{P}) + \text{O}_2 \rightarrow \text{O} + \text{O}_2$	$9.4 \cdot 10^{-16}$	114

Continuation of table A3: Oxygen-oxygen reactions

#	Reaction	K_r [$\text{m}^{3+3(N_r-2)}\text{s}^{-1}$]	Ref.
240	$\text{O}(^3\text{P}) + \text{O}_2(\text{a}^1\Delta_u) \rightarrow \text{O} + \text{O}_2$	$9.4 \cdot 10^{-16}$	114 ^c
241	$\text{O}(^3\text{P}) + \text{O}_2(\text{b}^1\Sigma_u^+) \rightarrow \text{O} + \text{O}_2$	$9.4 \cdot 10^{-16}$	114 ^c
242	$\text{O}(^3\text{P}) + \text{O}_3 \rightarrow \text{O} + \text{O}_3$	$9.4 \cdot 10^{-16}$	114 ^c
243	$\text{O}(^3\text{P}) + \text{O} \rightarrow \text{O} + \text{O}$	$9.4 \cdot 10^{-16}$	114 ^c
244	$\text{O}(^3\text{S}) + \text{O}_2 \rightarrow \text{O} + \text{O}_2$	$9.4 \cdot 10^{-16}$	114 ^c
245	$\text{O}(^3\text{S}) + \text{O}_2(\text{a}^1\Delta_u) \rightarrow \text{O} + \text{O}_2$	$9.4 \cdot 10^{-16}$	114 ^c
246	$\text{O}(^3\text{S}) + \text{O}_2(\text{b}^1\Sigma_u^+) \rightarrow \text{O} + \text{O}_2$	$9.4 \cdot 10^{-16}$	114 ^c
247	$\text{O}(^3\text{S}) + \text{O}_3 \rightarrow \text{O} + \text{O}_3$	$9.4 \cdot 10^{-16}$	114 ^c
248	$\text{O}(^3\text{S}) + \text{O} \rightarrow \text{O} + \text{O}$	$9.4 \cdot 10^{-16}$	114 ^c
249	$\text{O}(^5\text{P}) + \text{O}_2 \rightarrow \text{O} + \text{O}_2$	$1.08 \cdot 10^{-15}$	115
250	$\text{O}(^5\text{P}) + \text{O}_2(\text{a}^1\Delta_u) \rightarrow \text{O} + \text{O}_2$	$1.08 \cdot 10^{-15}$	115 ^d
251	$\text{O}(^5\text{P}) + \text{O}_2(\text{b}^1\Sigma_u^+) \rightarrow \text{O} + \text{O}_2$	$1.08 \cdot 10^{-15}$	115 ^d
252	$\text{O}(^5\text{P}) + \text{O}_3 \rightarrow \text{O} + \text{O}_3$	$1.08 \cdot 10^{-15}$	115 ^d
253	$\text{O}(^5\text{P}) + \text{O} \rightarrow \text{O} + \text{O}$	$1.08 \cdot 10^{-15}$	115 ^d
254	$\text{O}(^5\text{S}) + \text{O}_2 \rightarrow \text{O} + \text{O}_2$	$1.4 \cdot 10^{-16}$	116
255	$\text{O}(^5\text{S}) + \text{O}_2(\text{a}^1\Delta_u) \rightarrow \text{O} + \text{O}_2$	$1.4 \cdot 10^{-16}$	116 ^e
256	$\text{O}(^5\text{S}) + \text{O}_2(\text{b}^1\Sigma_u^+) \rightarrow \text{O} + \text{O}_2$	$1.4 \cdot 10^{-16}$	116 ^e
257	$\text{O}(^5\text{S}) + \text{O}_3 \rightarrow \text{O} + \text{O}_3$	$1.4 \cdot 10^{-16}$	116 ^e
258	$\text{O}(^5\text{S}) + \text{O} \rightarrow \text{O} + \text{O}$	$1.4 \cdot 10^{-16}$	116 ^e

^a The collisional quenching coefficient for $\text{O}(^1\text{D}) + \text{O}_2$ is measured in Ref. 112. Here, the same quenching coefficient is used for the marked reactions, due to a lack of specific data.

^b The collisional quenching coefficient for $\text{O}(^1\text{S}) + \text{O}_2$ is measured in Refs. 101,113. Here, the same quenching coefficient is used for the marked reactions, due to a lack of specific data.

^c The collisional quenching coefficient for $\text{O}(^3\text{S}) + \text{O}_2$ is measured in Ref. 114. Here, the same quenching coefficient is used for the marked reactions, due to a lack of specific data.

^d The collisional quenching coefficient for $\text{O}(^5\text{P}) + \text{O}_2$ is measured in Ref. 115. Here, the same quenching coefficient is used for the marked reactions, due to a lack of specific data.

^e The collisional quenching coefficient for $\text{O}(^5\text{S}) + \text{O}_2$ is measured in Ref. 116. Here, the same quenching coefficient is used for the marked reactions, due to a lack of specific data.

Table A4: Argon-argon reactions. Electron temperature, T_e , in eV and neutral and ion temperature, T_N , in K. N_r is the number of reactants.

#	Reaction	K_r [$\text{m}^{3+3(N_r-2)}\text{s}^{-1}$]	Ref.
259	$2\text{Ar}^m \rightarrow 2\text{Ar}$	$2.0 \cdot 10^{-13}$	45
260	$\text{Ar}^m + \text{Ar}^r \rightarrow \text{Ar} + \text{Ar}^+ + e$	$2.1 \cdot 10^{-15}$	45,144
261	$\text{Ar}(4\text{p}) + \text{Ar}(4\text{p}) \rightarrow \text{Ar} + \text{Ar}^+ + e$	$5.0 \cdot 10^{-16}$	45,110
262	$2\text{Ar}^m \rightarrow \text{Ar} + \text{Ar}^+ + e$	$6.4 \cdot 10^{-16}$	45,111
263	$\text{Ar} + \text{Ar}^m \rightarrow 2\text{Ar}$	$2.1 \cdot 10^{-21}$	45,144

Table A5: Argon-oxygen reactions. Electron temperature, T_e , in eV and neutral and ion temperature, T_N , in K. N_r is the number of reactants.

#	Reaction	K_r [$\text{m}^{3+3(N_r-2)}\text{s}^{-1}$]	Ref.
264	$\text{O} + \text{Ar}^m \rightarrow \text{O} + \text{Ar}$	$4.1 \cdot 10^{-17}$	45, 145
265	$\text{O} + \text{Ar}^r \rightarrow \text{O} + \text{Ar}$	$4.1 \cdot 10^{-17}$	45 ^a
266	$\text{O}_2 + \text{Ar}(4\text{p}) \rightarrow \text{O} + \text{O} + \text{Ar}$	$2.96 \cdot 10^{-16}$	45
267	$\text{O}_2(\text{a}^1\Delta_u) + \text{Ar}(4\text{p}) \rightarrow \text{O} + \text{O} + \text{Ar}$	$2.96 \cdot 10^{-16}$	45 ^a
268	$\text{O}_2(\text{b}^1\Sigma_u^+) + \text{Ar}(4\text{p}) \rightarrow \text{O} + \text{O} + \text{Ar}$	$2.96 \cdot 10^{-16}$	45 ^a
269	$\text{O}_2 + \text{Ar}(4\text{p}) \rightarrow \text{O} + \text{O}({}^1\text{D}) + \text{Ar}$	$3.34 \cdot 10^{-16}$	45
270	$\text{O}_2(\text{a}^1\Delta_u) + \text{Ar}(4\text{p}) \rightarrow \text{O} + \text{O}({}^1\text{D}) + \text{Ar}$	$3.34 \cdot 10^{-16}$	45 ^a
271	$\text{O}_2(\text{b}^1\Sigma_u^+) + \text{Ar}(4\text{p}) \rightarrow \text{O} + \text{O}({}^1\text{D}) + \text{Ar}$	$3.34 \cdot 10^{-16}$	45 ^a
272	$\text{O}_2 + \text{Ar}^+ \rightarrow \text{O}_2^+ + \text{Ar}$	$4.90 \cdot 10^{-17}(300/T_N)^{0.78}$	45, 146
273	$\text{O}_2(\text{a}^1\Delta_u) + \text{Ar}^+ \rightarrow \text{O}_2^+ + \text{Ar}$	$4.90 \cdot 10^{-17}(300/T_N)^{0.78}$	45 ^a
274	$\text{O}_2(\text{b}^1\Sigma_u^+) + \text{Ar}^+ \rightarrow \text{O}_2^+ + \text{Ar}$	$4.90 \cdot 10^{-17}(300/T_N)^{0.78}$	45 ^a
275	$\text{O} + \text{Ar}^+ \rightarrow \text{O}^+ + \text{Ar}$	$6.40 \cdot 10^{-18}$	45, 147
276	$\text{O}_2 + \text{Ar}^m \rightarrow \text{O} + \text{O} + \text{Ar}$	$1.035 \cdot 10^{-16}$	28, 148, 149
277	$\text{O}_2(\text{a}^1\Delta_u) + \text{Ar}^m \rightarrow \text{O} + \text{O} + \text{Ar}$	$1.035 \cdot 10^{-16}$	28, 148, 149
278	$\text{O}_2(\text{b}^1\Sigma_u^+) + \text{Ar}^m \rightarrow \text{O} + \text{O} + \text{Ar}$	$1.035 \cdot 10^{-16}$	28, 148, 149
279	$\text{O}_2 + \text{Ar}^m \rightarrow \text{O} + \text{O}({}^1\text{D}) + \text{Ar}$	$1.17 \cdot 10^{-16}$	28, 148, 149
280	$\text{O}_2(\text{a}^1\Delta_u) + \text{Ar}^m \rightarrow \text{O} + \text{O}({}^1\text{D}) + \text{Ar}$	$1.17 \cdot 10^{-16}$	28, 148, 149
281	$\text{O}_2(\text{b}^1\Sigma_u^+) + \text{Ar}^m \rightarrow \text{O} + \text{O}({}^1\text{D}) + \text{Ar}$	$1.17 \cdot 10^{-16}$	28, 148, 149
282	$\text{O}_2 + \text{Ar}^m \rightarrow \text{O} + \text{O}({}^1\text{S}) + \text{Ar}$	$4.5 \cdot 10^{-18}$	28, 148, 149
283	$\text{O}_2(\text{a}^1\Delta_u) + \text{Ar}^m \rightarrow \text{O} + \text{O}({}^1\text{S}) + \text{Ar}$	$4.5 \cdot 10^{-18}$	28, 148, 149
284	$\text{O}_2(\text{b}^1\Sigma_u^+) + \text{Ar}^m \rightarrow \text{O} + \text{O}({}^1\text{S}) + \text{Ar}$	$4.5 \cdot 10^{-18}$	28, 148, 149

Continuation of table A5: Argon-oxygen reactions.

#	Reaction	K_r [$\text{m}^{3+3(N_r-2)}\text{s}^{-1}$]	Ref.
285	$\text{O}_2 + \text{Ar}^r \rightarrow \text{O} + \text{O} + \text{Ar}$	$1.288 \cdot 10^{-16}$	28, 148, 149
286	$\text{O}_2(\text{a}^1\Delta_u) + \text{Ar}^r \rightarrow 2\text{O} + \text{Ar}$	$1.288 \cdot 10^{-16}$	28, 148, 149
287	$\text{O}_2(\text{b}^1\Sigma_u^+) + \text{Ar}^r \rightarrow 2\text{O} + \text{Ar}$	$1.288 \cdot 10^{-16}$	28, 148, 149
288	$\text{O}_2 + \text{Ar}^r \rightarrow \text{O} + \text{O}(^1\text{D}) + \text{Ar}$	$1.456 \cdot 10^{-16}$	28, 148, 149
289	$\text{O}_2(\text{a}^1\Delta_u) + \text{Ar}^r \rightarrow \text{O} + \text{O}(^1\text{D}) + \text{Ar}$	$1.456 \cdot 10^{-16}$	28, 148, 149
290	$\text{O}_2(\text{b}^1\Sigma_u^+) + \text{Ar}^r \rightarrow \text{O} + \text{O}(^1\text{D}) + \text{Ar}$	$1.456 \cdot 10^{-16}$	28, 148, 149
291	$\text{O}_2 + \text{Ar}^r \rightarrow \text{O} + \text{O}(^1\text{S}) + \text{Ar}$	$5.6 \cdot 10^{-18}$	28, 148, 149
292	$\text{O}_2(\text{a}^1\Delta_u) + \text{Ar}^r \rightarrow \text{O} + \text{O}(^1\text{S}) + \text{Ar}$	$5.6 \cdot 10^{-18}$	28, 148, 149
293	$\text{O}_2(\text{b}^1\Sigma_u^+) + \text{Ar}^r \rightarrow \text{O} + \text{O}(^1\text{S}) + \text{Ar}$	$5.6 \cdot 10^{-18}$	28, 148, 149
294	$\text{O}(^1\text{D}) + \text{Ar} \rightarrow \text{Ar} + \text{O}$	$3.0 \cdot 10^{-19}$	28, 121
295	$\text{O}(^1\text{S}) + \text{Ar} \rightarrow \text{Ar} + \text{O}$	$4.8 \cdot 10^{-24}$	28, 121
296	$\text{O} + \text{Ar}^m \rightarrow \text{Ar} + \text{O}(^3\text{P})$	$7.6 \cdot 10^{-17}$	28, 150
297	$\text{O}(^3\text{P}) + \text{Ar} \rightarrow \text{Ar} + \text{O}(^5\text{P})$	$2.80 \cdot 10^{-18}$	28, 151
298	$\text{O}(^3\text{P}) + \text{Ar} \rightarrow \text{O} + \text{Ar}$	$1.4 \cdot 10^{-17}$	114
299	$\text{O}(^3\text{S}) + \text{Ar} \rightarrow \text{O} + \text{Ar}$	$1.4 \cdot 10^{-17}$	114 ^b
300	$\text{O}(^5\text{P}) + \text{Ar} \rightarrow \text{O} + \text{Ar}$	$1.4 \cdot 10^{-17}$	114 ^b
301	$\text{O}(^5\text{S}) + \text{Ar} \rightarrow \text{O} + \text{Ar}$	$1.4 \cdot 10^{-17}$	114 ^b

^a The reaction is an extension from the reactions in Ref. 45.^b The collisional quenching coefficient for $\text{O}(^3\text{P}) + \text{Ar}$ is measured in Ref. 114. Here, the same quenching coefficient is used for the marked reactions, due to a lack of specific data.

Table A6: Recombination reactions. Neutral and ion temperature, T_N , in K, and N_r is the number of reactants.

#	Reaction	K_r [$\text{m}^{3+3(N_r-2)}\text{s}^{-1}$]	Ref.
302	$\text{O}^+ + \text{O}^- \rightarrow 2\text{O}$	$3.10 \cdot 10^{-14}(300/T_N)^{1.1}$	[48, reaction 186], 152
303	$\text{O}^+ + \text{O}^- + \text{O}_2 \rightarrow 2\text{O} + \text{O}_2$	$1.00 \cdot 10^{-37}(300/T_N)^{2.5}$	[48, reaction 187], 153
304	$\text{O}^+ + \text{O}^- + \text{O}_2 \rightarrow 2\text{O}_2$	$1.00 \cdot 10^{-37}(300/T_N)^{2.5}$	[48, reaction 188], 153
305	$\text{O}^- + \text{O}_2^+ \rightarrow 3\text{O}$	$1.61 \cdot 10^{-14}(300/T_N)^{1.1}$	[48, reaction 207], 152
306	$\text{O}^- + \text{O}_2^+ \rightarrow \text{O} + \text{O}_2$	$1.61 \cdot 10^{-14}(300/T_N)^{1.1}$	[48, reaction 208], 152
307	$\text{O}^- + \text{O}_3^+ \rightarrow \text{O} + \text{O}_3$	$3.07 \cdot 10^{-14}(300/T_N)^{1.1}$	[48, reaction 212], 152
308	$\text{O}^- + \text{O}_4^+ \rightarrow \text{O} + 2\text{O}_2$	$1.54 \cdot 10^{-14}(300/T_N)^{0.9}$	[48, reaction 213], 152
309	$\text{O}^- + \text{O}_4^+ \rightarrow \text{O}_2 + \text{O}_3$	$1.54 \cdot 10^{-14}(300/T_N)^{0.9}$	[48, reaction 214], 152
310	$\text{O}_2^+ + \text{O}^- + \text{O}_2 \rightarrow \text{O} + 2\text{O}_2$	$1.00 \cdot 10^{-37}(300/T_N)^{2.5}$	[48, reaction 237], 153
311	$\text{O}_2^+ + \text{O}^- + \text{O}_2 \rightarrow \text{O}_2 + \text{O}_3$	$1.00 \cdot 10^{-37}(300/T_N)^{2.5}$	[48, reaction 238], 153
312	$\text{O}_2^+ + \text{O}_2^- + \text{O}_2 \rightarrow 3\text{O}_2$	$2.00 \cdot 10^{-37}(300/T_N)^{2.5}$	[48, reaction 239], 153
313	$\text{O}_2^+ + \text{O}_3^- + \text{O}_2 \rightarrow 2\text{O}_2 + \text{O}_3$	$2.00 \cdot 10^{-37}(300/T_N)^{2.5}$	[48, reaction 240], 153
314	$\text{O}_2^+ + \text{O}_4^- + \text{O}_2 \rightarrow 4\text{O}_2$	$2.00 \cdot 10^{-37}(300/T_N)^{2.5}$	[48, reaction 241], 153
315	$\text{O}_2^+ + \text{O}_2^- \rightarrow \text{O}_2 + 2\text{O}$	$1.60 \cdot 10^{-14}(300/T_N)^{1.1}$	[48, reaction 242], 152
316	$\text{O}_2^+ + \text{O}_2^- \rightarrow 2\text{O}_2$	$1.60 \cdot 10^{-14}(300/T_N)^{1.1}$	[48, reaction 243], 152
317	$\text{O}_2^+ + \text{O}_3^- \rightarrow 2\text{O} + \text{O}_3$	$2.90 \cdot 10^{-14}(300/T_N)^{0.9}$	[48, reaction 244], 152
318	$\text{O}_2^+ + \text{O}_3^- \rightarrow \text{O}_2 + \text{O}_3$	$2.90 \cdot 10^{-14}(300/T_N)^{0.9}$	[48, reaction 245], 152
319	$\text{O}_2^+ + \text{O}_4^- \rightarrow 3\text{O}_2$	$6.07 \cdot 10^{-14}(300/T_N)^{0.9}$	[48, reaction 246], 152
320	$\text{O}_2^- + \text{O}_3^+ \rightarrow \text{O}_2 + \text{O}_3$	$3.29 \cdot 10^{-14}(300/T_N)^{1.1}$	[48, reaction 248], 152
321	$\text{O}_2^- + \text{O}_4^+ \rightarrow 2\text{O} + 2\text{O}_2$	$1.60 \cdot 10^{-14}(300/T_N)^{1.1}$	[48, reaction 249], 152
322	$\text{O}_2^- + \text{O}_4^+ \rightarrow 3\text{O}_2$	$1.60 \cdot 10^{-14}(300/T_N)^{1.1}$	[48, reaction 250], 152

Continuation of table A6: Recombination reactions.

#	Reaction	K_r [$\text{m}^{3+3(N_r-2)}\text{s}^{-1}$]	Ref.
323	$\text{O}^+ + \text{O}_2^- \rightarrow \text{O} + \text{O}_2$	$3.22 \cdot 10^{-14}(300/T_N)^{1.1}$	[48, reaction 190], 152
324	$\text{O}^+ + \text{O}_2^- + \text{O}_2 \rightarrow \text{O} + 2\text{O}_2$	$1.00 \cdot 10^{-37}(300/T_N)^{2.5}$	[48, reaction 191], 153
325	$\text{O}^+ + \text{O}_2^- + \text{O}_2 \rightarrow \text{O}_2 + \text{O}_3$	$1.00 \cdot 10^{-37}(300/T_N)^{2.5}$	[48, reaction 192], 153
326	$\text{O}_2 + \text{O}_2^- + \text{O}_3^+ \rightarrow 2\text{O}_2 + \text{O}_3$	$2.00 \cdot 10^{-37}(300/T_N)^{2.5}$	[48, reaction 219], 153
327	$\text{O}_2 + \text{O}_2^- + \text{O}_4^+ \rightarrow 4\text{O}_2$	$2.00 \cdot 10^{-37}(300/T_N)^{2.5}$	[48, reaction 220], 153
328	$\text{O}_3^+ + \text{O}_3^- \rightarrow 2\text{O}_3$	$5.19 \cdot 10^{-14}(300/T_N)^{0.9}$	[48, reaction 252], 152
329	$\text{O}_3^+ + \text{O}_4^- \rightarrow 2\text{O}_2 + \text{O}_3$	$5.37 \cdot 10^{-14}(300/T_N)^{0.9}$	[48, reaction 253], 152
330	$\text{O}_3^- + \text{O}_4^+ \rightarrow \text{O} + 3\text{O}_2$	$2.43 \cdot 10^{-14}(300/T_N)^{0.9}$	[48, reaction 255], 152
331	$\text{O}_3^- + \text{O}_4^+ \rightarrow 2\text{O}_2 + \text{O}_3$	$2.43 \cdot 10^{-14}(300/T_N)^{0.9}$	[48, reaction 256], 152
332	$\text{O}_4^+ + \text{O}_4^- \rightarrow 4\text{O}_2$	$4.97 \cdot 10^{-14}(300/T_N)^{0.9}$	[48, reaction 257], 152
333	$\text{O}^+ + \text{O}_3^- \rightarrow \text{O} + \text{O}_3$	$7.33 \cdot 10^{-14}(300/T_N)^{0.9}$	[48, reaction 194], 152
334	$\text{O}^+ + \text{O}_3^- + \text{O}_2 \rightarrow \text{O} + \text{O}_2 + \text{O}_3$	$2.00 \cdot 10^{-37}(300/T_N)^{2.5}$	[48, reaction 195], 153
335	$\text{O}^+ + \text{O}_4^- \rightarrow \text{O} + 2\text{O}_2$	$7.87 \cdot 10^{-14}(300/T_N)^{0.9}$	[48, reaction 196], 152
336	$\text{O}^+ + \text{O}_4^- + \text{O}_2 \rightarrow \text{O} + 3\text{O}_2$	$2.00 \cdot 10^{-37}(300/T_N)^{2.5}$	[48, reaction 197], 153
337	$\text{O}_2 + \text{O}_3^+ + \text{O}_3^- \rightarrow \text{O}_2 + 2\text{O}_3$	$2.00 \cdot 10^{-37}(300/T_N)^{2.5}$	[48, reaction 223], 153
338	$\text{O}_2 + \text{O}_3^+ + \text{O}_4^- \rightarrow 3\text{O}_2 + \text{O}_3$	$2.00 \cdot 10^{-37}(300/T_N)^{2.5}$	[48, reaction 224], 153
339	$\text{O}_2 + \text{O}_3^- + \text{O}_4^+ \rightarrow 3\text{O}_2 + \text{O}_3$	$2.00 \cdot 10^{-37}(300/T_N)^{2.5}$	[48, reaction 225], 153
340	$\text{O}_2 + \text{O}_4^+ + \text{O}_4^- \rightarrow 5\text{O}_2$	$2.00 \cdot 10^{-37}(300/T_N)^{2.5}$	[48, reaction 226], 153
341	$\text{O}^- + \text{O}_2 + \text{O}_3^+ \rightarrow \text{O} + \text{O}_2 + \text{O}_3$	$2.00 \cdot 10^{-37}(300/T_N)^{2.5}$	[48, reaction 201], 153
342	$\text{O}^- + \text{O}_2 + \text{O}_4^+ \rightarrow \text{O} + 3\text{O}_2$	$2.00 \cdot 10^{-37}(300/T_N)^{2.5}$	[48, reaction 202], 153
343	$\text{O}^- + \text{Ar}^+ \rightarrow \text{O} + \text{Ar}$	$4.0 \cdot 10^{-14}(300/T_N)^{0.43}$	45